ECOLE DE TECHNOLOGIE SUPÉRIEURE
UNIVERSITÉ DU QUÉBEC

MANUSCRIPT-BASED THESIS PRESENTED TO
ÉCOLE DE TECHNOLOGIE SUPÉRIEURE

IN PARTIAL FULFILLMENT OF THE REQUIREMENTS FOR
THE DEGREE OF DOCTOR OF PHILOSOPHY
Ph. D.

BY
Martin BRUMMUND

STUDY OF THE OCCLUSION EFFECT INDUCED BY AN EARPLUG: NUMERICAL MODELLING AND EXPERIMENTAL VALIDATION

MONTREAL, DECEMBER 19, 2014

BOARD OF EXAMINERS (THESIS PH.D.)

THIS THESIS HAS BEEN EVALUATED

BY THE FOLLOWING BOARD OF EXAMINERS

Mr. Frédéric Laville, Thesis Supervisor
Department of Mechanical Engineering at École de technologie supérieure

Mr. Yvan Petit, Thesis Co-supervisor
Department of Mechanical Engineering at École de technologie supérieure

Mr. Franck Sgard, Thesis Co-supervisor
Scientific Division at Institut de recherche Robert-Sauvé en santé et en sécurité du travail

Mrs. Nicola Hagemeister, President of the Board of Examiners
Department of Automated Manufacturing Engineering at École de technologie supérieure

Mr. Jérémie Voix, Member of the jury
Department of Mechanical Engineering at École de technologie supérieure

Mr. Raymond Panneton, External Evaluator
Department of Mechanical Engineering at Université de Sherbrooke

THIS THESIS WAS PRENSENTED AND DEFENDED

IN THE PRESENCE OF A BOARD OF EXAMINERS AND PUBLIC

NOVEMBER 27, 2014

AT ÉCOLE DE TECHNOLOGIE SUPÉRIEURE

ACKNOWLEDGMENT

I would like to express my deepest gratitude to my thesis supervisors Professors Franck Sgard, Yvan Petit and Frédéric Laville who have guided and supported me on countless occasions throughout this research project. Your expertise and dedication make you exceptional mentors and I feel privileged to be given the opportunity to research with and learn from you. Thank you for everything you have contributed to realize this study.

I would like to gratefully acknowledge the Institut de recherche Robert-Sauvé en santé et en sécurité du travail (IRSST) for funding this work. Additionally, I would like to gratefully acknowledge the funding received in form of prizes and scholarships from: École de technologie supérieure (ÉTS), Équipe de recherché en sécurité du travail – Réseau de recherche en santé et en sécurité du travail du Québec (ÉREST-RRSSTQ), Canadian Acoustical Association (CAA) and Acoustical Society of America (ASA).

I would like to thank the members of the Scientific Advisory Committee: Elliott H. Berger (3M), William J. Murphy (NIOSH), Karl Buck (ISL), and Nicolas Trompette (INRS) for sharing a tremendous amount of expert knowledge and experience. Your continued guidance throughout this research project has contributed significantly to the outcome of this study. I feel privileged to have been given the opportunity to present our research work to some of the most renowned researchers in hearing protection.

I would like to gratefully acknowledge Stefan Stenfelt (Linköping University) and Sabine Reinfeldt (Chalmers University of Technology) for kindly sharing occlusion effect data for the present study. Additionally, I would like to thank Hugues Nélisse (IRSST), Cécile Le Cocq (ÉTS) and Jérôme Boutin (IRSST) for providing experimental occlusion effect measurements for the present work and for their help and support during the experimental testing of the artificial external ear test fixture.

I would like to thank Professor Jérémie Voix of the Sonomax-ÉTS industrial research chair in in-ear technologies for his expertise and support as well as for providing earplug samples for the present study.

I would like to thank Annie Levasseur and Jaëlle Tremblay (both LIO - HSCM) for their help and support with the medical image processing and material testing.

I would like to acknowledge Mario Corbin and Olivier Bouthot (both ÉTS) for the technical support and help during the implementation of the artificial external ear prototype and the subsequent experimental tests.

I would like the express my gratitude to the board of examiners for their active participation during my doctoral exam and for evaluating the present doctoral thesis.

I would like to thank my colleague and great friend Guilhem Viallet for the many great moments we shared together at the office, at conferences and after work. Thanks to you I am starting to master the French language, my friend! I would also like to thank Sylvain Boyer for being a great colleague and friend.

Finally, I would like to thank my fiancée Vanessa Tamim for her love, help and support throughout the past years.

Gewidmet meinen Eltern

Eure tatkräftige Unterstützung trug maßgeblich zum Entstehen dieser Arbeit bei.

ÉTUDE DE L'EFFET D'OCCLUSION INDUIT PAR UN PROTECTEUR AUDITIF DE TYPE BOUCHON D'OREILLE : MODÉLISATION NUMÉRIQUE ET VALIDATION EXPÉRIMENTALE

Martin BRUMMUND

RESUME

Malgré l'existence de limites d'exposition au bruit en milieu du travail, la perte d'audition professionnelle constitue un problème important au Québec et à l'échelle mondiale. Plusieurs approches existent pour protéger les travailleurs exposés à des niveaux sonores nocifs. La solution à court terme la plus souvent rencontrée en pratique demeure l'utilisation de protecteurs individuels contre le bruit (PIB), tels que les bouchons d'oreilles et les protecteurs de type coquille.

Les PIBs représentent un moyen de protection efficace et ils se distinguent d'autres approches par leur coût économique faible et leur facilité d'utilisation. Néanmoins, à cause de problèmes d'inconfort il arrive souvent que la durée de port recommandée pour limiter l'exposition au bruit n'est pas respecter par les travailleurs et qu'ils risquent par conséquent de développer une perte d'audition professionnelle.

L'inconfort associé au port des PIBs peut être associé à deux grandes catégories. L'inconfort « physique » regroupe, pour les PIBs de type bouchon d'oreille, par exemple une sensation de pression sur les parois du conduit et l'échauffement de l'oreille. L'inconfort « auditif » regroupe des phénomènes liés à la modification de la perception de sons et de la parole ainsi que des difficultés de communication. Une source d'inconfort « auditif » qui joue un rôle important est l'effet d'occlusion.

L'effet d'occlusion apparaît lors de l'insertion d'un bouchon d'oreille dans le canal auditif et décrit un phénomène d'amplification sonore en basses fréquences par rapport au niveau habituel en oreille ouverte. Cette amplification sonore est perceptible par le porteur et mesurable par le niveau de pression dans le canal auditif (mesure objective) et la modification du seuil d'audition (mesure subjective). De plus, l'effet d'occlusion entraîne une sensation désagréable qui résulte du fait que la propre voix du porteur est déformée (elle est perçue comme plus caverneuse) et que les bruits physiologiques (tels que la respiration et la circulation sanguine) sont également amplifiés par le port des bouchons.

La réduction de l'effet d'occlusion contribuerait à augmenter le confort auditif des PIBs et donc aiderait à prévenir la surdité professionnelle. Afin de contribuer à résoudre les problématiques présentement associées au port des PIBs, l'institut de recherche Robert-Sauvé en santé et en sécurité du travail (IRSST) et l'École de technologie supérieure (ÉTS) ont mis en place un projet conjoint de recherche scientifique visant à mieux comprendre le fonctionnement des PIBs dans un but d'une meilleure conception acoustique.

La présente étude fait partie de cette collaboration et a pour but d'étudier l'effet d'occlusion induit par un bouchon d'oreille inséré dans le canal auditif grâce au développement de nouveaux modèles numériques prédictifs et de méthodes expérimentales.

Deux modèles couplés elasto-acoustiques linéaires à géométrie complexe et à géométrie simplifiée (axisymétrique) sont présentés pour simuler l'effet d'occlusion induit par un bouchon d'oreille dans le cadre d'une excitation par voix osseuse.

Le premier modèle 3D à géométrie complexe est utilisé pour simuler l'effet d'occlusion d'un bouchon d'oreille à plusieurs profondeurs d'insertions. Des bilans de puissances sont utilisés pour étudier la circulation d'énergie dans l'oreille occluse à faible, moyenne et profonde insertion pour mieux comprendre comment contribuent la surface intérieure du bouchon ainsi que les parois non-occlues à l'effet d'occlusion. Les effets d'occlusions numériques obtenus à partir du modèle sont validés à l'aide de mesures expérimentales disponible dans la littérature. Le modèle numérique 3D est utilisé pour étudier les modèles qualitatifs de l'effet d'occlusion à l'aide de bilans de puissances.

Le deuxième modèle à géométrie axisymétrique est utilisé pour étudier les fonctions de transferts (oreille ouverte et occluse) ainsi que l'effet d'occlusion dans trois conditions d'excitation différentes. Tout d'abord une excitation purement par voie osseuse est considérée. Ensuite un bruit aérien est ajouté de manière incohérente à la stimulation par voie osseuse pour étudier l'effet d'une excitation mixte. Cette excitation mixte est ensuite étudiée dans le cas (i) d'une occlusion parfaitement étanche et (ii) sous présence de petites fuites acoustiques dans les modèles géométriques du bouchon. Chaque type d'excitation est considéré pour quatre configurations de conditions aux limites et d'excitation. Toutes les simulations numériques sont comparées à des mesures expérimentales.

Le modèle axisymétrique est utilisé pour simuler l'effet d'occlusion pour étudier le rôle que joue le type du bouchon par rapport à l'effet de l'occlusion. Ce travail est réalisé en trois temps. Dans un premier temps le modèle numérique est validé à l'aide de mesures expérimentales faites sur deux groupes indépendant de sujets humains, chaque groupe étant équipé d'un bouchon différent. Dans un deuxième temps le modèle axisymétrique est validé à l'aide de deux modèles électriques équivalents de l'effet d'occlusion issus de la littérature. Dans un troisième temps des calculs de bilans de puissances sont effectués pour mieux comprendre comment l'énergie circule dans le système dépendamment du type de bouchon utilisé. Ces calculs sont effectués dans le canal occlus ainsi que dans les bouchons en contact avec les parois du canal à une moyenne et une très faible profondeurs d'insertions.

Le prototype d'un nouveau dispositif expérimental d'une oreille externe artificielle est proposé pour mesurer l'effet d'occlusion de manière objective et standardisé. Des résultats expérimentaux issus de ce prototype sont présentés pour démontrer la fonctionnalité du dispositif dans le but de mesurer l'effet d'occlusion d'un bouchon d'oreille. Premièrement la mise œuvre d'une oreille externe artificielle axisymétrique est présentée. Deuxièmement, le dispositif expérimental est utilisé pour étudier la contribution des différents chemins de transmission sonore. Troisièmement l'effet d'occlusion d'un bouchon en mousse à moyenne

profondeur d'insertion est mesuré à l'aide du dispositif expérimental. La mesure de l'effet d'occlusion est répétée à plusieurs niveaux d'excitation mécanique pour étudier la linéarité du système.

Mots-clés : Santé et sécurité du travail, protection auditive, effet d'occlusion, méthode d'éléments finis, étude numérique, mesure expérimentale, dispositif expérimental

STUDY OF THE OCCLUSION EFFECT INDUCED BY AN EARPLUG: NUMERICAL MODELLING AND EXPERIMENTAL VALIDATION

Martin BRUMMUND

ABSTRACT

Despite existing limits for occupational noise exposure, professional hearing loss remains a high priority problem both in Québec and worldwide. Several approaches exist to protect workers from harmful noise levels. The most frequently employed short term solution includes the distribution of hearing protection devices (HPD) such as earplugs and ear muffs. While HPDs offer an inexpensive (e.g. direct cost) and efficient means of protection workers often only tend to wear HPDs for limited amounts of time and, thus, remain at risk of developing professional hearing loss.

Discomfort while using HPDs contributes to HPD underutilization and non-use. Two more general categories of discomfort can be distinguished. The category physical discomfort includes, for instance, problems such as heating of the ear and irritation of the ear canal that that occur upon earplug insertion. The category auditory discomfort refers to alterations in the auditory perception of sounds and one's own voice as well as hindered workplace communications. One important auditory discomfort that promotes HPD non-use is the occlusion effect.

The occlusion effect occurs upon earplug insertion and describes sound amplification phenomena in the occluded ear canal at the low frequencies. The sound amplification is both perceivable and measurable (e.g., open and occluded sound pressure levels, hearing threshold shift). Additionally, the occlusion effect causes the HPD wearer to perceive his/her own voice as being distorted (e.g. hollow sounding) and physiological noises (e.g. respiration, blood circulation) are amplified also subsequent to earplug insertion.

Reducing the occlusion effect has the potential to increase the auditory comfort of HPDs and could help preventing occupational hearing loss in the future. In order to improve this and other shortcomings observed with currently existing HPDs a large research collaboration between the Robert-Sauvé research institute in occupational health and safety (IRSST) and the École de technologie supérieure (ÉTS) has been launched.

The present study represents a part of this collaboration and aims at studying the occlusion effect of the system earplug – ear canal through the development of novel numerical models and experimental methods.

A 3D (complex geometry) and an axisymmetric (simplified geometry) linear elasto-acoustic finite element model are presented in this study to simulate the objective bone conduction earplug occlusion effect.

The 3D model of complex geometry is used to predict the occlusion effect induced by a silicone earplug at several insertion depths. Power balance computations are used to explain how the ear canal walls and the medial earplug surface contribute to observed occlusion effect magnitudes at varying occlusion depths. The numerical occlusion effect predictions are validated with experimental reference data that were retrieved from the literature. The 3D model is used to investigate two well established qualitative occlusion effect models using power balance computations.

The axisymmetric occlusion effect model is used to predict open and occluded transfer function levels as well as the occlusion effect across three different excitation scenarios. First, only structure borne excitation is considered. Next, airborne noise is added incoherently to the structure borne excitation to study the effect of a mixed excitation. The mixed excitation is considered (i) for a leak free (perfect seal) earplug insertion and (ii) under the presence of small earplug leaks. Each stimulation scenario is examined across four different boundary and load conditions. All predicted transfer function levels and occlusion effects are compared to experimental data.

An adapted version of the axi-symmetric occlusion effect model is employed to investigate the contribution of the earplug type to the occlusion effect magnitude. First, the numerical model is validated with the help of experimental occlusion effect data which were measured in two independent human reference groups which each use a different earplug type (silicone earplug and foam earplug). Second, the numerical model is further validated through comparison with two gold standard lumped element occlusion effect models which were drawn from the literature. Third, power balance computations are employed to investigate the power flow inside the occluded ear canal cavity as well as the earplug body (coupled to the ear canal walls) of the numerical external ear model. The power balances are computed both for the foam and the silicone earplug models at medium and very shallow earplug insertion depths.

A prototype of a novel artificial external ear test fixture for objective and standardized measurement of the occlusion effect is developed. Details on the implementation of the artificial external ear and the assembly of the occlusion effect test fixture are presented. The experimental test fixture is used to investigate the contribution of the structure and airborne sound transmission pathways. Experimental data is provided to demonstrate that the test fixture is functional and that it can be used to measure the occlusion effect of a foam earplug. The occlusion effect measurement is repeated for several mechanical stimulation levels to study the system’s linearity.

Keywords: Occupational health and safety, hearing protection, occlusion effect, finite element method, numerical study, experimental measurements, artificial test fixture

TABLE OF CONTENTS

LIST OF TABLES

Page

LIST OF FIGURES

Page

LIST OF ABREVIATIONS

ABS	Acrylonitrile butadiene styrene
AC	Air conduction
ANSI	American National Standards Institute
ASA	Acoustical Society of America
ASTM	American Society for Testing and Materials
ATF	Artificial test fixture
BC	Bone conduction
ÉTS	École de technologie supérieure
FE	Finite element
FEM	Finite element method
HL	Hearing loss
HPD	Hearing protection device
IEC	International Electrotechnical Commission
IRSST	Institut de recherche Robert-Sauvé en santé et en sécurité du travail
ISO	International Organization for Standardization
L	Length
NRR	Noise reduction rating
OE	Occlusion effect
PIB	Protecteur individuel contre le bruit
PDTM	Power dissipated at the tympanic membrane
PSD	Power spectral density
R	Radius

REAT	Real-ear attenuation at threshold
RMS	Root mean square
S.D.	Standard deviation
SPL	Sound pressure level
T	Thickness
TFL	Transfer function level
VHP	Visible human project

INTRODUCTION

0.1 Research problem

0.1.1 Hazardous occupational noise exposure and means of protection

Exposure to high noise levels can cause permanent damage to the auditory system. In the context of occupational health and safety prolonged noise exposure is often inevitable as the work task (e.g. construction industry) might require workers to spend entire shifts in noisy environments. To protect these employees the Canadian federal and provincial legislations have defined maximum noise exposure levels that must be met. For instance, in Québec the maximum noise exposure during an 8 hour work shift is limited to 90 dB(A) (Québec, 2014).

Despite the existing limits for occupational noise exposure professional hearing loss remains a high priority problem. In Québec, impairment of the sense of hearing and the ear was the most frequently encountered professional disorder in 2011, 2012 and 2013 (Lamarche et al., 2011, 2013, 2014). In 2013 the number of accepted cases even increased from 2600 (accepted cases in 2012) to 3303 accepted cases (Lamarche et al., 2014). Worldwide, an estimated 120 million workers are regularly exposed to noise levels that can permanently damage the auditory system (Organisation mondiale de la santé (OMS), 2001).

Several approaches exist to protect workers from harmful noise exposure. They include (i) treating the noise emitting source and surrounding workspace in an attempt to achieve more moderate noise levels, (ii) structurally reorganizing the work tasks to limit the cumulated noise exposure and (iii) distributing hearing protection devices (HPD) such as earplugs and earmuffs to attenuate the ambient noise levels in such way that existing noise exposure limits are met. Due to financial, spatial and temporal restrictions observed in the first two methods HPDs remain, to date, the most frequently utilized short term solution to protect the workers, because they are easy-to-use, fast in implementation and at the same time cost efficient (e.g. direct cost).

The acoustic performance of a HPD is influenced by the achieved noise attenuation and amount of time the protector is being worn (Sgard et al., 2008). If worn correctly, HPDs provide an efficient means of protection (Berger et al., 2003). When HPDs are removed even during short periods of time their overall performance is reduced. The decrease in HPD net-performance due to temporary protector removal is hereby greater for higher noise reduction rated (NRR) HPDs. For instance, removing an HPD of nominal NRR 25 dB for only 15 minutes during an 8 hour shift reduces the net NRR of that protector to 20dB. On the other hand if the nominal NRR equals 15dB, the net NRR reduces to about 14 dB if the protector is not being worn for 15 min throughout the entire work shift (Berger et al., 2003).

0.1.2 Causes for HPD underutilization

0.1.2.1 General causes

Numerous empirical studies have been conducted to examine HPD use across different industries and countries. These studies unambiguously express the need to increase consistent HPD use especially among non-users and occasional HPD users. Melamed et al. (1994) and Tak et al. (2009), for example, provide overviews of some of the research work that has been carried out in order to better explain why HPDs are underutilized in the workplace environment. Contributing factors include:

- Unavailability of HPDs in noisy environments
- Lack of knowledge on the ability of an HPD to reduce harmful noise
- Lack of confidence to adequately use HPDs
- Physical discomfort while using HPDs (e.g. irritation of the ear canal, headband force)
- Interference of the HPD with other work equipment (e.g. headgear)
- Interference of the HPD with the work task
- Fear of a decrease in the worker's prestige among co-workers
- Fear of blocking out useful auditory cues such as warning signals
- A perceived sense of isolation while wearing a HPD (Hughson et al., 2002)
- Impression that the HPD negatively affects the communication with co-workers

Many of the aforementioned causes that contribute to non-use of HPDs can be approached through educational and motivational steps as part of a broader hearing conservation program (Berger et al., 2003) and adequate HPD selection.

Another important factor that contributes to HPD non-use is the occlusion effect. Often the occlusion effect is not specifically mentioned as cause for HPD non-use by test subjects. This could, hypothetically, originate from a certain degree of unawareness among the examined test subjects. As the present work is dedicated to studying the occlusion effect induced by an earplug the link between the occlusion effect and HPD underutilization is going to be discussed in detail in section 0.1.2.3. Prior to this discussion, a definition of the occlusion effect is presented as support for the reader.

0.1.2.2 Definition of the occlusion effect

The occlusion effect describes perceivable and measurable (e.g. sound pressure level inside the ear canal, hearing threshold shift) sound amplification phenomena that occur upon earplug insertion into the ear canal. Thus, the occlusion effect causes the HPD wearer to perceive his/her own voice as being distorted, hollow sounding and, most noticeably, amplified at the lower frequencies. Additionally, physiological noises (e.g. respiration, blood circulation) are amplified also subsequent to earplug insertion (Berger and Kerivan, 1983).

0.1.2.3 The role of the occlusion effect in the context of HPD underutilization

As was previously mentioned, the occlusion effect is often omitted as cause for HPD non-use by test subjects. Nevertheless, the occlusion effect contributes considerably for instance to the impression that HPDs hinder workplace communication as was discussed in Berger et al. (2003). Berger et al. (2003) provide a summarizing overview of the research work that has been carried out with regards to the effects of HPDs on auditory perception. It can be seen that HPDs can negatively affect speech intelligibility in conditions where the HPD wearer is listening to his own voice and in situations where co-workers, that are each wearing HPDs,

communicate (e.g. Howell and Martin, 1975). While the talker experiences the occlusion effect, the ambient noise is attenuated through his HPD at the same time. Thus, the talker gets the impression that his/her voice is louder with respect to the ambient noise than actually is the case and tends to lower his/her vocal effort. The latter decrease in signal level and signal to noise ratio hinders the intelligibility on the listener side and thus causes an overall reduction in speech intelligibility. Consequently, the HPD wearers are prone to removing their HPDs and, thus, remain at risk of developing professional hearing loss.

0.2 Research objectives

The preceding paragraphs provide a contextual overview on how the occlusion effect contributes to HPD underutilization and occupational hearing loss. In the following paragraphs the general and specific research objectives of the present study are presented.

0.2.1 General research objective

To improve the shortcomings observed in currently existing HPDs the Institut de recherche Robert-Sauvé en santé et en sécurité du travail (IRSST) and the École de technologie supérieure (ÉTS) have launched a research collaboration that aims at the development of tools and methods to better assess and design hearing protectors (IRSST research project 0099-7630).

The present study represents a sub domain of the outlined research collaboration. It aims at better understanding the occlusion effect induced by an earplug through the development of novel numerical models and experimental methods. The developed numerical models and experimental methods have the potential to provide valuable insight into the manner in which the earplug contributes to the occlusion effect and to identify earplug constituents (e.g. material properties) crucial to reducing the occlusion effect magnitude. In a future study, this work could serve as a foundation to specifically guide the design and implementation of a passive low occlusion effect earplug. As was outlined in section 0.1 the occlusion effect is an important factor that contributes to HPD non-use. It is, thus reasonable to assume that

reducing the occlusion effect could contribute to increasing the auditory comfort of HPDs. In return, this could help to reduce HPD non-use among workers that are exposed to harmful noise levels and, thus, assist in preventing occupational hearing loss in the future. Note that the present study only considers earplug type HPDs. Ear muff type HPDs are not considered in this work, because incorporating ear muffs would increase model complexity as the pinna and more of the head would have to be considered. In the future such model could definitely be implemented presently, however, it goes beyond the scope of the present study.

0.2.2 Specific research objectives

For the present study four specific objectives are defined to achieve the general objective outlined in the preceding paragraph. Under objective 1 a numerical model of complex geometry is implemented to model the human external ear as realistically as possible (note that several limitations apply which are outlined throughout the study). Under objective 2 a second numerical model is implemented. The degree of geometrical complexity of this model is reduced to increase the ease of use. Under objective 3 the numerical model implemented under objective 2 is used to further study the earplug induced occlusion effect. Lastly, objective 4 aims at developing a novel experimental method to measure the earplug occlusion effect. Note that detailed explanations of the relevance are provided with each specific objective. The four research objectives are:

O1: *Implement a 3D human external ear finite element model of complex geometry using anatomical images to simulate and study the earplug induced occlusion effect in the case of a mechanical stimulation applied on the ipsilateral mastoid process. Validate the numerical occlusion effect data obtained with the model against experimental measurements from the literature.*

Relevance of a 3D human external ear model: To date only a few studies have aimed at modelling the occlusion effect (see section 1.3.3 for details). All existing models rely on lumped elements (electrical equivalent circuits) to model the occlusion effect. While obtained results generally tend to be in good agreement with experimental measurements, lumped

element models seem less suitable than finite element models, especially, to improve the earplug design. For instance, finite element models make it possible to analyze three-dimensional sound propagation (lumped elements limited to one-dimensional sound propagation) in substructures of the external ear (e.g. ear canal walls) and the earplug. Furthermore, the link between the model parameters and the physical properties of, for instance, the earplug are clearer in a finite element model than in a lumped model and it is easier to represent the tissue domains that surround the ear canal. Additionally, finite element models allow for calculating the power flows between subsystems of the external ear in 3D. Exchanged and dissipated powers can also be calculated from 3D displacement fields in the tissues and the earplug and from pressure fields in the ear canal. These indicators can be very helpful to further understand the occlusion effect mechanisms and particularly how the earplug contributes to the occlusion effect and which earplug parameters (e.g. material properties) play key roles.

O2: *Implement an axi-symmetric simplified external ear model on the basis of average external ear dimensions taken from the literature to simulate and study the occlusion effect in the case of a mechanical stimulation applied on the model's circumference. Validate the numerical data with experimental measurements.*

Relevance of an axisymmetric human external ear model: While 3D finite element models allow anatomically correct reconstruction of the geometrical complexity of the ear canal and its surrounding tissues (e.g. temporal bone, cartilage tissue, skin tissue), which facilitates adequate model excitation, they are also accompanied by several disadvantages. For instance, the 3D reconstruction of the external ear is very tedious especially when skin and cartilage tissues ought to be distinguished. The number of anatomical datasets available for 3D reconstruction of the external ear is very limited. 3D models can, due to their geometrical complexity, be very difficult to manipulate (e.g. meshing) and can require excessive computational resources. In addition to that, the geometrical complexity makes 3D models also cumbersome for the implementation of sensitivity analyses (e.g. earplug material properties, external ear geometry). Lastly, it is very challenging to implement an artificial test fixture on the basis of an anatomically correct 3D external ear geometry. For example, it is

very difficult to cast the skin covered ear canal walls. During the casting process an insert would be required. Upon curing, the insert would have to be removed from the ear canal which is challenging given the ear canal's s-shape. Besides, 3D reconstructed external ear geometries are based on individual data. For an artificial test fixture it would be desirable to have an average ear canal model. Axi-symmetric, finite element models could contribute to alleviate the abovementioned difficulties, because they rely on simpler geometries, are easier to manipulate and require less computational resources. Existing averaged geometrical data of the human external ear (ear canal length, wall skin thickness etc.) can be employed for the implementation of such an axi-symmetric model which renders the tedious 3D ear reconstruction unnecessary. Additionally, an axi-symmetric external ear model can also serve as a blueprint for the implementation of an artificial external ear test fixture, because they can be manufactured more easily (e.g. see preliminary work by Brummund et al. (2013) and chapter 5). In this context the question arises whether a simplified axi-symmetric model is sufficient to model the occlusion effect or whether the geometrical complexity of the external ear needs to be considered. Stinson and Lawton (1989) demonstrated that the sound pressure level inside the human ear canal can be approximated using a cylinder for frequencies up to 6 kHz. Unfortunately, Stinson and Lawton (1989) limited their study to the open ear canal (no surrounding tissues) and airborne excitation. During the present work the feasibility to develop a 3D equivalent, simplified axi-symmetric occlusion effect model could be demonstrated. Obtained results were presented to the scientific community at 162nd Meeting of the Acoustical Society of America (Brummund et al., 2011). The presentation was granted the "Best Paper Award for Young Presenters in Noise".

O3: *Numerically predict the occlusion effects of two earplug types using the simplified model developed under O2, validate the obtained occlusion effects with experimental data and interpret observed occlusion effect differences with the help of power balance calculations.*

Necessity to further investigate earplug type dependent occlusion effect: To date only very few experimental studies have aimed at examining the occlusion effect as a function of earplug type (please refer to section 1.3.2.5 for a review of the existing literature). Obtained

experimental results suggest that the earplug type can influence the occlusion effect at medium insertion depth, whereas it appears to be of secondary importance at very shallow insertion. These experimental results are highly relevant, because they imply that it could be possible to reduce the occlusion effect through an improved earplug design (e.g. material properties, geometry). Yet, it is not well understood how different earplug types contribute to the observed occlusion effect differences. Numerical occlusion effect modeling could contribute to bridge this gap through an analysis of the exchanged and dissipated time averaged acoustical powers both inside the ear canal cavity (e.g. unoccluded ear canal walls, medial earplug surface, eardrum) as well as inside the earplug domain (e.g. occluded ear canal walls, earplug body, medial earplug surface). Note that no occlusion effect model can be found in the literature that has aimed at studying the contribution of the earplug to the occlusion effect numerically.

O4: *Design and implement an artificial occlusion effect test fixture of similar geometry as the simplified numerical occlusion effect model (see O2) to examine the general feasibility of such a device and to experimentally measure the earplug occlusion effect objectively.*

Relevance to implement an artificial external ear test fixture: To date, no commercially available artificial test fixture allows measuring the occlusion effect of either earplugs or earmuffs. In part, this might be due to the circumstance that it is challenging to implement a structure borne excitation that would result in a vibration of the ear canal walls and sound radiation into the ear canal cavity (see section 1.3 for details on the occlusion effect mechanisms). Some information on the advantages of using a simplified external ear geometry for the implementation of an artificial occlusion effect test fixture was already provided with objective 2 (e.g. easier to manufacture as complex model, easier to implement an average external ear geometry). Once implemented such a test fixture could be employed to test and rate existing earplug designs with respect to the occlusion effect they cause. Additionally, a test fixture equivalent numerical model could serve to better understand the contribution of each part of the system ear canal/earplug to the occlusion effect (e.g. using power balances). In the future, this mixed experimental-numerical approach could contribute

to more efficiently guide the earplug design process in order to realize an earplug that exhibits both adequate noise attenuation and a reduced occlusion effect.

0.3 Thesis structure and research methodology

The previous paragraph lists the specific research objectives of the present work. The following section details the structure of the present thesis along with an overview of the methodology used to attain each specific objective.

0.3.1 Chapter 1: Literature review

Chapter 1 provides a comprehensive literature review on hearing by bone conduction and the occlusion effect. A brief overview of the anatomical structures of the human ear that are crucial to bone conduction hearing is provided. The different bone conduction sound transmission pathways are discussed. The bone conduction pathway that is most important for the occlusion effect is presented along with qualitative models that have been established to explain the occlusion effect. Additionally, experimental literature data is reviewed which explains the contributions of the chosen measurement technique (objective versus subjective), the occlusion volume, the bone conduction stimulation position, and the earplug occlusion device to the occlusion effect magnitude. Lastly, existing lumped element occlusion effect models are reviewed.

0.3.2 Chapter 2: Development of a 3D human external ear model of complex geometry

0.3.2.1 Chapter contents

In chapter 2 the first research article is presented. This article is entitled “Three-dimensional finite element modeling of the human external ear: simulation study of the bone conduction occlusion effect”. The purpose of this research article is to complete specific objective 1. A

3D coupled linear elasto-acoustic finite element model of the human ear canal and surrounding structure to simulate the occlusion effect is proposed.

0.3.2.2 Overview of the methodology used to implement the 3D external ear model

Geometrical external ear reconstruction: To reconstruct the 3D human external ear model, anatomical color images of a female cadaver head are retrieved from the Visible Human Project® database of the US National Library of Medicine. The images are segmented using a contour detection tool in order to separate bony, cartilaginous and skin tissues as well as the ear canal. Upon completion of the segmentation the outer surfaces of each anatomical structure is created. The resulting geometry is imported into a computer assisted design tool for post-processing of the 3D solid model.

Material properties of external ear tissues and earplugs: The 3D model is imported into a commercially available finite element simulation tool. The material properties of the bony, cartilage and skin tissues are applied to each domain. The isotropic, linear elastic material properties (density, Young's modulus, Poisson's ration, loss factor) used in the model are drawn from the literature, when possible. While the assumption of linear elasticity is reasonable for small tissue deformations, assuming isotropy represents a simplification of the considered human tissues which are anisotropic and viscoelastic. Due to a lack of more accurate material property data, however, such simplification seems presently inevitable. Additionally, the material properties of two earplug types (silicone and foam earplugs) are applied to the earplug models of the occluded external ear. The earplug models are assumed to adapt to the shape of the ear canal without deforming its walls and to occlude the ear canal leak free. Again, isotropic linear elastic material behavior is assumed and all material properties are taken from the literature. To model the ear canal itself the speed of sound and density of air at 20°C are applied to this domain.

Boundary conditions and excitation: Boundary conditions are applied to the circumference of the external ear domains to express the connections that exist between the model domains

and their environment. The skin tissue of ear canal entrance region and the boundaries of the temporal bone are modeled as free boundary conditions. The circumference of the skin and cartilage tissue that back the ear canal are fixed. Between solid domains continuity of stress vectors and displacements is assumed. Interfaces between a solid domain and ear canal cavity are expressed through fluid-structure coupling. The eardrum is expressed using a locally reacting specific acoustical impedance boundary condition. Another locally reacting impedance boundary condition which corresponds to the radiation impedance of a baffled flat circular piston is applied over the entrance of the open ear canal. The external ear system is excited mechanically via the ipsilateral mastoid process using a constant total force of 1N which applies normally to a flat surface area.

Model meshing: The 3D model is meshed using tetrahedral quadratic elements for all domains. The mesh uses a convergence criterion of four elements per wavelength at 3 kHz. The meshed model is solved for the sound pressure at the eardrum. The sound pressures of the open and occluded external ear models are used to calculate the earplug occlusion effect. Other acoustical indicators such as the acoustical normal particle velocity are retrieved to calculate exchanged and dissipated powers.

Data analysis: Obtained numerical results are used to investigate the influence of the temporal bone's boundary conditions on the transfer function levels and occlusion effect magnitude. The open ear and occluded transfer function levels and occlusion effect are predicted at several earplug insertion depths. The predicted occlusion effects at medium insertion depth are compared to experimental occlusion effect data measured in human subjects (the data were kindly provided by Stenfelt and Reinfeldt (2007)). Note that comparing the 3D finite element (FE) predictions to experimental data is presently the most suitable way to validate the numerical model due to the circumstance that no model equivalent test fixture exists. Besides, implementing an artificial external ear test fixture of complex geometry is a challenging task by itself. Power balances are used to explain how the ear canal walls and the medial earplug contribute to observed occlusion effect magnitudes at varying occlusion depths between 1 kHz and 2 kHz. Furthermore, power balance

computations and transfer function level predictions are used to investigate Tonndorf's (1966) and Huizing's (1960) qualitative occlusion effect models. Detailed discussions of the obtained results along with conclusions can be found in CHAPTER 2 where the journal article is presented. In section 6.2 a synthesis of the main results is presented along with a critical discussion of the scientific and technological contributions as well as the limitations. Future recommendations are drawn based on current limitations.

0.3.3 Chapter 3: Implementation of a simplified axisymmetric external ear model of average geometry

0.3.3.1 Chapter contents

In chapter 3 the second research article entitled “Prediction of the bone conduction occlusion effect using a two-dimensional axi-symmetric finite element model” is presented. The purpose of this article is to specify an axi-symmetric linear elasto-acoustic finite element model of the human external ear for simulation of the bone conduction occlusion effect using geometrical and material properties found in the literature. This purpose is coherent with specific research objective 2 (see section 0.2.2).

0.3.3.2 Overview of the methodology used to implement the axisymmetric external ear model

Geometrical model layout: The implementation of the axisymmetric external ear geometry is carried out using commercially available finite element software. The ear canal and earplug (occluded model) are represented as straight cylinders of identical cross sectional areas. The ear canal walls are formed by a cylindrical skin layer. Half of the ear canal walls are surrounded by a cylindrical cartilage layer and the remaining half are surrounded by a bone layer. The anatomical landmarks of the pinna are disregarded mainly to ensure axisymmetry. To model the ear canal entrance region (zone where ear canal merges into the cavum conchae) the cartilage layer and the ear canal walls are continued outwards in such

way that they protrude with respect to the ear canal entrance. The dimensions of the external ear domains (e.g. ear canal length, ear canal radius, ear canal wall thickness, entrance protrusion, bone and cartilage thicknesses) are obtained on the basis of an extensive literature review.

Material properties of external ear tissues and earplug: The material properties of the bony, cartilage and skin tissues are applied to the finalized axisymmetric geometry. The same isotropic, linear elastic material properties density, Young's modulus, Poisson's ration, loss factor) that are used for the 3D model of complex geometry (see section 0.3.2.2) are applied to each of the tissue domains of the simplified axisymmetric model. One silicone earplug type is considered with this model. The earplug model is assumed to adapt to the shape of the ear canal without deforming its walls. Both a perfect seal and leaks of small diameters are investigated. When earplug leaks are included, airborne noise is presented in phase to study their combined effect. Note that the hypothesis of the airborne noise and the structure borne excitation being in phase is a simplification which is presently inevitable as it is very challenging to measure the phase difference. The isotropic linear elastic material properties of the silicone earplug are taken from the literature. The speed of sound and density of air at 20°C are applied to the ear canal cavity.

Boundary and load conditions: Four different boundary and load conditions are considered with the axisymmetric model. All configurations use fixed, free, impedance and boundary load conditions. The four configurations mainly differ in terms of how much of the bone and/or cartilage tissue is stimulated by the boundary load. The power spectral density of a bone transducer's RMS-force (obtained trough calibration with an artificial mastoid) serves as boundary load. The latter is always introduced normally and uniformly. This loading condition represents an idealization of the real stress vectors which act on the human tissues and which likely vary in terms of amplitude and direction along the tissue boundaries. Additionally, the RMS-force measured at the artificial mastoid (which would also apply to the mastoid process of a human subject) likely changes in terms of magnitude once it reaches the external ear. Applying this RMS-force directly to the circumference of the axisymmetric

external ear thus introduces another simplification which seems presently inevitable do to a lack of more accurate data. The open ear canal entrance is expressed using the radiation impedance of a baffled flat circular piston and the eardrum is modeled as a locally reacting specific acoustical impedance boundary condition. Between solid domains continuity of stress vectors and displacements is assumed. Interfaces between a solid domain and ear canal cavity are expressed through fluid-structure coupling.

Model meshing: The axisymmetric model is meshed using quadratic triangular elements for all domains. Like for the 3D model, the mesh uses a convergence criterion of four elements per wavelength at 3 kHz. The meshed axisymmetric model is solved for the sound pressure at the eardrum. The mean square pressure and the RMS-input force are related to approximate the transfer function levels. Occluded and open ear transfer function levels are subtracted to calculate the earplug occlusion effect.

Data analysis: Obtained numerical results are used to investigate the contribution of the four boundary and load condition configurations to the predicted transfer function levels and occlusion effects. Each boundary and load configuration is examined (i) with structure borne excitation only (no earplug leaks, no airborne noise), (ii) with simultaneous structure borne and airborne excitation (noise added incoherently), (iii) with simultaneous structure and airborne stimulation (added incoherently) and presence of small earplug leaks (considering viscous and thermal effects). Detailed discussions of the obtained results along with conclusions can be found in chapter 3 where the journal article is presented. In section 6.3 a synthesis of the main results is presented along with a critical discussion of the scientific and technological contributions as well as the limitations. Future recommendations are drawn based on current limitations.

0.3.4 Chapter 4: Numerical investigation of the earplug type dependent occlusion effect using an axisymmetric external ear model

0.3.4.1 Chapter contents

In chapter 4 the third research article "An axi-symmetric finite element model to study the earplug contribution to the bone conduction occlusion effect" is presented. The purpose of this article is to investigate the occlusion effect as a function of earplug type (two earplugs considered) for similar earplug insertion depths using an axi-symmetric linear elasto-acoustic finite element model of the human external ear of average geometry. This purpose is coherent with specific research objective 3 of section 0.2.2.

0.3.4.2 Overview of the methodology used to investigate the earplug type dependent occlusion effect

Geometrical model layout: The outlined investigation is carried out using a commercially available finite element software tool. The geometrical layout of the axisymmetric external ear model used for this analysis is the same as the one described in section 0.3.3.2. The geometrical dimensions (e.g. ear canal length) used, however, slightly differ for the present model. This difference originates from the circumstance that two independent test subject groups are used to measure the occlusion effects of a silicone and a foam earplug (both at similar insertion depths). Thus, it is attempted to adjust the external ear model's dimensions in such way that one axisymmetric model can be used to predict the earplug type dependent occlusion effects of both experimental test groups with sufficient precision. To identify the most suited geometrical dimensions of the model a sensitivity analysis is implemented within naturally occurring limits. All upper and lower limits used during this sensitivity analysis are obtained on the basis of an extensive literature review. A two level factorial design is implemented using a commercially available statistics software tool. The obtained run sheet is imported into the abovementioned finite element tool and a parametric sweep with respect to the model dimensions is carried out numerically. Subsequently the obtained numerical transfer function levels are re-imported into the statistics software for multi-response optimization which allows identification of one configuration that provides satisfying occlusion effect predictions for both earplug test groups.

Material properties of external ear tissues and earplug: The material properties of the bony, cartilage and skin tissues are applied to the axisymmetric geometry. The same isotropic, linear elastic material properties (density, Young's modulus, Poisson's ration, loss factor) that are used for model described in section 0.3.2.2 are applied. A silicone and a foam earplug are used during this investigation. The earplug models are assumed to adapt to the shape of the ear canal without deforming its walls. Only leak free occlusion is considered here. The isotropic linear elastic material properties of the silicone and foam earplugs are taken from the literature and correspond to those used in the 3D external ear model of complex geometry. The speed of sound and density of air at 20°C are applied to the ear canal cavity.

Boundary and load conditions: One boundary and load condition is considered. It uses a free condition on the area around the ear canal entrance. Fixed boundary conditions are applied to the horizontal ear canal entrance region as well as the medial vertical model boundaries. The power spectral density of the bone transducer's RMS-force described in section 0.3.3.2 serves as boundary load which is introduced normally and uniformly on the horizontal boundaries of the cartilage and bony model boundaries. All limitations with respect to the excitation that are outlined in section 0.3.3.2 also apply to this model. The ear canal entrance is expressed via a locally reacting impedance condition that corresponds to the radiation impedance of a flat baffled piston. The eardrum is modeled via a locally reacting specific acoustical impedance boundary condition. Between solid domains continuity of stress vectors and displacements is assumed. Interfaces between a solid domain and ear canal cavity are expressed through fluid-structure coupling

Model meshing: Meshing of the model is carried out following the same procedure described in section 0.3.3.2. The meshed model is solved for the sound pressure at the eardrum. The sound pressures of the open and occluded external ear models are used to calculate the earplug occlusion effect. Other acoustical indicators such as the acoustical normal particle velocity as well as the stress and strain tensors are retrieved to calculate exchanged and dissipated powers inside the ear canal cavity and the earplug models.

Data analysis: Obtained numerical results are used to validate the axisymmetric model of this study against experimental occlusion effect data obtained in two independent healthy reference groups that are tested using comparable earplug types and similar earplug insertion depths as the numerical model. Furthermore, the axisymmetric numerical model is validated against two existing gold standard electro-acoustical occlusion effect models. Numerical earplug dependent occlusion effect differences are investigated using power balance computations in the ear canal cavity and the earplug domains. The contribution of the earplug to the occlusion effect is investigated at very shallow and medium insertion depths. Detailed discussions of the obtained results along with conclusions can be found in chapter 4 where the journal article is presented. In section 6.4 a synthesis of the main results is presented along with a critical discussion of the scientific and technological contributions as well as the limitations. Future recommendations are drawn based on current limitations.

0.3.5 Chapter 5: Implementation of an artificial external ear test fixture to measure the occlusion effect

0.3.5.1 Chapter contents

Chapter 5 is an additional chapter which is entitled “Implementation of a simplified, artificial external ear test fixture for measurement of the earplug induced auditory occlusion effect”. The purpose of this chapter is to propose a preliminary axisymmetric external ear test fixture to experimentally measure the earplug occlusion effect. This purpose is coherent with specific research objective 4 of section 0.2.2. The work presented in chapter 5 has not yet been the subject of a fourth journal submission. Obtained results have, however, been published in the conference proceedings (peer reviewed) of the International Congress on Acoustics 2013 (Brummund et al., 2013). Additionally, obtained results were orally presented to the scientific community at the aforementioned conference. It is anticipated to complete and submit a journal article in the near future during a continuation of the present research project.

0.3.5.2 Overview of the methodology used to implement artificial occlusion effect test fixture

Geometrical test fixture layout: The geometrical layout of the artificial external ear test fixture resembles that of the axisymmetric finite element model presented in section 0.3.3.2. The test fixture comprises the ear canal and its surrounding skin cartilage and bone tissues. Minor adjustments of the model's dimensions (e.g. ear canal radius) are carried out in order to facilitate using standardized measurement equipment such as the IEC-60711 coupler to measure the sound pressure level at the artificial eardrum. Additionally, the suggested prototype exhibits a constant ear canal wall thickness mainly to facilitate the silicone casting described further below. In a future version an ear canal wall of variable thickness could definitely be implemented.

Implementation of the artificial external ear: Solid rigid polyurethane foam is used to mimic the bony external ear tissue. The cartilage and skin tissues are made up of two types of silicones. The cartilage silicone exhibits a shore A hardness of 55 whereas the softer skin silicone exhibits a shore A hardness of 30. A steel slip-on flange houses the artificial external ear. Using a slip-on flange offers two advantages. First, its central bore hole, into which the external ear components are pressed and casted, imposes a clamped boundary condition. Second, when other artificial external ear configurations (e.g. materials, geometries) are to be tested the slip-on flange can be easily removed from the test fixture installation. During the fabrication process of the artificial external ear, part of the rigid polyurethane foam cylinder (bone) is press fitted into the central bore hole of the slip on flange. Prior to press fitting the bone cylinder is drilled open concentrically. This opening leaves room for the ear canal walls and the ear canal cavity. A first ABS pin (same diameter as hole in bone cylinder) is inserted into the bore hole of the bone cylinder. A batch of the cartilage silicone is casted into the bone-flange subassembly to mimic the cartilage tissue. After completion of the curing process the ABS insert is removed. The bony and cartilage portions that back the ear canal are complete. Next a second ABS pin is inserted into the cartilage-bone-flange subassembly. The insert's diameter corresponds to the ear canal diameter thus leaving enough room to cast

the ear canal walls and the skin at the ear canal entrance region using the second silicone. Upon completion of the curing process the second insert is removed and the artificial external ear geometry is complete.

Stimulation of the artificial external ear: To mechanically stimulate the artificial ear a small mechanical dynamic shaker is used. Its mechanical excitation is transferred to the bony part of the artificial ear with the help of a custom made coupling cage. The anterior part of the cage is press-fitted to the bony portion of the artificial external ear. The main advantage of this setup is that it allows axisymmetric stimulation of the artificial external ear. In the future this axisymmetry will be beneficial for the implementation of a test fixture equivalent numerical FE-model, which together with the test fixture could be used to further study the occlusion effect. One disadvantage of the stimulation mechanism includes the circumstance that a shear excitation is generated whereas bone transducers that are frequently used for occlusion effect measurements in human subject cause a compressional stimulation of, for instance, the mastoid process. Bone transducers and several other compressional excitation methods cannot be used in the present test fixture due to the axisymmetry requirement as well as other limitations which are discussion in detail in section 5.2.3.

Data analysis: The described occlusion effect test fixture is used to investigate the sound transmission pathways to ensure that the sound pressure level reading at the artificial eardrum originates from structure borne excitation. The open and occluded sound pressure readings are subtracted to calculate the earplug occlusion effect obtained for a foam earplug at medium insertion depth. A linearity analysis of the occlusion effect with respect to the stimulation magnitude is carried out. More detailed discussions of the obtained results along with conclusions can be found in chapter 5.

0.3.6 Chapter 6: Synthesis and conclusion

In chapter 6 a synthesis of the main results obtained during this work in the context of the general and specific research objectives is provided. The scientific and technological

contributions, the limitations and future recommendations for each article are presented. A brief general conclusion is presented.

CHAPTER 1

LITERATURE REVIEW

This chapter provides a comprehensive review on hearing by bone conduction and the occlusion effect. In section 1.1 a brief overview of the anatomy of the human ear is presented. Section 1.2 introduces the notion of hearing by bone conduction which is crucial in order for the occlusion effect to occur. In Section 1.3 a detailed description of the outer-ear transmission pathway is provided. This bone conduction pathway causes the occlusion effect. Additionally, qualitative occlusion effects models, experimental occlusion effect information and a review of existing occlusion effect models are presented in section 1.3.

1.1 Brief overview of the anatomy of the human ear

The following section aims at providing a simplified overview of the ear components that are crucial to bone conduction hearing and the occlusion effect. To facilitate reading this section an overview of the anatomical orientations is provided in Figure 1.1 and Figure 1.2 illustrates a schematic overview of the human ear.

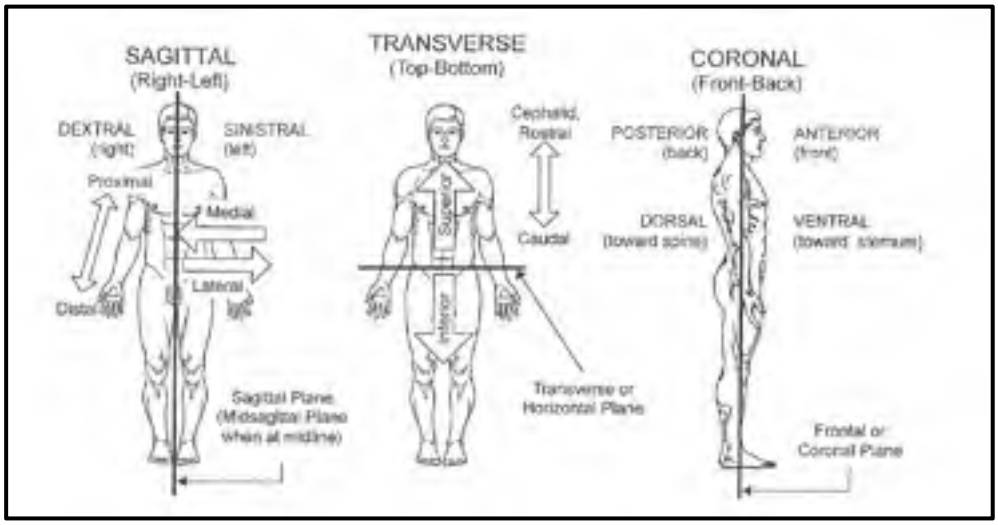

Figure 1.1: Overview of the anatomical orientations used throughout this chapter. The original image can be found in (Gelfand, 2010)

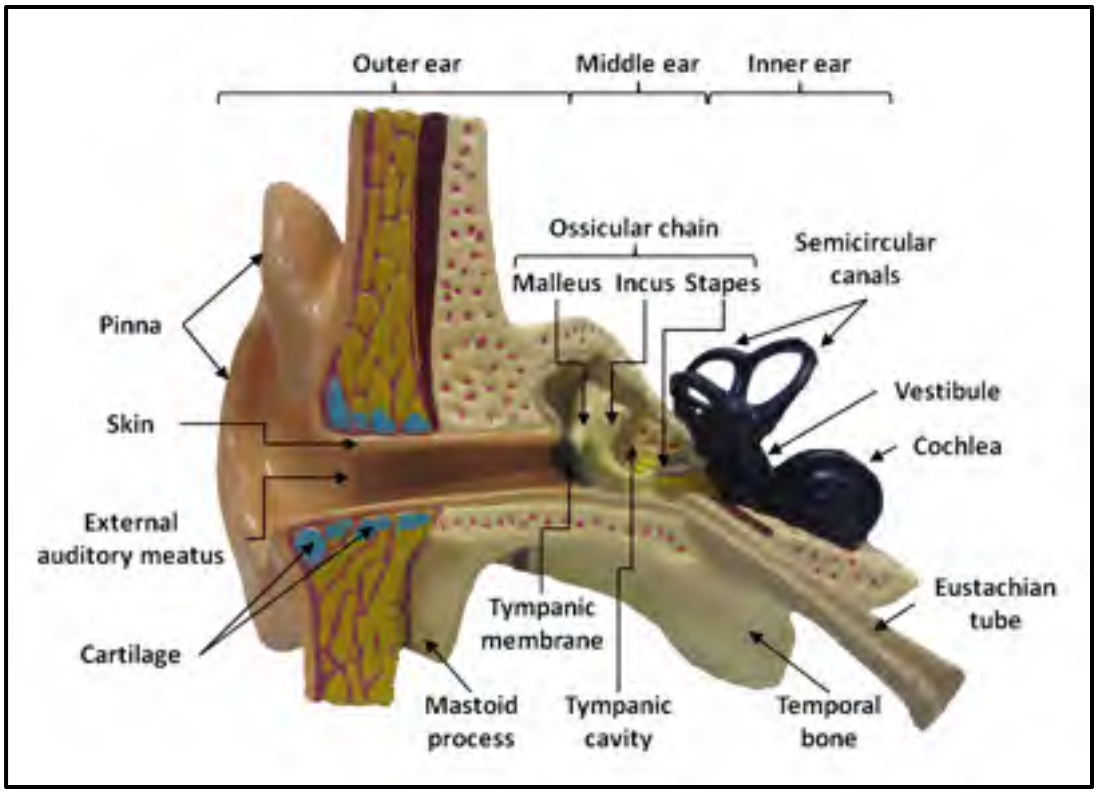

Figure 1.2: Cross sectional schematic view of the human outer, middle and inner ear

The human ear can be divided into three major sections including the outer ear, the middle ear and the inner ear. The *outer ear* spans the region from the pinna to the tympanic membrane. The tympanic membrane separates the outer from the middle ear. The *middle ear* comprises the tympanic membrane, the tympanic cavity, the ossicular chain as well as the Eustachian tube. The stapes footplate of the ossicular chain is in contact with oval window (not indicated in Figure 1.2). The oval window marks the beginning of the inner ear. The *inner ear* is composed of sensory organs pertaining to both hearing and balance (e.g. semicircular canal). The hearing organs of the inner ear, beyond the oval window, include the vestibule and the cochlea (Gelfand, 2010). For BC hearing in general all three ear sections are of importance. The relative contribution of each ear component to BC hearing, however, is frequency dependent. For the occlusion effect, on the other hand, only the outer ear, especially the ear canal, is of highest importance (see section 1.3).

The ear canal (external auditory meatus) is of S-shaped geometry and exhibits a length of about 25 to 30 mm. It extends from the concha of the pinna to tympanic membrane. Due to the inclined orientation of the tympanic membrane the ear canal is shorter on its superior-posterior limit than on its inferior-anterior limit (Lucente et al., 1995).

Approximately half[1] of the ear canal as well as the entire middle and inner ears is embedded in the temporal bone. Anatomically landmarks of particular interest for the present study include the *tympanic*, *petrous* and *mastoid* portions of the temporal bone. The tympanic portion forms the floor as well as the anterior and inferoposterior walls of the medial ear canal. The petrous portion houses the cochlea as well as the semicircular canals. Lastly, the mastoid portion which is located on the posterior part of the temporal bone projects into the mastoid process on its caudal limit. The latter is often used for bone conduction stimulation (Gelfand, 2010).

The lateral cartilaginous half of the ear canal is not embedded in the temporal bone. It is connected to the periosteum of the bony canal through firm connective tissue (Lucente et al., 1995). The cartilage of the pinna represents the external expansion of the cartilaginous auditory meatus. It is connected to the skull through three muscles and ligaments (Lucente et al., 1995).

The pinna and the external auditory meatus (both cartilaginous and bony portions) are covered with skin tissue which is closely attached to the perichondrium of the cartilage as well as the periosteum of the bony meatus. In the cartilaginous meatus the skin tissue measures about 0.5 to 1 mm in thickness and comprises an epidermis, dermis and a subcutaneous layer. In the bony meatus the skin tissue is about 0.2 mm thin and it is continuous with the external layer of the tympanic membrane (Lucente et al., 1995).

---

[1] In the literature different cartilage to bone tissue volume ratios around the ear canal have been reported. While some authors report tissue ratios of 0.5:0.5 other studies mention ratio of 0.33:0.66 (e.g. Alvord and Farmer, 1997; Lucente et al., 1995; Oliveira and Hoeker, 2003; Stenfelt et al., 2003).

1.2 Bone conduction sound transmission pathways

A sound source can either be located outside (external source) or inside the human body (internal source). Examples for external sources include environmental noise such as traffic, television, radio etc.. Internal sound sources include physiological noises such as one's own heart beat and one's own voice. The sound emitted from a source can get transmitted to the inner ear principally via two conduction routes. The first route is the so called air conduction (AC) which conducts the sound through the outer and middle ear components to the cochlea (Gelfand, 2010). The second route is the so called bone conduction (BC) during which the bones of the skull transmit the sound to the cochlear (Gelfand, 2010). Due to the important impedance mismatch between the skull and its surrounding air, bone conduction requires a strong airborne stimulus (about 40 dB to 50 dB above open ear air conduction threshold (Berger et al., 2003). Alternatively, bone transducers that are directly applied to the skull are frequently used during audiological measurements to stimulate the skull. Békésy (1932) and Lowy (1942) provide experimental proof that air conduction and bone conduction result in the same travelling waves in the cochlea (Gelfand, 2010).

For the present study the bone conduction route is of highest importance. Hearing by bone conduction has been the subject of many research studies over the past decades. The results of these studies have helped to distinguish different BC pathways and to better understand how these pathways act together across different frequency bands to create a hearing sensation. Comprehensive reviews on BC sound can, for example, be found in Tonndorf (1972) and Stenfelt and Goode (2005). To date, four pathways have been identified to explain hearing by bone conduction (Figure 1.3). While additional theories have been suggested in the past, only these pathways seem coherent with both clinical and experimental observations. They include:

1) Sound radiation into the ear canal (outer ear path);
2) Inertial movement of the middle ear ossicles (Bàràny, 1938);
3) Inertial movement of the cochlea fluid;

4) Elastic compression of the cochlea walls.

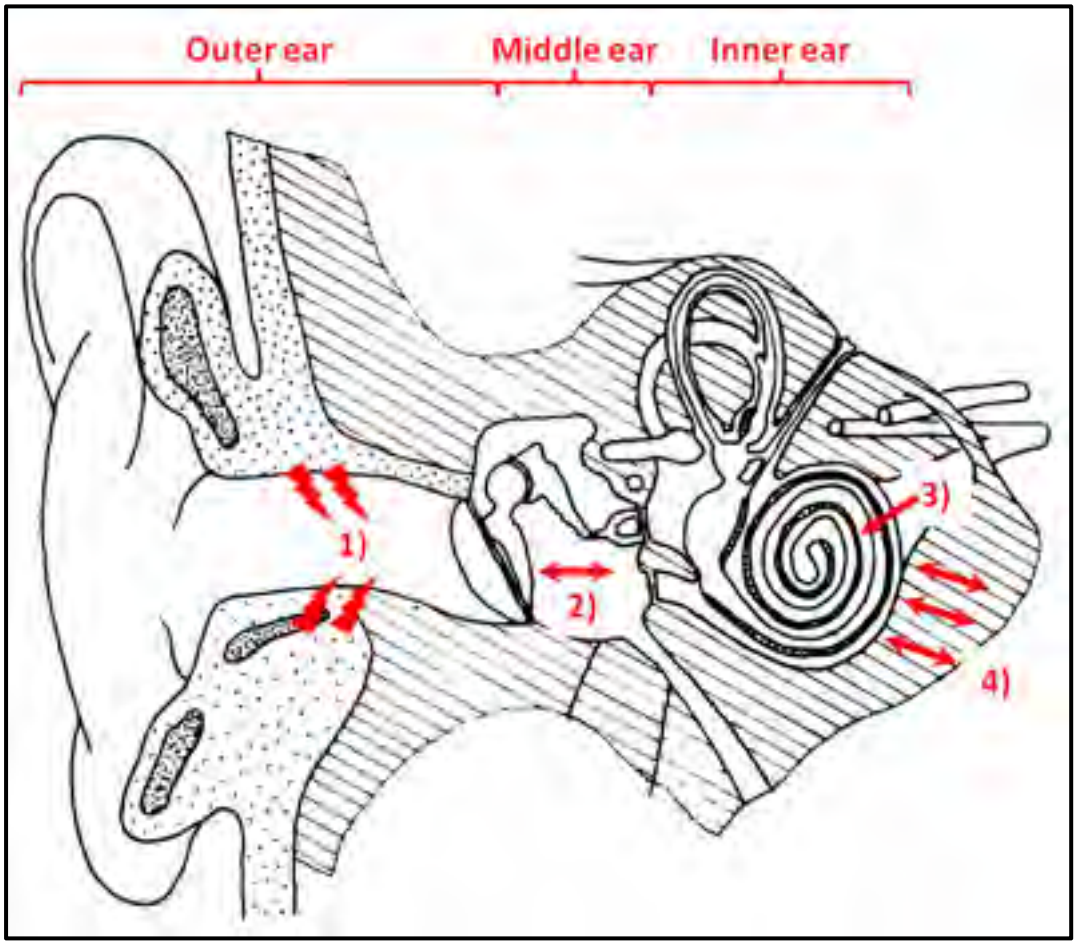

Figure 1.3: Schematic illustration of the BC conduction pathways. 1) sound radiation into the ear canal, 2) middle ear ossicle inertia, 3) inertial movement of cochlea fluids, 4) elastic compression of cochlea walls

The relative contribution of each of BC pathways to bone conduction hearing has been subject to discussion over the past decades (e.g. Allen and Fernandez, 1960; Wever and Lawrence, 1954; Kirikae, 1959).

To explain the occlusion effect the sound radiation into the ear canal is of highest importance (Khanna et al., 1976; Stenfelt et al., 2003). Thus, it is going to be discussed in more detail in the following paragraph.

1.3 The outer-ear transmission path and occlusion effect

The outer ear path (corresponds to sound radiation into the ear canal) is intriguing, because its overall contribution to BC hearing can be increased through occlusion of the external auditory meatus.

In the open canal, the outer ear path is, to date, not considered to contribute markedly to BC hearing (Stenfelt and Goode, 2005). Nevertheless, opposing data exist. For instance, on the basis of AC/BC cancellation experiments, Khanna et al. (1976) demonstrated that the external ear component dominates hearing by BC for frequencies up to 0.8 kHz in the open ear. More recently, however, Stenfelt et al. (2003) demonstrated, using laser Doppler vibrometry on human cadaver heads, that the outer ear path may not contribute to BC hearing in the open ear. Several explanations for these contradicting results obtained for the open ear can be found elsewhere (Stenfelt et al., 2003; Stenfelt and Goode, 2005).

When the *ear canal is occluded* through for instance a HPD the external ear path dominates BC hearing at the low frequencies. Khanna et al. (1976) state that the external ear component dominates BC hearing in the occluded ear canal for frequencies up to 2 kHz while Stenfelt et al. (2003) report that the outer ear path dominates BC hearing for frequencies < 1 kHz in the occluded ear.

The increased contribution of the occluded ear canal to BC hearing (as compared to the open ear canal) is referred to as occlusion effect. The occlusion effect manifests itself in two manners. *Objectively*, an increase (with respect to the open ear canal) in the sound pressure level can be measured in the occluded ear canal at the low frequencies. This increased sound pressure is measureable for frequencies < 2 kHz. *Subjectively*, the test subject (e.g. HPD wearer) will experience a hollow sounding low frequency amplification of his/her own voice and an amplification of physiological noises (e.g. respiration, blood circulation) (Berger and Kerivan, 1983). In addition to using one's voice, bone transducer stimulation devices can be used as sources to generate the sound pressure level in the ear canal.

As was outlined in the introduction the occlusion effect plays an important role in HPD underutilization and professional hearing loss. It contributes to reducing the auditory comfort of a HPD and can negatively affect communications in the workplace environment.

1.3.1 Qualitative explanation of the occlusion effect

Understanding the mechanisms that govern the occlusion effect has been a challenging problem in bone conduction theory (Tonndorf, 1972). To date, two models have been established to qualitatively explain the occlusion effect at low- and mid-frequencies. These models are going to be explained in the following paragraphs.

1.3.1.1 The high pass filter effect model (low frequencies)

Tonndorf (1966) suggested that the sound which gets radiated from the ear canal walls into the *open* ear canal cavity will split up and follow two pathways. Some of the radiated sound will get transmitted to the inner ear via the tympanic membrane and the ossicular chain. The remaining sound that does not get transmitted to the inner ear will get radiated outward at the ear canal opening. The sound radiation is more efficient at the low frequencies and thus the open ear canal behaves in a similar manner as a high pass filter element due to the unoccluded ear canal entrance.

Occlusion of the ear canal entrance removes the high pass filter like behavior of the ear canal. In part, this is due to the circumstance that the low frequency sound radiation becomes impossible with leak free occlusion. More importantly, however, the input impedance of the ear canal, as seen by the ear canal walls, increases upon occlusion (Tonndorf, 1966; Schroeter and Poesselt, 1986; Stenfelt and Reinfeldt, 2007; Brummund et al., 2014). Consequently, more sound power gets radiated into the ear canal and the sound pressure level increases at the low frequencies.

1.3.1.2 The ear canal resonance shift model (mid frequencies)

Rinne (1855) proposed a theory according to which the occlusion effect could be explained via resonance phenomena in the ear canal (e.g Tonndorf (1972)). Later, this theory was scientifically elaborated by Huizing (1960). It states that the open ear canal corresponds to a closed tube and as such it exhibits a quarter wavelength resonance frequency.

Occlusion of the ear canal through a HPD alters the acoustic properties of the ear canal and shifts the ear canal resonance frequency. The quarter wavelength resonance becomes a half wavelength resonance upon occlusion. The frequency shift obtained for the open and occluded ear canals directly affects the occlusion effect calculation in the mid frequency range where the open ear canal resonance occurs.

1.3.2 Experimental analysis of the occlusion effect

In addition to the qualitative models of Huizing (1960) and Tonndorf (1966), numerous experimental studies have been conducted to quantitatively explain the occlusion effect. The following paragraphs are meant to provide a summarizing overview of these findings.

1.3.2.1 Subjective and objective occlusion effect

The occlusion effect is usually measured either subjectively or objectively (e.g. Békésy, 1941; Watson and Gales, 1943; Huizing, 1960; Goldstein and Hayes, 1965; Tonndorf, 1966; Berger and Kerivan, 1983; Stenfelt and Reinfeldt, 2007; Reinfeldt et al., 2007). The subjective occlusion effect describes a positive shift (for frequencies < 2 kHz) in the test subject's *hearing threshold* upon occlusion of the external auditory meatus. The objective occlusion effect, on the other hand, describes an increase (for frequencies < 2 kHz) in *sound pressure level* inside the test subject's ear canal upon occlusion. The latter method requires the insertion of miniature microphones inside ear canal (commonly in close proximity to the tympanic membrane) to measure the ear canal sound pressure levels. Huizing (1960)

observed that the objective occlusion effect is some 10 to 15 dB larger in magnitude as compared to the subjective occlusion effect and points out that both occlusion effect measures are not correlated in any particular manner. More recently, similar observations were made by Stenfelt and Reinfeldt (2007), Reinfeldt et al. (2007) and Reinfeldt et al. (2013). The authors trace the observed phenomenon back to different BC pathways in the open ear. While the ear canal sound pressure level (*objective occlusion effect*) relies mainly on sound radiation from the ear canal walls, the open ear threshold (*subjective occlusion effect*) is influenced by other BC pathways (see section 1.2). It is also important to point out that the obtained differences in objective and subjective occlusion effects are influenced by the stimulation position (e.g. ipsilateral mastoid versus forehead stimulation) (e.g. Stenfeldt and Reinfeldt, 2007; Reinfeldt et al., 2013).

1.3.2.2 The contribution of the external ear components to the sound pressure in the occluded ear

In the occluded ear, the outer ear path dominates BC hearing (Khanna et al., 1976; Stenfelt and Goode, 2005). The increased sound pressure level inside the occluded ear canal could potentially originate from (i) airborne noise masking at the ear canal entrance (Pohlmann, 1930; Guild, 1936), (ii) sound outflow ("Schallabflusztheorie") from the cochlea into the ear canal via the middle ear and tympanic membrane (Mach, 1863) and/or (iii) sound radiation at the ear canal walls (Khanna et al., 1976; Stenfelt et al., 2003).

The airborne noise masking theory (i) of the occlusion effect supposes that ambient AC noise would increase the open ear BC threshold. Thus, the occlusion effect (decrease of the BC threshold) would result from an elimination of this masking influence of the AC noise. The masking theory originates from the observation that the threshold occlusion effect decreases when measured in an anechoic chamber (Huizing (1960) citing Pohlman (1930)) and justifies the necessity to conduct occlusion effect measurements under low ambient noise levels. Nevertheless, the masking effect of ambient airborne noise is insufficient to fully explain the

occlusion effect. For instance, Tonndorf (1966) demonstrated occlusion effects in cats using cochlear microphones that are not sensitive to airborne noise masking (Tonndorf, 1972).

The outflow theory (ii) hypothesizes that the occlusion effect originates from BC sound transmission to the cochlear. The cochlear would inversely leak sound energy into the ear canal via the ossicles and tympanic membrane. This sound pressure level would increase upon occlusion. First direct evidence against the outflow theory was presented by Tonndorf (1966) who showed that removing the tympanic membrane did not alter the occlusion effect (Tonndorf, 1972). Similarly, additional research studies (e.g. a comprehensive review can be found in Stenfelt and Goode (2005)) provided further evidence against this theory

As was previously mentioned, sound radiation from the ear canal walls (iii) is presently considered to be at the origin of the occlusion effect. Originally this explanation was proposed by von Békésy (1941) who argued that the vibration of the ear canal wall is caused by a relative motion between the skull and the mandible whose condyles are in contact with the cartilaginous portion of the ear canal. Thus, BC sound would result in a periodical excitation of the ear canal wall.

While a relative motion between the skull and the mandible can be measured experimentally (e.g. Franke et al., 1952) this out of phase motion cannot fully explain the sound radiation from the ear canal walls. For example, Allen and Fernandez (1960) demonstrated occlusion effects in two patients that were unilaterally missing the mandibular condyle (Tonndorf, 1972). More recently, Stenfelt et al. (2003) provided further evidence that the contribution of the mandible to the ear canal sound radiation might be of secondary importance through complete removal of the lower jaw in human cadaver heads.

Additionally, Stenfelt et al. (2003) also provided experimental evidence that, at the low frequencies, the sound transmission through the cartilage tissue of the external ear is the most important contributor to ear canal sound pressure for bone conduction. Upon removal of the cartilage and soft tissue Stenfelt et al. (2003) observed occlusion effect magnitudes of 5-10

dB for frequencies up to 2 kHz. The latter observation indicates a small contribution of the bony ear canal to the ear canal sound pressure level.

1.3.2.3 The contribution of the occlusion volume to the occlusion effect magnitude

In addition to varying as a function of frequency, the occlusion effect magnitude is also influenced by the occlusion volume. As can be seen from Figure 1.4 different trends can be observed for different HPD types.

For instance, the occlusion effect becomes minimal when earmuffs of large earcup volume are used and it (occlusion effect) increases as the earcup volume decreases. Following Tonndorf's (1966) model this observation can be explained as follows at the low frequencies. For large earcup volumes the acoustical properties of the occluded ear canal are fairly similar to the acoustical properties of the open ear canal (e.g. mass-like behaviour of the open ear canal entrance). Thus, the occluded ear canal entrance continues to radiate some of the sound power exchanged at the ear canal walls outwards. More importantly, however, the input impedance seen by the occluded ear canal walls also remains fairly constant for large earcup volumes thus the same amount (as compared to the open ear canal) of acoustical power should get radiated from the ear canal walls into the occluded ear canal cavity. Huizing's (1960) model can be used to explain the inverse relationship between earcup volume and occlusion effect magnitude at the mid-frequencies. Because the acoustical properties of the occluded ear canal remain similar to the properties of the open ear canal for large earcup volumes the quarter wavelength resonance does not become a half wavelength resonance upon occlusion. Lastly, as the earcup volume decreases the acoustical properties of the open and occluded ear canal cavities become increasingly different. On the one hand this causes more power to be radiated from the ear canal walls into the occluded ear canal (low frequency occlusion effect) and on the other hand the half wavelength resonance becomes a quarter wavelength resonance (mid-frequency occlusion effect).

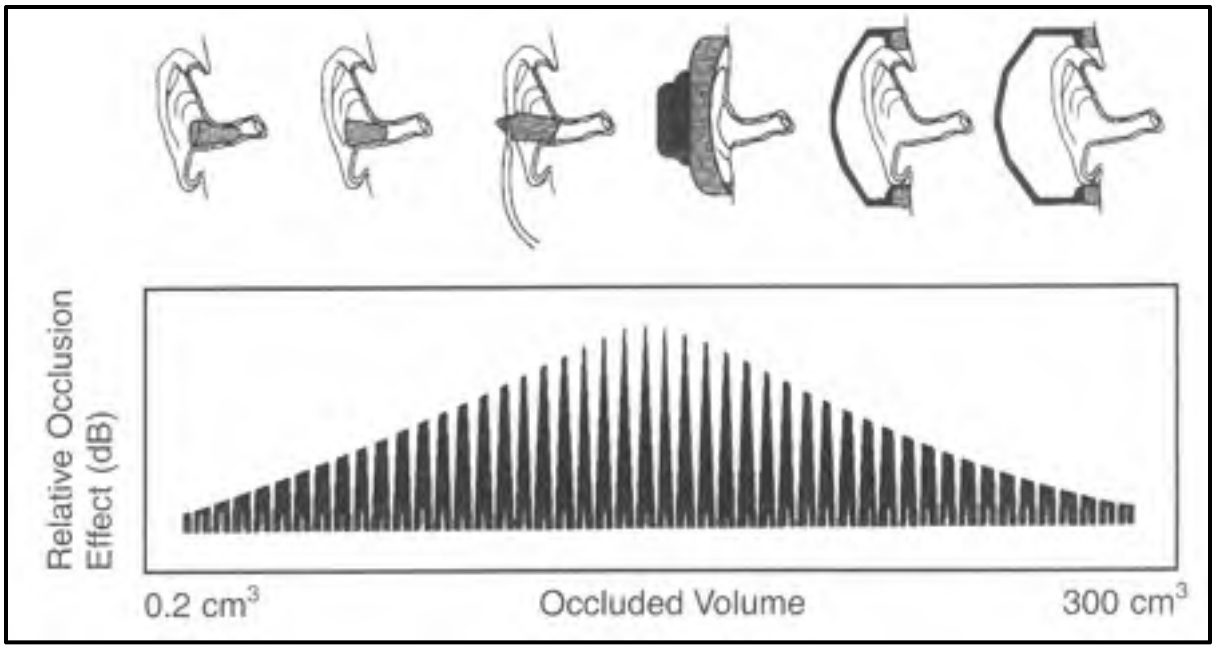

Figure 1.4: Schematic illustration of the relationship between the occlusion volume and the occlusion effect magnitude for earplug and earmuff HPDs (Taken from Berger et al. (2003))

For earplugs an opposite behaviour (as compared to earmuffs) can be observed. Here, the occlusion effect magnitude is maximal for large occluded volumes (e.g. shallow earplug insertion) and the occlusion effect magnitude decreases proportional to the occlusion volume (e.g. Békésy, 1941). The latter observation has been attributed to several mechanisms. Firstly, increasing the occlusion depth causes a reduction of the radiating surface area of the ear canal walls (Tonndorf, 1972). Secondly, increasing the insertion depth causes a gradual immobilization of the tympanic membrane (Tonndorf, 1972). Thirdly, the stiffer bony tissue radiates less energy into the ear canal as compared to the soft tissue, greater insertion depth causes less power to be radiated from the bone backed ear canal wall (Berger and Kerivan, 1983). Fourthly, deeper earplug insertion gradually stiffens the unoccluded ear canal walls (Berger and Kerivan, 1983).

1.3.2.4 The contribution of the stimulation position to the occlusion effect magnitude

The occlusion effect is often examined with the help of bone transducers that are securely attached to either the test subject's mastoid process (e.g. ipsilateral) or forehead. Nevertheless, other stimulation positions (e.g. incisors Békésy (1941)) and methods such as one's own voice exist. In a recent study, Reinfeldt et al. (2013) re-examined occlusion effect magnitudes as a function of stimulation position. Reinfeldt et al. (2013) report lower occlusion effect magnitudes for ipsilateral mastoid excitation as compared to forehead and contra lateral bone transducer placement. This observation was made for both objective and subjective occlusion effect measurements. While the former was statistically significantly smaller at 0.125 kHz the latter exhibited statistically significantly smaller occlusion effect magnitudes up to 0.5 kHz. Similar results were published by Klodd and Edgerton (1977) as well as Stenfelt and Reinfeldt (2007). The former, however, only examined threshold occlusion effect differences as a function of stimulation position.

The origin of the objective occlusion effect differences as a function of stimulation position is not fully understood. The subjective occlusion differences as a function of transducer placement for frequencies < 1 kHz have been attributed to the directivity of the excitation placement that would cause different vibration patterns of the outer, middle and inner ear (Stenfelt and Reinfeldt, 2007). Additionally, Reinfeldt et al. (2013) suggest a possible contribution of the soft tissue of the external ear (ipsilateral mastoid stimulation) to explain threshold occlusion effect differences at 0.125 kHz.

1.3.2.5 The contribution of the earplug to the occlusion effect

Previously, it was shown that the earplug insertion depth contributes to the occlusion effect magnitude. Research on whether the geometrical and material properties of the earplug contribute to the occlusion effect magnitude at a given occlusion depth, however, is sparse. To the best of our knowledge only one experimental study (Lee, 2011) has examined the effect the earplug type on the occlusion effect magnitude. Among others, Lee (2011)

statistically compared a foam earplug and a medical balloon type earplug at two insertion depths (2 mm and 11 mm) in one third octave band centered at 0.5 kHz. The results obtained by Lee (2011) showed statistically significant effects of the earplug type on the occlusion effect at 11 mm insertion. At 2 mm insertion, the author observed only a small, statistically insignificant, difference between both earplug types. While the foam earplug caused less occlusion effect at 11 mm insertion it led to slightly more occlusion effect at 2 mm insertion as compared to the medical balloon type earplug.

1.3.3 Occlusion effect modelling

A few studies have proposed occlusion effect models. In the following, three relevant models are reviewed. To date, all existing occlusion effect models rely on lumped elements (electrical equivalent circuits). Hence, they are limited to one dimensional sound wave propagation and only allow for analyzing acoustic pressure and volume velocity along the ear canal axis.

1.3.3.1 The Schroeter and Poesselt (1986) model

Schroeter and Poesselt (1986) published a comprehensive study on modelling of the external human ear. Among others, the authors propose an occlusion effect model to predict earplug and earmuff occlusion effects (both subjective and objective). For the present study, only the *earplug occlusion effect* is considered.

Schroeter and Poesselt (1986) approximate the ear canal using an acoustic transmission line of constant diameter (7.5 mm) and 18 mm length (see Figure 1.5).

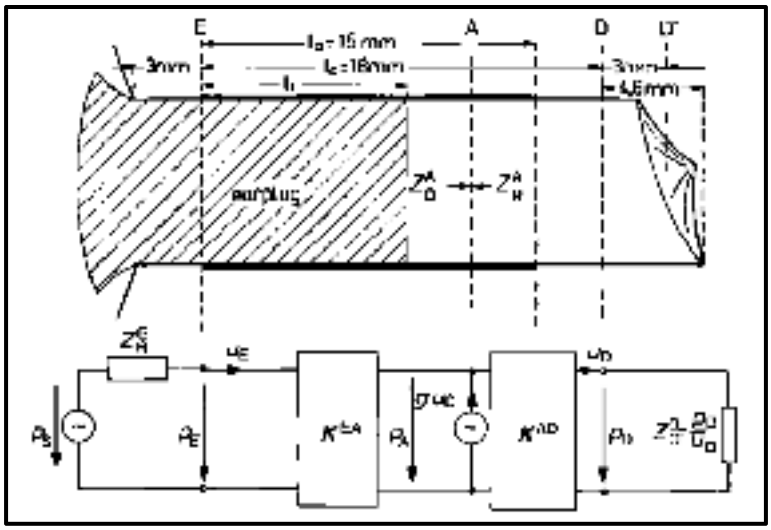

Figure 1.5: Layout of Schroeter and Poesselt's (1986) ear canal model. The original image can be found in (Schroeter and Poesselt, 1986)

To model the *earplug occlusion effect* Schroeter and Poesselt (1986) combine their external ear model with a modified version of Shaw and Stinson's (1981) middle ear model (lumped element model). The modification consisted in adding a volume velocity source to model the middle ear inertia (Bàràny, 1938). Additionally, the authors added a second volume velocity point source in the cartilaginous portion (15 mm length) of the ear canal to model the sound radiation from the ear canal walls into the ear canal cavity. The gain of the latter source is adjustable to the earplug insertion depth. The bony portion of the ear canal was not excited. The volume velocities of the middle ear and ear canal were calculated with the help of experimental sound pressure level measurements that were obtained at hearing threshold in the occluded ear canal following airborne and structure borne excitation.

The open ear canal entrance radiation impedance and the occlusion impedance of the earplug were measured experimentally using a modified acoustic test fixture.

The earplug occlusion effect model proposed by Schroeter and Poesselt (1986) agreed very well with the experimental subjective occlusion effect data of Berger and Kerivan (1983). Furthermore, the model provided occlusion effect differences (subjective versus objective

occlusion effect predictions) that exhibited similar trends as the data published by Huizing (1960).

1.3.3.2 The Stenfelt and Reinfeldt (2007) model

Stenfelt and Reinfeldt (2007) proposed a lumped element model to predict the *objective occlusion effect* at various insertion depths (earplug model) and occlusion volumes (earmuff model).

Stenfelt and Reinfeldt (2007) approximate the ear canal via four acoustic impedance blocks. Each impedance block consists of a symmetrical T-lattice containing acoustic masses, an acoustic compliance and three resistive elements. The latter introduce losses which are due to viscosity effects as well as thermal conduction and absorption.

While the model's mass and compliance elements are derived from a uniform tube, Stenfelt and Reinfeldt (2007) use average ear canal surface data (Stinson and Lawton, 1989) to calculate the mass and compliance magnitudes for each of the four impedance blocks.

Stenfelt and Reinfeldt's (2007) ear canal model exhibits a length (straight axis) of about 29 mm. The ear canal is divided into a cartilaginous (medial 15 mm of the ear canal) and a bony part. Figure 1.6 provides a schematic overview of the model.

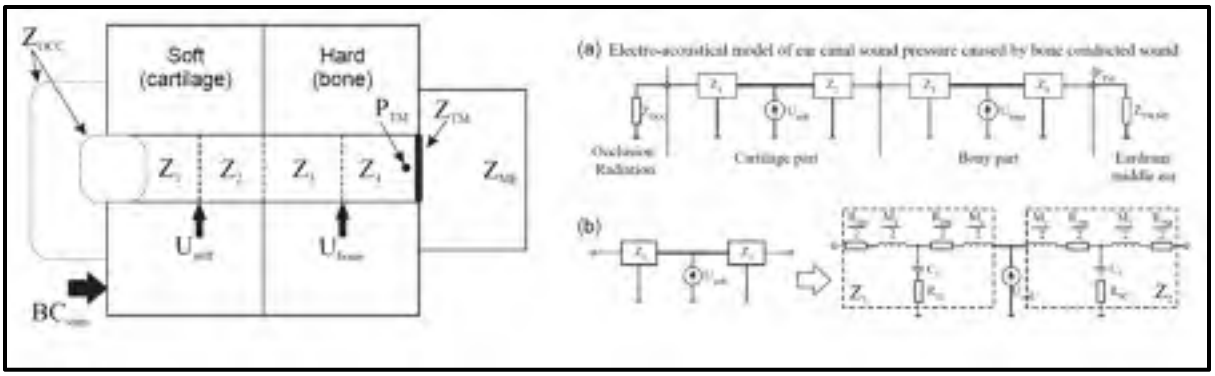

Figure 1.6: Layout of Stenfelt and Reinfeldt's (2007) occlusion effect model. Adapted version of original images (Stenfelt and Reinfeldt, 2007)

Two linked volume velocity point sources excite the ear canal model. The first source is located at the center of the cartilaginous ear canal region while the second point source is located at the center of the bony ear canal region. The bony source magnitude is set to equal a fraction of the cartilage source magnitude (1 m^3/s) through multiplication with a term that consists of two constants and the frequency. The latter constants were estimated by curve fitting experimental ear canal sound pressure data (Stenfelt et al., 2003) between 0.3 and 1.5 kHz.

The open ear canal's radiation impedance is expressed using Hudde and Engel's (1998) radiation impedance. Similarly, the eardrum impedance is expressed using Hudde and Engel's (1998) tympanic and middle ear impedance. Unlike Schroeter and Poesselt (1986) who experimentally measured the occlusion impedance of the earplug, Stenfelt and Reinfelt (2007) set the occlusion impedance to infinity.

The objective occlusion effect predictions obtained with Stenfelt and Reinfeldt's (2007) model agree fairly well with experimental objective occlusion effect measurements (median value) obtained at shallow and deep earplug insertion. For shallow insertion, Stenfelt and Reinfeldt (2007) report overestimation of around 5 dB for frequencies <1 kHz. Greater deviations are found especially at the low frequencies. Similarly, for deep insertion the

authors also report occlusion effect predictions that are about 5 dB too large for frequencies between 0.3 kHz and 0.7 kHz.

1.3.3.3 Hansen's (1998) model

Hansen (1998) published a comprehensive study on both measuring and modelling of the objective occlusion effect. Hansen (1998) mainly focused on modelling the objective occlusion effect of various hearing aid moulds subjected to excitation with one's own voice. Thus, the model was excited simultaneously through air and bone conduction.

Hansen (1998) approximates the concha (no pinna) and ear canal using acoustic transmission lines. The concha model measures 6 mm in depth and 22 mm in diameter whereas the ear canal model exhibits a length of 23.5 mm and a diameter of 7.1 mm. The ear canal is expressed as a chain of rigid cylindrical tubes and it is supposed to be equally backed by cartilage and bone tissue (ratio 50:50).

The volume velocity body source is placed 3 mm behind the medial limit of the earmould (insertion depth 7.8 mm). Its magnitude and phase are calculated using the sound pressure level that is generated in the open ear canal under simultaneous excitation with air borne and structure borne sound.

Hansen (1998) states that, in the occluded ear canal, the distribution of the volume velocity produced during speech will be influenced by the loading of a given ear canal section. Hansen (1998) distinguishes three zones: the bony wall, the free cartilage, and the cartilage loaded by the earmould. To incorporate the influence of loading at a given insertion depth on the distribution of the structure borne volume velocity, Hansen (1998) added a lumped element network to the occluded ear canal model. Figure 1.7 provides a schematic overview of Hansen's (1998) occlusion effect model.

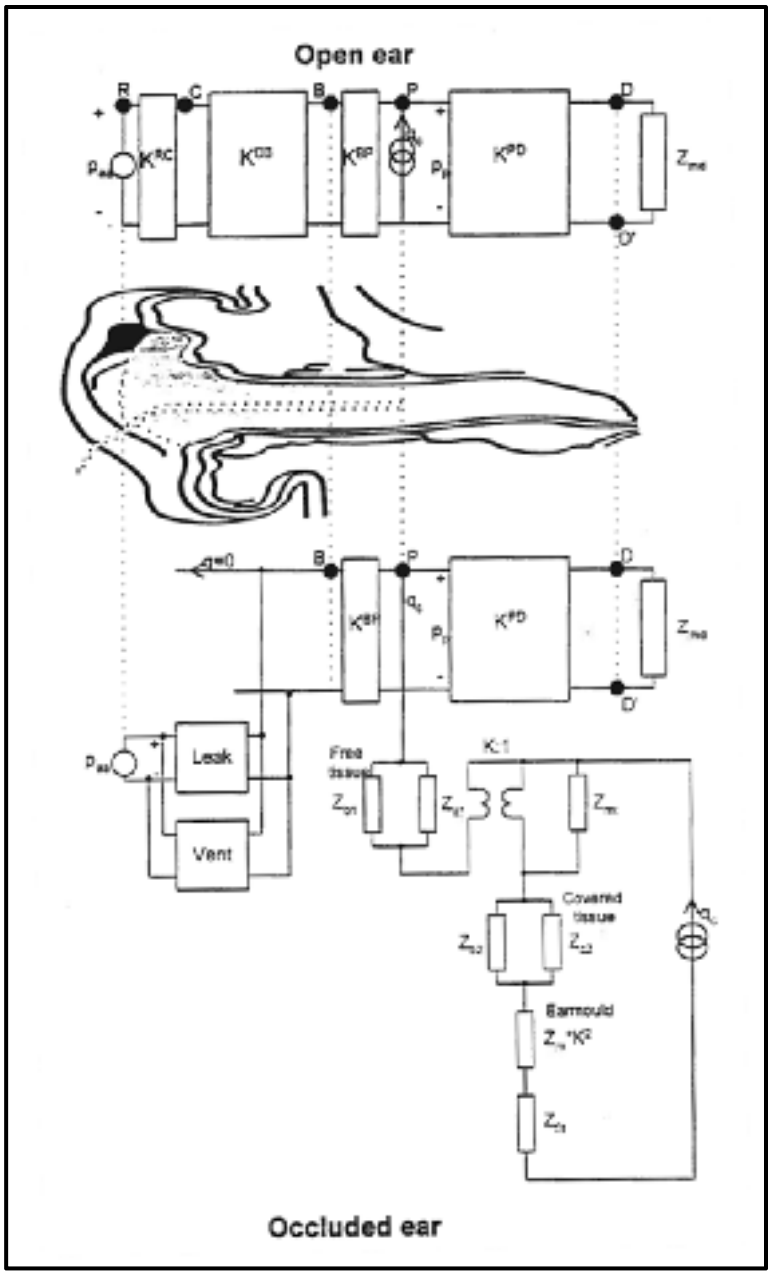

Figure 1.7: Layout of Hansen's (1998) occlusion effect model. The original image can be found in (Hansen, 1997)

In Hansen's (1998) model the open ear canal radiation impedance was expressed with the help of a rigid piston in an infinite baffle. The eardrum and middle impedance was expressed using the modified Zwislocki network (Shaw, 1977; Shaw and Stinson, 1981). Hansen's model (1998) assumed that the earmould can be expressed using an acoustically rigid wall.

Additionally, Hansen (1998) included natural leaks and vents in the earmould of the occluded ear model (see Figure 1.7).

Hansen (1998) reports that the occlusion effect predictions obtained with the model agree fairly well with average experimental occlusion effect data (uncertainty of about 5 dB). Furthermore, the author points out that the model has difficulty to predict individual occlusion effects. Hansen (1998) attributes this difficulty mainly to the fitting of the earmould which among other variables changes from one subject to another.

1.4 Concluding remarks

The occlusion effect originates from sound radiation into the ear canal (a pathway of hearing by bone conduction). To explain the occlusion effect at the low-and-mid frequencies two qualitative models have been established. Additionally numerous experimental studies were conducted and have helped to quantitatively study and understand the occlusion effect. While the contributions of factors such as the external ear components (e.g. mandible, ear canal wall area), the stimulation position (e.g. forehead versus mastoid process) and the measurement technique (e.g. objective versus subjective measurements) are well documented in the literature, information on the role of occlusion device (e.g. earplug) is mostly limited to the effect of the occlusion volume. Only one experimental study could be found that has examined the occlusion effect as a function of earplug type in one third octave band. Nevertheless, it remains unclear how the examined earplug types contribute to the observed occlusion effect differences at medium insertion depth. Additionally, no occlusion effect model can be found in the literature that has aimed at studying the contribution of the earplug to the occlusion effect numerically. The present literature review indicates the need to further study the occlusion effect to gain insight into the manner in which the earplug contributes to the occlusion effect and to identify earplug constituents (e.g. material properties) crucial to reducing the occlusion effect magnitude. The present thesis attempts to reduce this shortcoming through the development of novel numerical models and experimental methods that are required (see section 0.2.2) in order to accomplish this objective.

CHAPTER 2

ARTICLE 1: THREE-DIMENSIONAL FINITE ELEMENT MODELING OF THE HUMAN EXTERNAL EAR: SIMULATION STUDY OF THE BONE CONDUCTION OCCLUSION EFFECT[a)]

Martin K. Brummund [b)]

Department of Mechanical Engineering, École de technologie supérieure

1100 rue Notre-Dame Ouest, Montréal, Québec, Canada, H3C 1K3

Franck Sgard

IRSST, Service de la recherche

505 Boulevard de Maisonneuve Ouest, Montréal, Québec, Canada, H3A 3C2

Yvan Petit [c)]

Department of Mechanical Engineering, École de technologie supérieure

1100 rue Notre-Dame Ouest, Montréal, Québec, Canada, H3C 1K3

Frédéric Laville

Department of Mechanical Engineering, École de technologie supérieure

1100 rue Notre-Dame Ouest, Montréal, Québec, Canada, H3C 1K3

Published in:

The Journal of the Acoustical Society of America, 2014, vol. 135, no. 3, pp. 1433-1444

[a)] Portions of this work were presented in "Development of a 3D finite element model of the human external ear for simulation of the auditory occlusion effect". Proceedings of Acoustics Week in Canada, Québec City, Canada, September 2011, pp 94-95.

[b)] Electronic address: martin.brummund.1@ens.etsmtl.ca

[c)] Also at Research Centre, Hôpital du Sacré-Cœur de Montréal, 5400 Boulevard Gouin Ouest, Montréal, Québec, Canada, H4J 1C5.

2.1 Abstract

A linear 3D elasto-acoustic finite element model was used to simulate the occlusion effect following mechanical vibration at the mastoid process. The ear canal and the surrounding soft and bony tissues were reconstructed using images of a female cadaver head (Visible Human Project®). The geometrical model was coupled to a 3D earplug model and imported into COMSOL Multiphysics (COMSOL®, Sweden). The software was used to solve for the sound pressure at the eardrum. Finite element modeling of the human external ear and of the occlusion effect has several qualities that can complement existing measuring and modeling techniques. Firstly, geometrically complex structures such as the external ear can be reconstructed. Secondly, various material behavioral laws and complex loading can be accounted for. Lastly, 3D analyses of external ear substructures are possible allowing for the computation of a broad range of acoustic indicators. The model simulates consistent occlusion effects (e.g. insertion depth variability). Comparison with an experimental dataset, kindly provided by Stenfelt et al. (2007), further demonstrates the model's accuracy. Power balances were used to analyze occlusion effect differences obtained for a silicone earplug and to examine the increase in sound energy when the ear canal is occluded (e.g. high-pass filter removal).

2.2 Introduction

Hearing by bone conduction has been the subject of many research studies over the past decades (a comprehensive review can be found e.g. in Stenfelt and Goode, 2005). The results of these studies have helped to distinguish different bone conduction pathways and to better understand how these pathways act together to create a hearing sensation. One route, the outer-ear path, is intriguing as its overall contribution to bone conduction hearing can be altered through obstruction of the external auditory meatus. While this route is negligible in the open ear, it dominates bone conduction hearing at frequencies below 1 kHz in the occluded ear canal (Stenfelt et al., 2003). This phenomenon is referred to as occlusion effect (e.g. Békésy, 1941; Goldstein and Hayes, 1965; Huizing, 1960; Tonndorf, 1966). For clinical tests the occlusion effect can be of benefit (e.g. Bing test). In non-clinical contexts, such as

occupational hearing protection and hearing aid usage, however, the occlusion effect can be a comfort limiting nuisance as it alters the perception of the wearer's own voice and amplifies physiological noises (e.g. Berger et al., 2003).

To qualitatively explain the occlusion effect two models have been established. The first model was scientifically elaborated by Huizing (1960). According to this model the open and occluded ear canals correspond to open and closed pipes of varying lengths. Therefore, the occlusion effect can be attributed to a frequency shift in the resonances of the ear canal that occurs subsequent to ear canal occlusion. Huizing's model applies to the mid frequencies where the resonances of open and occluded ear canals occur. The second model was proposed by Tonndorf et al. (1966). Using an electrical analogy, Tonndorf stated that the open external ear acts as a high pass filter and that occlusion of the ear canal would remove this high pass filter effect. Tonndorf's model applies to the low frequencies where the wavelength is much larger than the ear canal length.

To quantitatively explain the occlusion effect and to understand how structure borne sound propagates in the external ear, numerous experimental studies have been conducted. Cited publications include both threshold and ear canal sound pressure occlusion effects. The present work only simulates the ear canal sound pressure occlusion effect that, for convenience, is referred to as occlusion effect. Research findings indicate that at low frequencies the sound transmission through the cartilage tissue of the external ear is the most important contributor to ear canal sound pressure for bone conduction (Stenfelt et al., 2003). Other potential sound transmission pathways such as conduction via the condyle of the mandible (Allen and Fernandez, 1960; Brinkman et al. 1965; Stenfelt et al., 2003; Tonndorf, 1966) or the compliance of the tympanic membrane (Stenfelt et al., 2002) were demonstrated to have little to no effect on the occlusion effect. Occlusion of the external auditory meatus alters the ear canal sound pressure level. The importance of this effect depends on occlusion depth and frequency. The magnitude of the occlusion effect varies strongly between subjects (e.g. Stenfelt and Reinfeldt, 2007). Nevertheless, a general order of magnitude of about 20 to 30dB can be found in the literature (Schroeter and Poesselt, 1986; Stenfelt et al., 2003). The magnitude of the occlusion effect is influenced by the occluded volume (Berger and Kerivan, 1983; Watson and Gales, 1943) and it decreases as the occlusion device gets introduced

deeper into the ear canal. The latter has been attributed to several mechanisms including the reduction of the radiating surface of the ear canal walls (Tonndorf, 1972), a gradual immobilization of the tympanic membrane (Tonndorf, 1972), the stiffer bony tissue that might radiate less energy as compared to the soft tissue (Berger and Kerivan, 1983), and a gradual stiffening of the unoccluded ear canal walls (Berger and Kerivan, 1983). Reinfeldt et al. (2013) showed that the ear canal occlusion effect is influenced little by the excitation location (ipsilateral mastoid, forehead, contralateral mastoid) except at 0.125 kHz where ipsilateral mastoid stimulation causes the smallest occlusion effect and at 0.5 kHz where forehead stimulation results in the smallest occlusion effect. Lastly, a study by Lee (2011) suggests that the earplug type becomes important once the occlusion is deep into the ear canal.

A few studies have attempted to model the occlusion effect (e.g. Schroeter and Poesselt, 1986; Stenfelt and Reinfeldt, 2007; Tonndorf, 1966; Hansen, 1998). All models that could be found in the literature are based on lumped elements. Obtained modeling results generally tend to be in good agreement with experimental results. Nevertheless, electrical circuit models are accompanied by several difficulties. Firstly, these models are limited to one dimensional sound wave propagation and therefore only allow for analyzing acoustic pressure and volume velocity along the ear canal axis. Secondly, the link between the model parameters and the physical properties is less clear than in a finite element model. Thirdly, it is very challenging to use lumped models to represent the tissue domains surrounding the ear canal and to define an adequate excitation for the soft and bone-backed ear canal regions.

The purpose of the present study is to propose a 3D linear elasto-acoustic finite element model of the ear canal and surrounding structures to simulate the occlusion effect. No record of using the finite element method to simulate the occlusion effect was found in the literature. This approach is valuable because it allows for an accurate reproduction of the geometrical complexity of the ear canal and its surrounding bony, cartilaginous, and skin tissues. At the same time, various material behavioral laws as well as complex loadings and boundary conditions can be accounted for. Furthermore, this modeling approach makes it possible to analyze sound propagation through three dimensional substructures of the external ear, such

as the ear canal walls, and to compute acoustic indicators such as exchanged and dissipated powers which are used to further understand the occlusion effect mechanisms. Nevertheless, it must also be noted that the numerical model is still a simplification of reality. These simplifications are outlined in the following paragraphs. All computations were carried out using COMSOL Multiphysics (COMSOL®, Sweden).

In section 2.3, details on the methodology to build the finite element model are provided. Afterwards, the numerical occlusion effect simulations are presented, discussed and compared to experimental literature findings. Finally, the conclusion section summarizes the main findings of this work.

2.3 Methodology

2.3.1 Geometrical reconstruction of the external ear

One hundred thirty-five anatomical images (transverse plane, 24 bits of color, voxel dimensions: 0.33mm x 0.33mm x 0.33mm) of a female cadaver head were used to reconstruct the complex external ear geometry. All images were retrieved from the Visible Human Project® database of the US National Library of Medicine. Image segmentation was performed using a contour detection tool to separate bony structures from cartilage and skin tissues on each image (Slice-O-Matic, ©Tomovision, QC, Canada). The outer surface of each structure was automatically created from the contours using the marching cube algorithm (Lorensen and Cline, 1987). The resulting 3D geometry was then imported into a computer-assisted design tool (CATIA v5, ©Dassault Systemes, France) for post-processing of the resulting 3D solid model. The entire ear canal (from entrance to tympanic membrane) was considered. While the location of the eardrum could be identified in the images the membrane itself could not be reconstructed as higher image resolution would be required. Instead, surfaces of the ear canal domain that adjoin to the eardrum were selected. The ossicular chain and middle ear cavity were not reconstructed, but are accounted for in Shaw and Stinson's (1981) lumped middle ear model (see also section 2.3.4).

Color images permit distinguishing skin and cartilaginous tissues that cover the ear canal walls, and the entrance region of the external ear (pinna region). Both tissue domains were modeled to account for the complex boundaries that exist between tissue domains and at the tissue-ear canal interface. While it would be more realistic to model the entire head including all soft tissues and bones this task seems presently impractical. Among other factors, this is due to the limited knowledge of material properties and the extreme complexity of the resulting model that would require excessive computational resources. As a first approximation, the pinna, skin, and cartilage tissue domains of the present model were cut to a cylindrical shape (diameter = 27mm) using CATIA v5 (©Dassault Systemes, France) to limit the circumference of the soft tissues. The diameter of 27mm was judged optimal following visual inspection of the color images. Furthermore, the diameter is sufficiently large to allow for the entire ear canal to be backed by both skin and cartilage tissue and sufficiently small to avoid modeling of neighboring anatomical regions of the head (e.g. cranial cavity). Other diameters were not considered in the present model.

The temporal bone was modeled completely, with the exception of the upper half of the squamous part and the styloid process to reduce model complexity. It is assumed here that the styloid process has very little influence on the ear canal sound pressure, because the wavelengths of the compressive (approximately 0.99m at 3kHz) and shear waves (approximately 0.53m at 3kHz) in the temporal bone model are much longer than the length of the styloid process (approximately 0.02m) up to 3 kHz. Therefore, the styloid process was excluded from the geometrical model. Furthermore, the mandibular condyles were excluded from the model. Hollow spaces and passages such as the middle ear cavity, the carotid canal and the internal acoustic meatus were filled with bony tissue in CATIA v5 (©Dassault Systemes, France) to reduce model complexity. A hole was made anterior-inferiorly to the internal acoustic meatus to gain access to the tympanic membrane (the hole was not filled with any material or fluid). At a later point in time the numerical model might serve as template for a physical prototype in which the hole could house a coupler to measure the response at the tympanic membrane. Furthermore, the hole could serve at a later point in time to include the model of a middle ear. For the present study it was confirmed that the presence/absence of the hole does not alter the simulation results markedly (largest occlusion

effect difference equals 2.4dB at 1.6 kHz, the mean occlusion effect difference equals 0.7dB). In the unoccluded model the surface area of the ear canal entrance equals 40.5 mm^2. Its location was chosen manually with the intention of avoiding excessively large entrance surface areas that would occur in the concha bowl. The final ear canal volume equals 803.4 mm^3. The ear canal length was calculated along a curved axis that connects the centers of gravity of thirty parallel (with respect to the ear canal entrance) ear canal cross-sections (spacing 1mm). The obtained ear canal has a length of 33.7 mm. The surface area of the conical tympanic membrane equals 55.7 mm^2. The average thickness of the skin tissue covering the lateral part (cartilage backed) of the ear canal equals about 2 mm. The skin tissue that covers the medial part (bone backed) of the ear canal exhibits an average thickness of about 1.5 mm. Figure 2.1 illustrates the resulting external ear geometry.

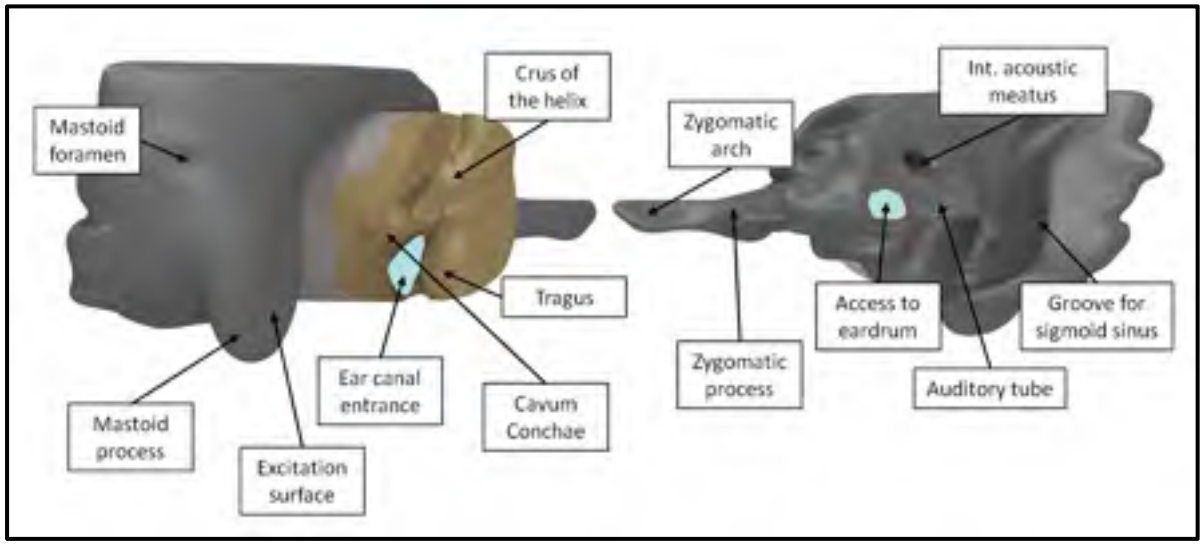

Figure 2.1: Final external ear geometry as obtained after 3D reconstruction using images of a human cadaver head (The Visible Human Project®). Left: Posterior-lateral view of temporal bone, cartilage tissue, and skin tissue at the ear canal entrance. Right: Medial view of the temporal bone geometry. Anatomical landmarks are indicated with arrows

2.3.2 Material properties of external ear tissues

The tissue domains included in the finite element model exhibit non-linear, anisotropic, viscoelastic material behavior and vary as a function of age and gender. Under the

assumption of small tissue deformation, however, it is reasonable to assume linear stress-strain behavior (e.g. Fung, 1993). Isotropic elastic material characteristics are hypothesized here because the literature exhibits a current lack of data in terms of anisotropy, homogeneity, pre-stress state and frequency dependence for the biological tissues considered here. The characterization of anisotropic, viscoelastic biological material parameters is in itself a challenge. Further research is necessary to accurately estimate the error introduced by these simplifications. The implementation of a linear elasto-acoustic model of the external ear requires Young's moduli, densities, Poisson's ratios, and loss factors of all solid domains to be known. For the present work, the material properties of modeled tissue domains were drawn from the literature, when possible. Material properties that could not directly be drawn from the literature were approximated using similar tissues in close anatomical proximity. For instance, human septum cartilage was used to model the auricular cartilage. It is assumed here that similar mechanical loading acts upon both cartilages. Hence, due to functional adaptation to mechanical stress, both cartilages might exhibit similar mechanical properties. This claim, however, can presently not be proven with quantitative data. Table 2.1 provides a summarizing overview of all material properties used. To model the air filled ear canal cavity a density of 1.20 kg/m^3 and a speed of sound of 343.20 m/s were used.

Table 2.1: Material properties of tissue domains included in the finite element model. For the air filled ear canal cavity ρ_{air} = 1.20 kg/m^3 and c_{air} = 343.20 m/s were used

		Density [kg/m^3]	Young's mod. [MPa]	Poisson's ratio	Loss factor
Bone	Value	1714	11316	0.3	0.01
	Anatomical site	Mean over skull	Mean over temporal bone	Mean over temporal bone	Assumed
	Reference	Delille et al. (2007)	Delille et al. (2007)	Peterson and Dechow (2003)	n/a
Cartilage	Value	1080	7.2	0.26	0.05
	Anatomical site	Human articular	Human septum	Human septum	Assumed
	Reference	Cox and Peacock (1979)	Grellmann et al. (2006)	Grellmann et al. (2006)	n/a
Skin	Value	1100	0.5	0.4	0.1
	Anatomical site	Average skin density	Breast skin model	Assumed	Assumed
	Reference	Duck (1990)	(Sarvazyan et al., 1995)	n/a	n/a

2.3.3 Geometrical and material properties of earplug model

To predict the occlusion effect, it is necessary to couple the open 3D external ear model to an earplug model. It was hypothesized in this work that earplug insertion would only deform the earplug and that the ear canal would keep its original shape. The earplug's circumferential surface is therefore assumed to perfectly adapt to the ear canal walls (no leaking, no slipping).

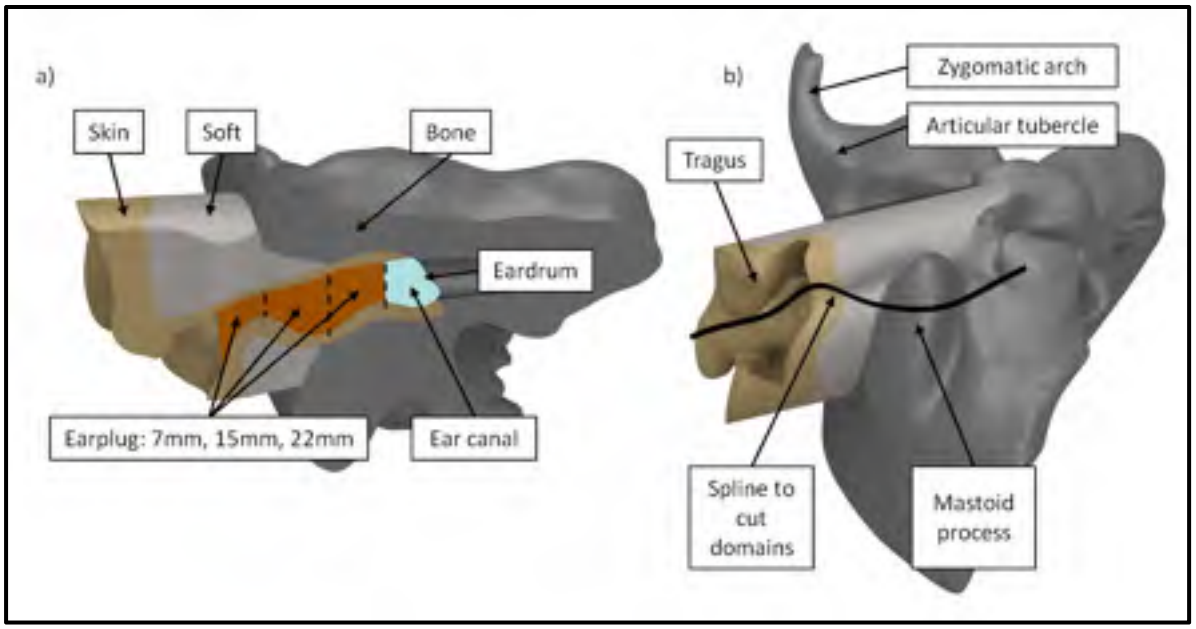

Figure 2.2: a) Anterior sectional view of occluded external ear model including all modeled tissue domains. The different occlusion depths are indicated using dashed lines. b) Inferior view of the complete model. Due to the bends in the ear canal the domains were cut along a spline curve instead of a plane. This also explains the narrow entrance region in a)

This is a reasonable hypothesis for custom made molded earplugs or soft foam earplugs. The earplug model was used to occlude the external ear model at the three different occlusion depths (Figure 2.2). Shallow occlusion corresponds to an earplug insertion of 7mm into the ear canal. Medium occlusion equals a 15 mm insertion and deep occlusion corresponds to an occlusion depth of 22 mm. The total earplug model length along a curved central axis is 25.3 mm (total earplug length along a straight central axis = 22 mm). During all occlusion conditions the lateral earplug surface is kept flush with the ear canal entrance. This choice is due to the circumstance that the circumferential earplug surface that is in contact with the ear canal walls as well as the medial earplug surface that is in contact with the ear canal cavity are the parts of the earplug that are of highest importance for the present study. Hence, to reduce model complexity protruding earplug pieces (into concha bowl) that would occur during shallow and medium occlusion were excluded from the model. Two earplug materials were tested and both earplugs were assumed to exhibit isotropic linear elastic material behavior. Firstly, a silicone earplug model of known material properties (Sgard et al., 2010)

was tested at all three occlusion depths. Secondly, a foam earplug model was tested at one occlusion depth (15mm). In this paper, the foam earplug's circumferential surface was assumed to be uniformly compressed at a radial strain of 18% relative to its initial radius. The foam material properties were taken from the literature (James, 2006). James (2006) also determined the material properties for a foam earplug under 6%, and 30% radial strain. Here, these material properties are disregarded, because the results were similar to the material properties obtained at18% radial strain. Table 2.2 summarizes the material properties of the tested earplugs.

Table 2.2: Material properties of earplugs tested with the finite element model

	Density [kg/m^3]	Young's mod. [MPa]	Poisson's ratio	Loss factor	Reference
Silicone plug	1050	0.85	0.48	0.1	(Franck Sgard et al., 2010)
Foam plug 18% radial strain	146	0.42	0.1	0.1 (assumed)	(James, 2006)

2.3.4 Boundary conditions and excitation

To account for the interactions between the modeled tissue domains and their environment several boundary conditions were defined. The skin tissue and the earplug surface (occluded models) in contact with the surrounding external air are modeled using a free boundary condition. The circumferential cartilage and skin tissue boundaries are fixed. All boundaries of the temporal bone model are free. The chosen boundary conditions provided the best results in terms of both the transfer function level inside the ear canal and the occlusion effect. It is noteworthy that switching from fixed to free boundary conditions on the bone domain strongly increases the amplitude (about 20dB) of the transfer function level inside the ear canal. The slope of the transfer function level graphs as well as the occlusion effects are influenced only very little when either fixed or free boundary conditions are used both on the temporal bone or the circumferential cartilage and skin tissue boundaries. At interfaces

between the different solid domains continuity of stress vectors and displacements is assumed. Interfaces between a solid domain and the fluid filled ear canal cavity (e.g. medial earplug surface – ear canal, ear canal skin – ear canal) are expressed through fluid-structure coupling. The tympanic membrane is expressed using Shaw and Stinson's model (Shaw and Stinson, 1981; Hahn, 1985). It is introduced as a locally reacting specific acoustical impedance boundary condition and applied to the ear canal surfaces that adjoin to the eardrum. While this approach reduces the model's complexity considerably, it also introduces a simplification, because the sound pressure which originates from the inertia of the middle ear ossicles is not accounted for. The latter has been shown to influence bone conduction sound in the mid-frequencies (around 1-3 kHz) (Stenfelt and Goode, 2005; Stenfelt et al., 2002). Other eardrum models were not considered in the present study. A locally reacting impedance boundary condition corresponding to the radiation impedance of a baffled flat circular piston is applied over the entrance of the open ear canal (Shaw, 1976).
The external ear system is excited mechanically via the ipsilateral mastoid process. A constant force of 1N (frequency sweep, 0.112 kHz to 2.8 kHz) is applied to a 175mm^2 flat surface area on the mastoid process of the temporal bone. A plane cut was used in CATIA v5 (©Dassault Systemes, France) to lower part of the mastoid process to obtain a flat excitation surface. The performed cut lowered the mastoid process by maximally 0.48 mm. The excitation surface size was chosen so that it corresponds to the contact area of a B-71 (©Radioear Corporation, PA, USA) bone transducer which is frequently used in clinical applications for mastoid or forehead stimulation.

2.3.5 Finite element modeling

The external ear system comprises solid and fluid domains. The solid domains are formed by the cartilage, bony, and skin tissues as well as the earplug. The ear canal represents a fluid filled cavity. To model this system, a three dimensional coupled linear elasto-acoustic model was implemented under the assumption of small material deformations. Assuming a temporal dependency $e^{j\omega t}$ for all fields, the governing equation of each solid domain is given by the classic linear elasto-dynamic equation

$$\hat{\sigma}_{ij}^{k}\left(\underline{\hat{u}}^{k}\right) + \omega^{2}\rho_{s}^{k}\hat{u}_{i}^{k} = 0 \tag{2.1}$$

where $\hat{\sigma}_{ij}^{k}$, ω, ρ_{s}^{k}, and $\hat{u}_{i}^{k}$ correspond to the stress tensor, angular frequency, density, and displacement vector of a given domain k, respectively. Structural damping is introduced as a multiplier $(1 + j\eta_{s}^{k})$ in the stiffness matrix. Here, η_{s}^{k} corresponds to the isotropic structural loss factor (see Table 2.1) of a given domain k and j is the imaginary unit. The governing equation of the fluid domain is given by the Helmholtz equation

$$\Delta\hat{p} + k^{2}\hat{p} = 0 \tag{2.2}$$

where $\hat{p}$ denotes the sound pressure and $k = {\omega}/{c}$ is the wave number. Coupling between the mechanical and acoustical domains is introduced via the continuity of stress vectors $\hat{\sigma}_{ij}^{k}n_{j} = -\hat{p}n_{i}$ and normal displacements $\frac{\partial\hat{p}}{\partial n} = \rho_{air}\,\omega^{2}\hat{u}_{i}^{k}n_{i}$ where n corresponds to the unit normal vector that points outward from a solid domain k.

The coupled elasto-acoustic finite element system was solved using COMSOL Multiphysics (COMSOL®, Sweden). All tissue domains were exported as .IGES files from CATIA v5 (©Dassault Systemes, France) and imported into COMSOL Multiphysics (COMSOL®, Sweden). The material properties and boundary conditions outlined in sections 2.3.2, 2.3.3, and 2.3.4 were applied to the model domains. Subsequently, all domains were meshed according to a criterion of four elements per wavelength at 3 kHz to ensure that the minimum element size is satisfied over the entire frequency range. Tetrahedral quadratic elements were used for all the domains. In total, the open ear model consisted of 88205 solid and 5015 acoustic elements. The occluded models consisted of 93196 solid and 4297 acoustic elements (7mm occlusion), 94861solid and 3149 acoustic elements (15mm occlusion), and 97121solid and 2089 acoustic elements (22mm occlusion). The open and occluded models were solved separately.

2.3.6 Computation of acoustical quantities

In the following, the computation of the acoustical quantities that are used in the results and discussion section are briefly summarized.

2.3.6.1 Transfer function levels and occlusion effects

First, the transfer function between the mechanical excitation and the sound pressure at the center of the tympanic membrane is calculated for the open ear model. Subsequently, the same calculation is carried out for the ear model occluded by an earplug (silicone or foam). The frequency resolution of the transfer function calculations is twenty equally spaced points in each third octave band. The third octave response is determined from the narrow band transfer functions (bands 125Hz to 2500Hz) through third octave integration which is carried out using an in-house MATLAB (MathWorks®, MA, USA) routine. Lastly, occlusion effects are calculated by subtracting the open ear transfer function level from the occluded ear transfer function levels.

2.4 Computation of exchanged powers

The time averaged acoustic powers that are exchanged at the ear canal wall – ear canal interface (open and occluded models) and at the medial earplug surface – ear canal interface (occluded models only) are calculated. Secondly, radiated average acoustic powers are computed for the ear canal entrance (open ear model only). The time averaged power exchanged at surface S_i between a solid domain and a fluid domain is calculated using (Pierce, 1991)

$$\bar{W}_{exc,i} = \frac{1}{2}\Re\left[\int_{S_i} \hat{p}\hat{v}_n^* dS\right]. \tag{2.3}$$

$\hat{p}$ corresponds to the complex acoustic pressure and $\hat{v}_n^*$ is the complex conjugate of the acoustical normal particle velocity. For the open ear case, $\hat{v}_n^*$ can be expressed in terms of the acoustic radiation impedance of the ear canal entrance $\hat{Z}_{ent}$. The exchanged power then reads

$$\bar{W}_{exc,ent} = \frac{1}{2}\Re\left[\int_{S_{ent}} \frac{|\hat{p}|^2}{\hat{Z}_{ent}^*} dS\right]. \tag{2.4}$$

2.5 Results and discussion

2.5.1 Finite element modelling of the occlusion effect

Figure 2.3 illustrates the occlusion effects that were obtained for varying earplug insertion depths. Shallow insertion (7mm) occludes the ear canal entrance region only. Medium insertion (15mm) occludes all of the ear canal's soft tissue. Deep insertion (22mm) occludes the soft and approximately half of the bony tissue.

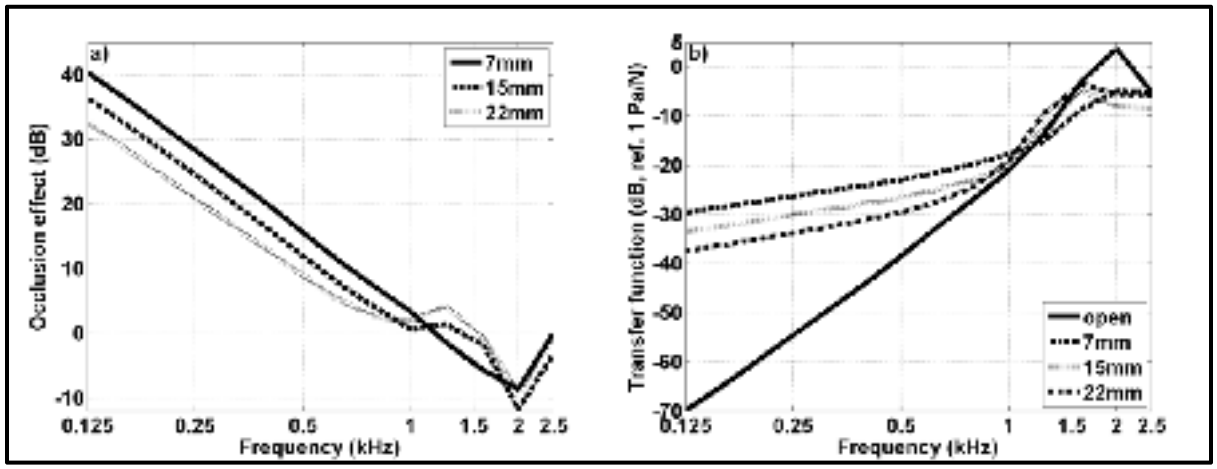

Figure 2.3: a): occlusion effect simulations obtained with 3D finite element model for silicone earplug at shallow, medium, and deep occlusions. All data are 1/3rd octave band filtered. b): corresponding transfer function levels at the center of the tympanic membrane in the open and occluded ear models for a silicone earplug. All data are 1/3rd octave band filtered

Below 1 kHz, shallow occlusion results in the largest occlusion effect. Medium and deep occlusion effects are about 3.7dB and 7dB smaller at frequencies up to 0.8 kHz. The simulated occlusion effects decrease as a function of insertion depth for frequencies < 1 kHz. The magnitude at which the occlusion effect decreases as a function of insertion depth is relatively small as compared to mean experimental data. Especially the deep occlusion condition causes an occlusion effect that seems to be quite large as compared to average experimental occlusion effect data at similar insertion depths. Figure 2.4 illustrates a power balance plot for the 22mm occlusion condition.

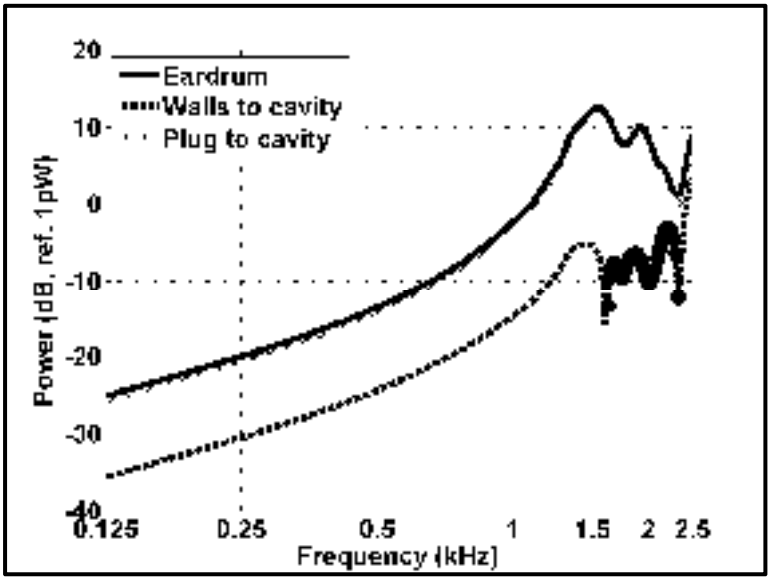

Figure 2.4: Power balance plot for the 22 mm occlusion condition (silicone earplug). The time averaged power that is dissipated at the eardrum (solid line) as well as the time averaged powers that are exchanged between the ear canal wall – ear canal (dashed line) and earplug – ear canal (dotted line) are depicted. Markers on the dashed curve indicate frequencies at which the ear canal walls receive power from the ear canal cavity (e.g. negative power flowing from the ear canal to walls). Narrow band spectra are shown

The contribution of the medial earplug surface to the total dissipated power is seen to be about ten times larger than the contribution of the ear canal walls at the low frequencies. This

suggests that the earplug contributes considerably to the observed occlusion effect at 22mm insertion. It is possible that the silicone material properties used in the model (which were determined at ambient temperature) might be inadequate to model the earplug in contact with the ear canal wall which is at body temperature. With respect to this, further research is necessary. This limitation also applies to the material properties of the modeled tissue domains. In particular, Poisson's ratio and Young's modulus of the skin tissue domain might be of importance in this respect as these properties were shown to have a relevant influence on numerical occlusion effect simulations when altered by +/- 20% (Brummund et al., 2012). Note that this sensitivity analysis has, to date, only been done with a simplified 2D model (equivalent to 3D model) due to large computational requirements for the 3D model. Nonetheless, it must also be mentioned that, although the obtained numerical occlusion effects may be large as compared with the mean experimental occlusion effect reported in the literature (Stenfelt et al., 2007), they do fit the experimental zone, albeit close to the upper boundary in the case of the deep occlusion. Above 0.9 kHz simulated occlusion effect curves cross, and between 1.1 kHz and 1.8 kHz the initial order is inverted with deep occlusion causing the largest occlusion effect. The initial occlusion effect order is reestablished for shallow and medium occlusion at frequencies above 1.8 kHz. Deep occlusion causes an occlusion effect similar to the one obtained for shallow occlusion above 1.8 kHz. Even though a direct comparison is difficult due to differences in the experimental protocol, a similar trend can be found in Berger and Kerivan (1983) who reported an inverted mean threshold occlusion effect order at 2 kHz for partially, standard and deeply inserted foam earplugs. To more closely examine the occlusion effect inversion between 1.1 and 1.8 kHz, power balances were determined for shallow, medium, and deep occlusion depths respectively.

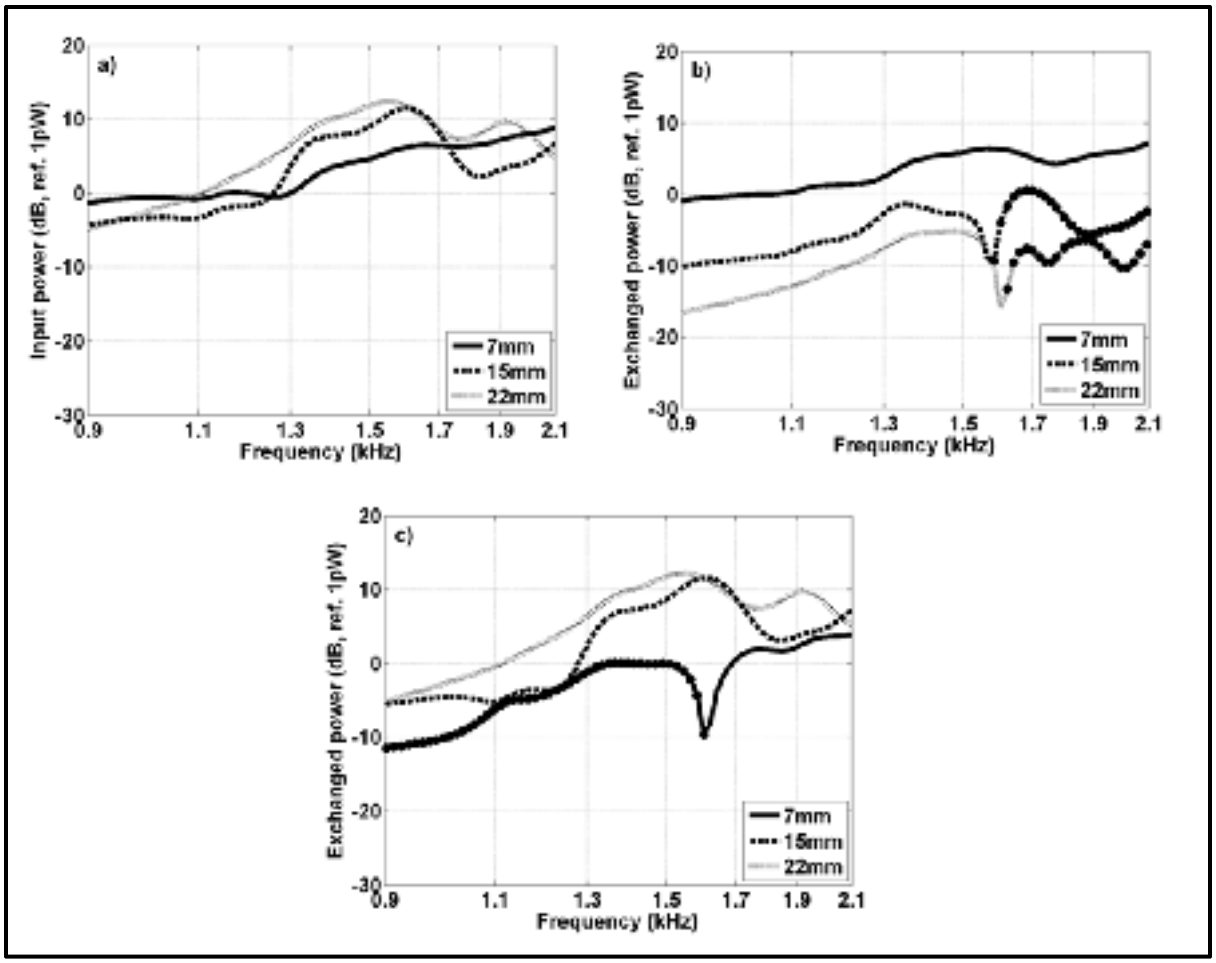

Figure 2.5: a): sum of the time averaged input power to the ear canal. b): time averaged power exchanged between the ear canal walls and the ear canal cavity. c): time averaged power exchanged between the medial earplug surface and the ear canal cavity. All time averaged powers are provided for shallow, medium, and deep occlusion using a silicone earplug between 0.9 kHz and 2.1 kHz. The markers on the graphs indicate frequencies at which the ear canal wall or earplug receives power from the ear canal cavity (e.g. negative power flowing from the ear canal to walls or earplug). Narrow band spectra are shown

Figure 2.5a) shows the input power to the ear canal cavity. It equals the sum of the power exchanged at the ear canal wall – ear canal cavity interface (Figure 2.5b)) and the power that is exchanged between the medial earplug surface and the ear canal (Figure 2.5c)). The input power increases with occlusion depth for frequencies above 1.26 kHz and below 1.6 kHz. The input power is furthermore equal to the power dissipated at the eardrum (not depicted in Figure 2.5). For shallow occlusion the input power is mainly due to the time averaged power

that is exchanged between the ear canal walls and the ear canal (see Figure 2.5b)). The inner earplug surface starts to contribute a little to the input power at frequencies above 1.7 kHz. Furthermore, the earplug receives power from the ear canal cavity at frequencies below 1.6 kHz which is indicated by the markers on the solid curve at these frequencies. In contrast, for medium and deep occlusion the input power is mainly driven by the time averaged power that is exchanged between the inner earplug surface and the ear canal cavity. The contribution of the power that is exchanged between the ear canal walls and the ear canal is small for medium occlusion and absent for deep occlusion. At these occlusion depths the medial earplug surfaces inject power at all frequencies whereas the ear canal walls receive power form the ear canal cavity at frequencies above 1.586 kHz (medium occlusion) and 1.624 kHz (deep occlusion). The latter is indicated through markers on the dashed and dotted curves.

2.5.2 Comparison of modelling results and experimental data

Figure 2.6 illustrates two occlusion effect simulations for a 15mm occlusion with a silicone and a radially constrained foam earplug. The numerical results are compared to experimental ear canal sound pressure occlusion effect data (n = 20 subjects). All experimental data were measured by Stenfelt and Reinfeldt (2007) and kindly shared for use in the present study. These experimental data were chosen because of their methodological similarity and because they are presently the only experimental data accessible (a larger experimental study is currently being run to measure more reference data (Nélisse et al., 2013), however, no data is readily available at this point in time). In their study, Stenfelt and Reinfeldt used the ipsilateral mastoid process to stimulate occlusion effects. A foam earplug was used as occlusion device. It was inserted 10 – 15mm into each subject's ear canal. For the present study, the mean ± one standard deviation as well as the individual results of Stenfelt's and Reinfeldt's experimental data were used and limited to the considered frequency range in order to create an experimental reference zone.

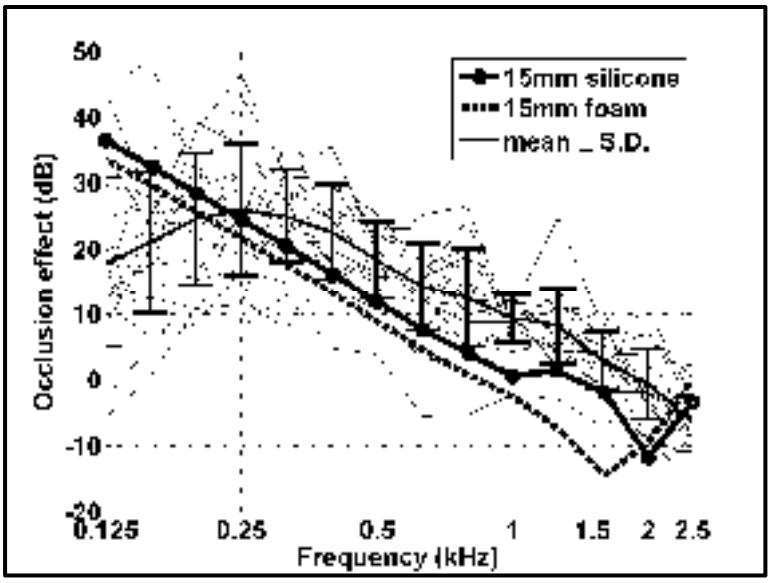

Figure 2.6: Comparison of experimental data and simulations (thick solid line with markers) for a silicone earplug and a foam earplug (thick dashed line) inserted at an occlusion depth of 15mm. The errorbar-plot (mean ± S.D) and individual occlusion effect plots (thin solid lines) define a reference zone that was measured experimentally by Stenfelt and Reinfeldt (2007). All data are 1/3rd octave band filtered

Comparison with the individual occlusion effect data (thin solid lines) shows that except between 1 – 2 kHz (foam earplug) and in the 2 kHz band (silicone earplug), simulated occlusion effects for both earplug models fall within the experimental reference zone. For frequencies <0.2 kHz the simulated occlusion effects are closer to the upper reference zone boundary. Above 0.2 kHz, the numerical occlusion effects lie closer to the lower boundary of the target zone. This way of comparing simulation and experimental data seems suitable, because the reconstructed 3D external ear geometry is unlikely to represent the average ear canal geometry (in contrast to the model of Stenfelt and Reinfeldt (2007), which was based on an average area canal geometry). Therefore, it is improbable that this specific geometry could be used to simulate an average occlusion effect. Nevertheless, such comparison is attempted. With respect to the mean occlusion effect it can been seen that at frequencies below 0.25 kHz simulated occlusion effects for both earplug types exceed the mean experimental data by 18.6dB, 11.4dB, and 3.8dB (silicone earplug) and by 15.7dB, 8.5dB,

and 1dB (foam earplug), respectively. Above 0.25 kHz the simulated occlusion effects fall below the mean experimental graph. This might be due to an uncertainty regarding the experimental occlusion depth (10 to 15mm). For the silicone earplug the simulated graph closely follows the lower boundary of the experimental standard deviation above 0.315 kHz and below 1.6 kHz with the exception of 1kHz where simulated graph is about 5dB smaller as compared to the experimental standard deviation data. The simulated graph of the foam earplug also follows the lower boundary of the experimental standard deviation for frequencies > 0.315 kHz and < 1 kHz, but the occlusion effect is smaller than the experimental standard deviation (on average 2.6dB) at these frequencies. At 1 kHz, 1.25 kHz and 1.6 kHz the foam earplug model results in an occlusion effect that is considerably smaller than the experimental standard deviation (8dB, 10dB and 13dB respectively). It is noticeable that the simulation graphs (in particular the silicone earplug data) have similar trends as the mean experimental data up to 1 kHz (foam earplug) and 2 kHz (silicone earplug). Above 1.5 kHz (foam earplug) and 2 kHz (silicone earplug) the simulation data start to increase whereas the experimental mean value continues to decrease. When compared to the silicone earplug, the foam earplug induces a smaller occlusion effect for frequencies <2 kHz and a larger occlusion effect above 2 kHz. Deviation magnitudes vary with frequency. Up to 1 kHz, the occlusion effect obtained for the foam earplug is about 3dB smaller than the occlusion effect of the silicone earplug. Between 1 kHz and 1.6 kHz the foam earplug results in a 10.6dB smaller occlusion effect. For frequencies >2 kHz the foam plug induced occlusion effect exceeds that of the silicone earplug by about 3dB.

Two factors may contribute to explain why the occlusion effect simulations exceed the experimental mean values at the lowest frequencies. Firstly, the numerical model considers complete earplug sealing and does not account for sound energy that gets lost through leaks. Leaks would reduce the transfer function levels in the occluded ear models especially at the low frequencies. Consequently, accounting for the leaks in the model could decrease the occluded transfer function level and shift the occlusion effect curves further into the experimental reference zone. Secondly, Stenfelt and Reinfeldt (2007) argued that the inter-subject variability observed at the lowest frequencies of the experimental data might also be

due to low microphone sensitivity and hence poor signal to noise ratios. Therefore, if the earplug seal was leak free then the low frequency deviation between experimental and numerical data could also be due to the in-ear microphone's noise floor.

The deviations that occur between the experimental and numerical data at the mid and higher frequencies could originate from uncertainties in terms of how well the modeled external ear geometry (ear canal length, ear canal volume etc.) compares to those of the examined healthy reference group. Large geometrical deviations between the 3D external ear model and the ears of the reference group might contribute to explain the observed results. Geometrical variability is especially important with respect to the subjects' ear canal lengths which can vary between 27 mm to 37 mm (Stinson and Lawton, 1989) and therefore cause a shift in the open ear canal resonance frequency of about 0.7 kHz (using the resonance frequency formula for a closed pipe with end correction based on an average ear canal diameter of 7.5 mm). Large length variability ultimately alters the relative occlusion depth (ratio between ear plug insertion depth and total ear canal length). While earplugs usually get inserted to a given depth (e.g. 15mm relative to the center of the tragus or the ear canal entrance) these constant insertion depths all result in different relative occlusion depths. Consequently this could cause inconsistencies regarding the radiating surface area of the unoccluded ear canal walls which could alter the time averaged power exchanged between the unoccluded ear canal walls and the ear canal. Secondly, limitations regarding the model implementation might be of importance to explain deviations between simulated and measured occlusion effect data. Among others, these limitations include: inaccuracies regarding the chosen material properties, differences that originate from the chosen boundary conditions and limitations that are due to simplification, such as modeling of the temporal bone as compared to the entire head and assuming isotropic linear elastic material behavior as compared to anisotropic, viscoelastic behavior.

2.5.3 The high-pass filter effect removal and the ear canal resonance frequency shift

Positive occlusion effects are obtained for frequencies <1.25 kHz for shallow occlusion, and <1.6 kHz for medium deep occlusion (Figure 2.3a). These results are due to a smaller transfer function level in the open ear model, as compared to the occluded ear models, at the aforementioned frequencies (Figure 2.3b). It has been suggested that the smaller open ear transfer function level originates from sound energy that is dissipated at the ear canal entrance, therefore causing the external ear to behave like a high pass filter element (Tonndorf, 1966). To examine how much power is radiated by the ear canal entrance into the environment a power balance was calculated for the open ear. Figure 2.7 illustrates the power that is flowing out through the ear canal entrance (specific acoustical radiation impedance of a baffled circular piston) relative to the input power exchanged between the ear canal walls and the ear canal. Because the power exchanged at the ear canal walls varies as a function of frequency, the normalized power flow is provided here to facilitate interpreting the data.

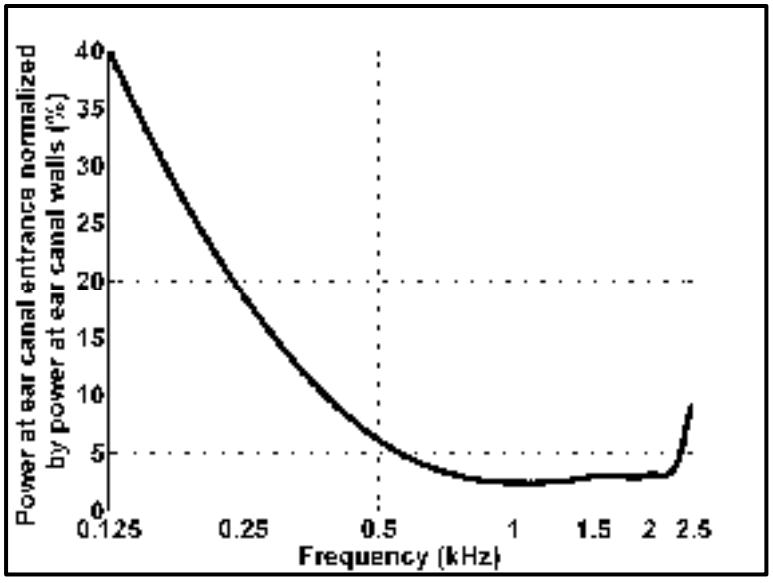

Figure 2.7: Time averaged power radiated into the environment normalized by the time averaged input power exchanged at the ear canal wall - ear canal cavity interface for the open ear model. Narrow band spectra are shown

It can be seen that the normalized power radiated outside by the ear canal entrance decreases as a function of frequency. At the lowest frequencies, about 40% of the input power that is exchanged between the ear canal walls and the ear canal is radiated into the environment. The remaining input power is absorbed by the eardrum. Around 0.5 kHz, the relative ear canal radiation reduces to about 6%. When the radiation impedance boundary condition at the ear canal entrance is removed and an earplug is inserted, the aforementioned sound radiation becomes impossible (assuming that the occlusion device is not leaking) and the transfer function level at the tympanic membrane increases, causing an occlusion effect. This phenomenon is referred to as the removal of the high pass filter effect (Tonndorf, 1966). One could think that the low frequency increase in sound pressure level at the tympanic membrane of the occluded ear might be due to excess sound power that does not get radiated into the environment. Yet, it is unclear whether the 40% sound radiation is sufficient to explain a 40 dB occlusion effect. To examine this relationship the radiation impedance boundary condition at the ear canal entrance is replaced by an infinite acoustic impedance to simulate a very shallow occlusion. Such an occlusion condition is very useful to study the removed high pass filter effect, because the ear canal wall area remains unaltered after occlusion. Therefore, if the removed high pass filter effect is due to excess sound power that does not get radiated into the environment, the amount of radiated sound power for the open ear should be equal to the difference in the sound power absorbed at the eardrums in the open and occluded cases for frequencies < 1 kHz above which the relative ear canal radiation becomes very small (Figure 2.7).

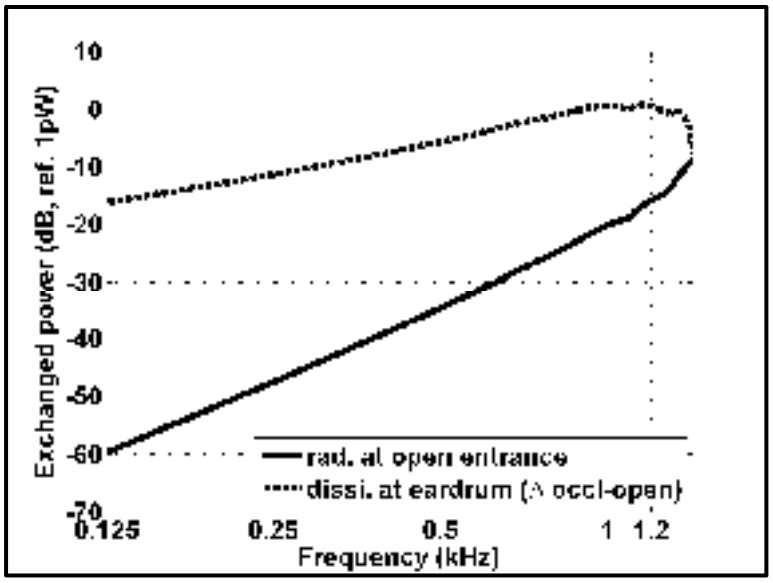

Figure 2.8: Time averaged power radiated into the environment (solid line) of the open ear. Difference in time averaged power dissipated at the eardrums of the occluded and open ear models (dashed line). Above 1.4 kHz (not depicted) the power dissipated at the open eardrum exceeds that of the occluded eardrum. Narrow band spectra are shown

From Figure 2.8 it can be seen that the 40% sound radiation at the entrance does not suffice to account for a 40dB occlusion effect. On the other hand, if the absence of sound radiation does not suffice to explain the occlusion effect, the increased sound power level at the occluded ear's eardrum can only originate from an increase in the input power at the ear canal walls, even though the excitation at the mastoid and the ear canal surface area remain constant upon occlusion. The input powers at the ear canal walls were determined for the open ear (specific acoustical radiation impedance of a circular piston) and for the occluded model (infinite impedance). Figure 2.9 confirms that the time averaged input power from the ear canal walls does increase upon occlusion for frequencies <1.3 kHz.

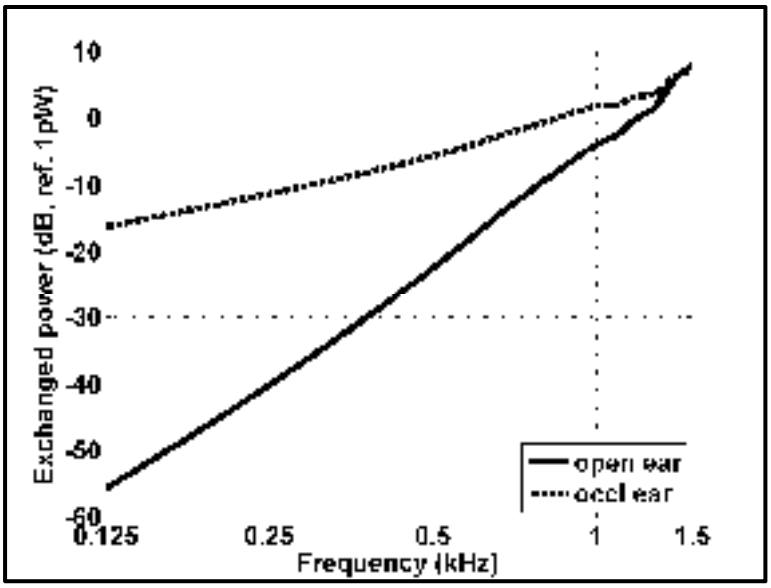

Figure 2.9: Time averaged input power from the ear canal walls for the open and occluded ear (infinite impedance at the ear canal entrance) models for frequencies below 1.5 kHz. Narrow band spectra are shown

This result is interesting, because it shows that the removed high pass filter effect / low frequency occlusion effect in the present model is not mainly driven by the absence of sound radiation into the environment but by an increase of input power at the ear canal walls even though the stimulation at the mastoid process and the surface area of the ear canal walls remain constant. The increased input power on the other hand must be caused by a larger input impedance seen by the ear canal walls, which is due to the introduction of the occlusion device that replaces the radiation impedance boundary condition (mass like behavior) at the ear canal entrance. This can be explained by rewriting the expression of the input power in terms of a surface averaged acoustical specific input impedance at the ear canal walls and the average mean square velocity of the ear canal walls. Equation (3.3) can be rewritten as:

$$\begin{aligned} \overline{W}_{in} &= \frac{1}{2}\,\Re[\langle\hat{p}\rangle\langle\hat{v}_n\rangle^*]S \\ &= \frac{1}{2}\,\Re\big[\langle\hat{Z}_{in}\rangle\langle\hat{v}_n\rangle\langle\hat{v}_n\rangle^*\big]S = \frac{1}{2}\,\Re\big[\langle\hat{Z}_{in}\rangle\big]|\langle\hat{v}_n\rangle|^2 S \end{aligned} \tag{2.5}$$

$$= \Re\left[\langle \hat{Z}_{in} \rangle\right] \overline{\langle \hat{v}_n \rangle^2} S.$$

Here, <.> denotes surface averaged quantities, $\langle \hat{Z}_{in} \rangle$ is the surface averaged acoustical specific input impedance of the ear canal walls.

$$\langle \hat{v}_n \rangle = \left| \frac{1}{S} \int_S \hat{v}_n dS \right| \tag{2.6}$$

is the surface averaged complex acoustical normal particle velocity, S corresponds to the coupling surface area between the ear canal walls and the ear canal cavity. $\overline{\langle \hat{v}_n \rangle^2}$ represents the time average of the squared surface averaged complex acoustical normal particle velocity of the ear canal walls, which is denoted as the average mean square velocity of the ear canal walls in the following. The numerical model is used to calculate the input power $\overline{W}_{in}$ at the ear canal walls, the coupling surface area S between the ear canal walls and the ear canal cavity, and the average mean square velocity of the ear canal walls. $\Re\left[\langle \hat{Z}_{in} \rangle\right]$ can then be calculated from equation (3.5). Figure 2.10 illustrates the average mean square velocity of the ear canal walls and real part of input impedances that were obtained for the open ear model and for the ear model whose entrance was occluded using the infinite impedance. From Figure 2.10a it can be seen that the average mean square velocity of the ear canal walls decreases little upon occlusion of the ear canal entrance (0.9dB for frequencies below 1 kHz and 1.7dB for frequencies >1 kHz). In contrast, the real part of the surface averaged acoustical specific input impedance increases considerably subsequent to occlusion (Figure 2.10b). These findings validate the explanation above regarding the increased input impedance seen by the ear canal walls. Furthermore, these findings are in agreement with existing lumped element models (e.g. Schroeter and Poesselt, 1986; Stenfelt and Reinfeldt, 2007; Tonndorf, 1966) that employ constant volume velocity sources for both open and occluded ears and which load the ear canal by switching from open radiation impedance to the impedance of the occlusion device.

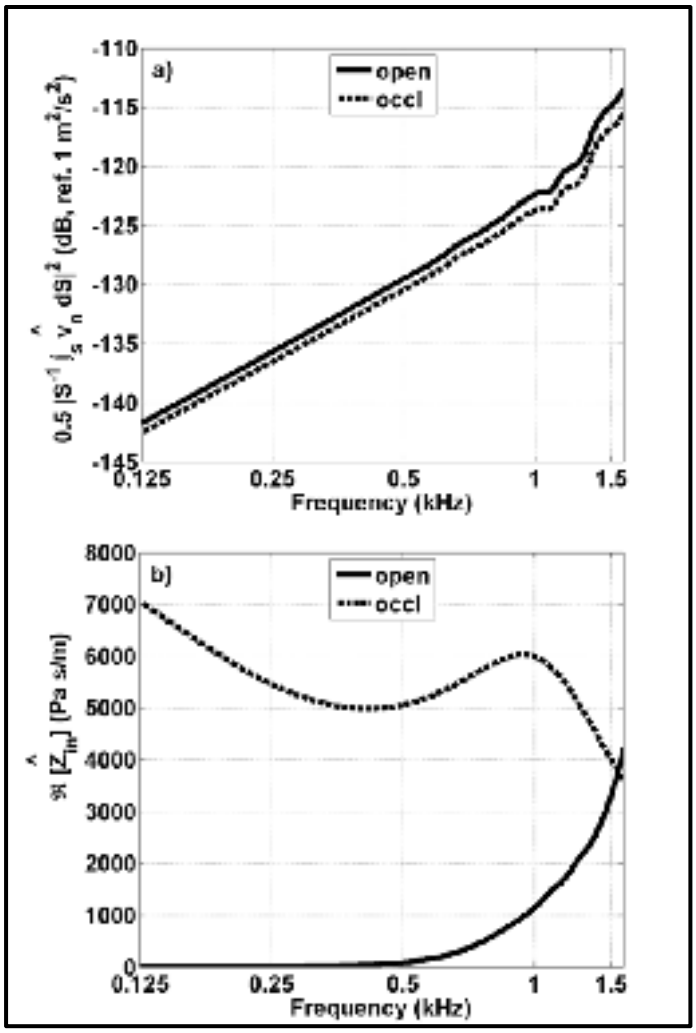

Figure 2.10: a): average mean square velocity of the ear canal walls obtained for the open and occluded (infinite impedance at ear canal entrance) ear models for frequencies below 1.5 kHz. b): real part of the surface averaged acoustical specific input impedance of the ear canal walls for the open and occluded (infinite impedance at ear canal entrance) ear models for frequencies below 1.5 kHz. Narrow band spectra are shown

Above 1.25 kHz (shallow occlusion), and 1.6 kHz (medium and deep occlusion) all simulated occlusion effects are negative (Figure 2.3a). This characteristic has been attributed to a change in the resonance frequencies of the open and occluded ear canal and was suggested by Huizing (1960). In the present study, the resonance frequency of the open ear

was found at 2.1 kHz (Figure 2.3b) which is in good agreement with the analytical solution obtained for an occluded tube of a length which corresponds to the model's effective ear canal length (end correction included). The occluded resonance frequency peak which usually occurs around 5 – 6 kHz, depending on ear canal length and occlusion depth, does not appear in the present data as simulations were limited to 2.8 kHz because the occlusion effect is most problematic at low frequencies and in order to ensure reasonable model solution times. Comparison of the open ear transfer function levels and the occluded ear transfer function levels (Figure 2.3b) shows that the open ear's transfer function level exceeds, due to a steeper slope, those of the occluded ear models around 1.25 kHz, and 1.60 kHz respectively. This results in negative occlusion effects above these frequencies.

2.6 Conclusions

A three dimensional finite element model of the external ear was developed for the simulation of the earplug induced occlusion effect. All computations were carried out using COMSOL Multiphysics (COMSOL®, Sweden). The model provides occlusion effect simulations that are more or less consistent with what has been reported in the literature. In particular, obtained occlusion effects are positive in the lower frequencies and become negative at higher frequencies. Furthermore, the magnitude of the obtained occlusion effects was shown to decrease as a function of earplug insertion depth for frequencies below 1 kHz. Between 1.1 kHz and 1.8 kHz an inversion of the occlusion effect magnitude occurred. In the present model this occlusion effect inversion is mainly due to an increase in the time averaged power that is exchanged between the medial earplug surface and the ear canal cavity for medium and deep occlusion. For shallow occlusion an inverse behavior can be observed (more power is transferred to the cavity from the walls than from the inner ear plug surface).The occlusion effect obtained at deep occlusion, however, appears to be quite large as compared to average experimental occlusion effect data. With the help of power balances it was possible to show that, in the present model, the relatively large occlusion effect at deep insertion might be due to the material properties of the silicone earplug.

Comparison with 20 individual occlusion effect plots shows that the obtained modeling results (15mm occlusion) fall within the experimental reference zone except between 1 – 2 kHz (foam earplug) and at 2 kHz (silicone earplug). Compared to the mean ± one standard deviation the occlusion effect simulations of both earplugs exceed the mean experimental data below 0.25 kHz. Above 0.25 kHz the simulated occlusion effects fall below the mean experimental graph. This might be due to an uncertainty regarding the experimental occlusion depth (10 to 15mm). For both earplug types the simulated graphs closely follow the lower boundary of one experimental standard deviation above 0.315 kHz and below 1 kHz (foam earplug) and 1.6 kHz (silicone earplug). While the graph for the silicone earplug coincides with the lower boundary of one experimental standard deviation the graph for the foam earplug is on average 2.6dB smaller than this lower boundary. Important mid frequency deviations between the experimental standard deviation and the numerical data occur at 1 and 2 kHz (foam and silicone earplug), 1.25 kHz and 1.6 kHz (foam earplug).

With respect to the two tested earplug materials it can be seen that, at medium occlusion, the foam earplug results in a smaller occlusion effect for frequencies below 2 kHz whereas it causes a larger occlusion effect above 2 kHz (3dB). For frequencies <1 kHz the foam earplug causes on average 3dB less occlusion effect. Between 1 kHz and 1.6 kHz the foam earplug causes considerably less occlusion effect (on average 10.6 dB). While the low frequency difference is small, it is not negligible, and this result indicates that the chosen earplug material properties can influence occlusion effect magnitudes. Further investigation of the contribution of the earplug material is necessary. Additionally, to reduce deviations between numerical and experimental results in a future study it might be beneficial to include the bone transducer's airborne noise emission in combination with possible earplug leaks in the model. Furthermore, it would be desirable, although quite difficult, to evaluate geometric properties and relative occlusion depths in experimental setups.

A high pass filter like behavior, as was suggested by Tonndorf (1966), was demonstrated through an analysis of the exchanged powers. In the open ear case, it was found that up to 40% of the power that is exchanged at the ear canal – ear canal wall interface gets radiated by

the ear canal entrance into the environment for the lowest frequencies. At frequencies around 0.5 kHz this sound radiation reduces to about 6%. The remaining power is dissipated at the tympanic membrane. When the ear canal entrance is rigidly occluded using an infinite impedance no sound gets radiated into the environment. It was demonstrated that the absence of sound radiation does not suffice to explain a 40dB occlusion effect. On the other hand, it was shown that the input power from the ear canal walls into the ear canal cavity is larger in the occluded model as compared to the open ear model even though the excitation at the mastoid process and the ear canal wall area remain constant. The average mean square velocity of the ear canal walls remained almost unaltered for open and occluded ears. Consequently, the input power increase is due to a larger input resistance seen by the ear canal walls which, in turn, originates from the introduction of the occlusion device.

While obtained modeling results are promising, care should be taken with regards to model limitations and simplifications that include the chosen material properties (anisotropy, homogeneity, preloading and frequency dependency) and boundary conditions, modeling of the temporal bone as compared to the entire head, and the assumption of isotropic material behavior. Additionally, it would be desirable to develop further 3D external ear models to study occlusion effect differences that might be related to geometry. Unfortunately, these data are sparse. A preliminary study had shown that the male images from the Visible Human Project® could not be used for complete external ear reconstruction, because the larger image spacing hindered the reconstruction of the skin tissue on the ear canal walls. The Visible Korean® dataset could be used to bridge this gap. Further research with respect to these limitations is needed.

2.7 Acknowledgements

The authors gratefully acknowledge the IRSST for funding this work. Furthermore, the authors thank S. Stenfelt and S. Reinfeldt for kindly sharing occlusion effect data for the present study.

CHAPTER 3

ARTICLE 2: PREDICTION OF THE BONE CONDUCTION OCCLUSION EFFECT USING A TWO-DIMENSIONAL AXI-SYMMETRIC FINITE ELEMENT MODEL [a)]

Martin K. Brummund [b)]

Department of Mechanical Engineering, École de technologie supérieure,

1100 rue Notre-Dame Ouest, Montréal, Québec, H3C 1K3, Canada,

Franck Sgard

IRSST, Direction scientifique

505 Boulevard de Maisonneuve Ouest, Montréal, Québec, H3A 3C2, Canada

Yvan Petit [c)] and Frédéric Laville

Department of Mechanical Engineering, École de technologie supérieure

1100 rue Notre-Dame Ouest, Montréal, Québec, Canada, H3C 1K3

Hugues Nélisse

IRSST, Service de la recherche

505 Boulevard de Maisonneuve Ouest, Montréal, Québec, Canada, H3A 3C2

Submitted for publication to:

The Journal of the Acoustical Society of America on February 19, 2014

[a)] Portions of this work were presented in "A simplified axi-symmetric finite element model of the human outer ear to determine the earplug induced auditory occlusion effect". Abstracts of 162nd Meeting: Acoustical Society of America, San Diego, CA, USA, October 2011, p. 2469.

[b)] Electronic address: martin.brummund.1@ens.etsmtl.ca

[c)] Also at Research Centre, Hôpital du Sacré-Cœur de Montréal, 5400 Boulevard Gouin Ouest, Montréal, Québec, Canada, H4J 1C5

3.1 Abstract

A simplified linear elasto-acoustic finite element model of the human external ear was developed. The model comprises the ear canal cavity and skin, as well as the bony and cartilaginous external ear domains. All geometrical and material properties were taken from the literature. The model was used to simulate the TFL (transfer function level) between a mechanical stimulation and the acoustic pressure in the ear canal. All computations were carried out using COMSOL Multiphysics (COMSOL®, Sweden). The TFLs also served to calculate the bone conduction OE (occlusion effect) of a silicone earplug. Both, TFLs (open and occluded) and OEs were compared to experimental measurements obtained from a healthy human reference group (18 subjects). The earplug type, insertion depth, and mechanical stimulus used in the experimental study were applied to the numerical model. Four different boundary condition configurations were examined. Additionally, the role of airborne noise and earplug leaks of varying diameters were examined with the model. Obtained results indicate that a simplified external ear model can predict experimental TFLs and OEs with satisfying precision. Deviation magnitudes vary with frequency. Furthermore, the numerical results are influenced by the boundary conditions and the presence of both airborne noise and earplug leaks.

3.2 Introduction

The occlusion effect (OE) originates from the outer-ear bone conduction pathway and describes a perceived low frequency sound increase when the ear canal is occluded for instance through a hearing protection device (e.g. earplug) or a hearing aid. While the outer-ear bone conduction path is negligible in the open ear, it dominates bone conduction hearing at frequencies below 1 kHz in the occluded ear canal (Stenfelt et al., 2003). To qualitatively explain the OE, two models have been established. Huizing (1960) elaborated that the open and occluded ear canals correspond to open and closed pipes of varying lengths and that the OE originates from a frequency shift in the resonance of the occluded ear canal. This explanation is reasonable in the mid frequencies where the resonances of open and occluded ear canals occur. Secondly, using an electrical analogy, Tonndorf (1966) demonstrated that

the open ear canal acts as a high pass filter and that occlusion of the ear canal opening removes this high pass filter effect. Tonndorf's model applies to the low frequencies where the wavelength is much larger than the ear canal length.

The outer ear comprises the ear canal cavity, skin tissue that covers the ear canal walls, entrance region, and pinna, cartilaginous tissue that backs the lateral ear canal and bony tissue that backs the medial ear canal. All of these domains exhibit complex geometrical shapes that vary between subjects (e.g. ear canal volume, length). A few studies have attempted to model the OE that results from structure borne excitation (Schroeter and Poesselt, 1986; Hansen, 1998; Stenfelt and Reinfeldt, 2007; Brummund et al., 2014). With the exception of Brummund et al. (2014), who used a 3D linear elasto-acoustic finite element model, all other models used lumped elements to simulate the OE. Finite element models are appealing because they allow for analyzing the sound propagation in a complex shaped ear canal coupled to an earplug over a wide frequency range. Furthermore, various material behavioral laws as well as complex loadings and boundary conditions can be accounted for. Yet, a current lack of material property data in terms of anisotropy, homogeneity, pre-stress state and frequency dependency for the external ear tissues limits finite element models to hypothesize isotropy and linear elasticity.

A major disadvantage of 3D finite element models is that they can require extensive computational resources thus causing unreasonable model solution times. A high degree of geometrical complexity makes the 3D reconstruction of the external ear very tedious especially when the skin and cartilage tissues need to be distinguished. Besides, the number of anatomical datasets available for complete geometrical reconstruction of the external ear is very limited and it is challenging to define standardized and meaningful geometrical characteristics for an anatomically correct 3D external ear model (e.g. the ear canal radius and wall thickness vary along the ear canal axis). Lastly, 3D models are cumbersome for the implementation of sensitivity analyses (e.g. material properties and geometry) and are therefore not adapted for optimizing hearing protection devices.

Axi-symmetric finite element models could contribute to alleviate the abovementioned drawbacks because they rely on simpler geometries and thus require less computational resources. Existing averaged geometrical data of the human external ear (ear canal length, wall skin thickness etc.) can be employed for the implementation of such an axi-symmetric model which renders the tedious 3D ear reconstruction unnecessary. Additionally, an axi-symmetric external ear model can also serve as a blueprint for the implementation of an artificial external ear test fixture (e.g. see preliminary work by Brummund et al., 2013) to measure and study the OE in a standardized and objective manner.

The objective of the present study is threefold. The first objective is to specify an axi-symmetric linear elasto-acoustic finite element model of the human external ear for simulation of the bone conduction OE using geometrical and material properties found in the literature. No attempt of simplifying the ear canal coupled to the external ear tissues for simulation of the OE could be found in the literature. The second objective is to use the axi-symmetric model to simulate transfer function levels (TFL) in open and occluded ears and to calculate bone conduction OEs of an earplug hearing protection device. The third objective is to compare the numerical model to experimental data (both TFL and OE) that were measured in a healthy human reference group.

3.3 Methodology

3.3.1 Geometrical layout of the axi-symmetric external ear model

The geometrical simplification of the ear canal and its surrounding soft and bony tissues is depicted in Figure 3.1.

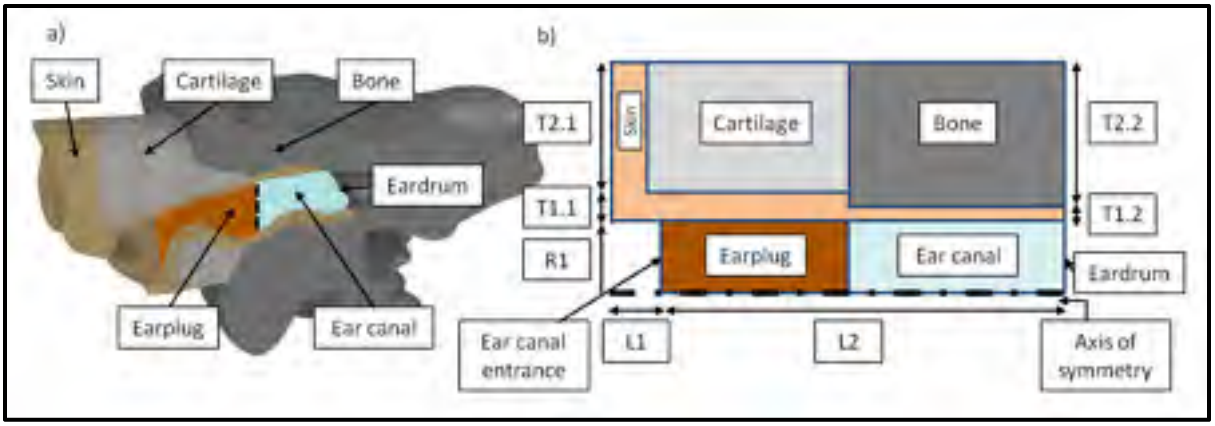

Figure 3.1: a) Anterior sectional view of a 3D reconstructed external ear geometry (The Visible Human Project® images were used). b) Simplified axi-symmetric geometry of the external ear including ear canal, earplug, skin tissue, cartilage tissue and bony tissue. The axis of symmetry is indicated through a dashed-dotted line. The model's dimension identifiers (see Table 3.1) are included using text boxes

The ear canal and earplug are represented as straight cylinders of identical cross-sectional areas. The ear canal walls are formed by a cylindrical skin layer which is surrounded by a cylindrical cartilage layer in the lateral outer ear (close to the ear canal opening) and a cylindrical bone layer in the medial outer ear (close to the ear drum). In the literature different cartilage to bone tissue volume ratios around the ear canal have been reported (e.g. Alvord and Farmer, 1997; Lucente et al., 1995; Oliveira and Hoeker, 2003; Stenfelt et al., 2003). The present model assumes that half of the ear canal is backed by cartilaginous tissue and the other half by bony tissue. The ear canal entrance region describes the zone where the external auditory meatus gradually merges into the cavum conchae. To model the ear canal entrance region the cartilage cylinder around the ear canal and the skin tissue that covers the ear canal walls were continued outwards in such a way that they protrude with respect to the ear canal entrance (see Figure 3.1, dimension L1). The cartilage tissue protrudes 0.6 mm and the skin tissue thickness equals 1.4 mm leading to a total length L1 of 2 mm. These dimensions are based on average thickness data of the auricular cutis, subcutis and cartilage (Danter et al., 1996). Other anatomical landmarks of the pinna were disregarded in the present model mainly to allow for the model to be axi-symmetric. Besides, no record could be found in the literature that suggests a major contribution of the anatomical landmarks of

the pinna to the bone conduction OE. The human ear canal length varies between subjects. Lengths of 27 mm to 37 mm along a curved central axis have been measured in human cadaver heads (Stinson and Lawton, 1989). Other studies report average ear canal lengths of 25 and 30 mm (e.g. Alvord and Farmer, 1997; Johansen, 1975; Oliveira and Hoeker, 2003). The obtained length differences can be explained by the inclination of the eardrum which causes the cranial ear canal wall to be shorter than the caudal wall (Alvord and Farmer, 1997). Additionally, measuring the length of a given ear canal along both a curved and a straight central axis influences the obtained result (Stinson and Lawton, 1989). For the present model, a length of 27mm was chosen for the unoccluded ear canal (see Figure 3.1, dimension L2). This length approximately corresponds to the average ear canal length of the test subjects that provide the experimental reference data for the present study (see section 3.3.6). The latter was estimated based on the individual head related transfer functions. To find a constant radius for a straight cylindrical ear canal two approaches can be considered. The radius can either be calculated from average volume and length data or from average surface area data. Information on volume, length and average surface area can be found in various studies (e.g. Johansen, 1975; Stinson and Lawton, 1989; Yu et al., 2012). Using these datasets and calculation methods causes the average constant ear canal radii to vary relatively little between 3.4 mm and 3.75 mm. Here, a radius of 3.4 mm is chosen (see Figure 3.1, dimension R1). The human ear canal walls are covered with a very thin layer of skin whose thickness decreases from lateral to medial direction. In the cartilage backed ear canal region an average skin thickness of 0.5 to 1.0 mm has been reported (Lucente et al., 1995). In the bone backed ear canal region depths of about 0.2 mm and as little as 15 µm to 30µm (for the epidermal layer) were observed (Jahn and Santos-Sacchi, 2001; Lucente et al., 1995). For the lateral ear canal wall of the axi-symmetric model a skin thickness of 1.0 mm (see Figure 3.1, dimension T1.1) and for the bone backed ear canal wall a thickness of 0.2 mm (see Figure 3.1, dimension T1.2) is assumed. The external ear includes the pinna and the ear canal with the tympanic membrane marking its medial limit. While the ear canal is partly backed by cartilaginous and bony tissues it is not self-evident where exactly the cartilaginous and bony tissues border to other anatomical regions of the head. As these transitions are likely gradual, it is challenging to define an adequate circumferential limit of the simplified external ear

geometry. Ideally, the entire head including all tissues (e.g. organs, nerves, blood vessels) should be accounted for. In the present study this is out of scope since the model is assumed to be axi-symmetric. As a first approximation, the thickness of the cartilage tissue that backs the medial ear canal was set to 10mm (see Figure 3.1, dimension T2.1). The bony tissue that backs the ear canal is slightly thicker (T2.2 = 10.8mm, see Figure 3.1), because the skin tissue on the medial ear canal is 0.8mm thinner than the skin at the lateral ear canal wall. Table 3.1 summarizes the dimensions used for the simplified external ear geometry.

Table 3.1: Overview of the dimensions used in the axi-symmetric external ear model

Identifier	Dimension name	Value [mm]	Comments
L1	Protrusion at canal entrance	2	1.4 mm skin 0.6 mm cartilage
L2	Ear canal length	27	50 % cartilage backed 50% bone backed
R1	Ear canal radius	3.4	n/a
T1.1	Lateral canal wall thickness	1	n/a
T1.2	Medial canal wall thickness	0.2	n/a
T2.1	Lateral skin and cartilage thickness	10	n/a
T2.2	Medial bone tissue thickness	10.8	n/a

3.3.2 Material properties of the external ear tissues and the earplug

The external ear tissues exhibit non-linear, anisotropic, viscoelastic material behavior and are influenced by factors such as age and gender. Under the assumption of small tissue deformation, however, it is reasonable to assume linear stress-strain behavior in these domains (e.g Fung, 1993). On the other hand, assuming isotropic elastic material characteristics is presently inevitable because of a current lack of property data in terms of anisotropy, homogeneity, pre-stress state, and parameter frequency dependency for the biological tissues considered here. Besides, especially the characterization of anisotropic,

viscoelastic biological material parameters is in itself a challenging task. Further research will be necessary to accurately estimate the error introduced by the outlined simplifications.

The implementation of a linear elasto-acoustic external ear model requires knowledge of Young's moduli, densities, Poisson's ratios, and loss factors of all solid domains. For the present model, the material properties that have been used in a previous study (Brummund et al., 2014) are re-used. Table 3.2 summarizes all material properties used in the axi-symmetric model. The density and the speed of sound of the air that fills the ear canal cavity were ρ_{air} = 1.20 kg/m^3 and c_{air} = 343.20 m/s.

Table 3.2: Material properties employed for modelling of the external ear tissues. The density of the air and the speed of sound of the air inside the ear canal are ρ_{air} = 1.20 kg/m^3 and c_{air} = 343.20 m/s

		Density [kg/m^3]	Young's mod. [MPa]	Poisson's ratio	Loss factor
Bone	Value	1714	11316	0.3	0.01
	Anatomical site	Mean over skull	Mean over temporal bone	Mean over temporal bone	Assumed
	Reference	Delille et al. (2007)	Delille et al. (2007)	Peterson and Dechow (2003)	n/a
Cartilage	Value	1080	7.2	0.26	0.05
	Anatomical site	Human articular	Human septum	Human septum	Assumed
	Reference	Cox and Peacock (1979)	Grellmann et al. (2006)	Grellmann et al. (2006)	n/a
Skin	Value	1100	0.5	0.4	0.1
	Anatomical site	Average skin density	Breast skin model	Assumed	Assumed
	Reference	Duck (1990)	(Sarvazyan et al., 1995)	n/a	n/a

The model of a cylindrical earplug is coupled to the open simplified external ear model to predict the numerical OE. The earplug model is assumed to fully adapt to the shape of the cylindrical ear canal without deforming it. This hypothesis seems reasonable for custom

molded earplugs and soft foam earplugs. One silicone earplug material is considered in the present study. The earplug material is assumed to exhibit isotropic linear elastic behavior and its properties are taken from Sgard et al. (2010) (see Table 3.3). Three occlusion depths (10.4mm, 11.7mm, and 13mm) were investigated. The chosen occlusion depths correspond to the average insertion depth (with respect to the ear canal entrance) and standard deviation of the custom molded silicone earplugs used in the experimental part of this study.

Table 3.3: Material properties of the earplug model used to occlude the external ear model

	Density [kg/m^3]	Young's mod. [MPa]	Poisson's ratio	Loss factor	Reference
Silicone earplug	1050	0.85	0.48	0.1	(Sgard et al., 2010)

3.3.3 Boundary and load conditions

Several boundary conditions need to be defined to account for the connections that exist between the external ear domains and their adjacent domains. Ideally, these connections should be expressed using transfer impedance boundary conditions. Their assessment, however, is challenging (Viallet et al., 2013). As a first approximation, more conventional boundary conditions, such as free and clamped conditions can be used. Nevertheless, it is not obvious which boundary and load conditions best represent the connections between the external ear and its adjacent tissue domains.

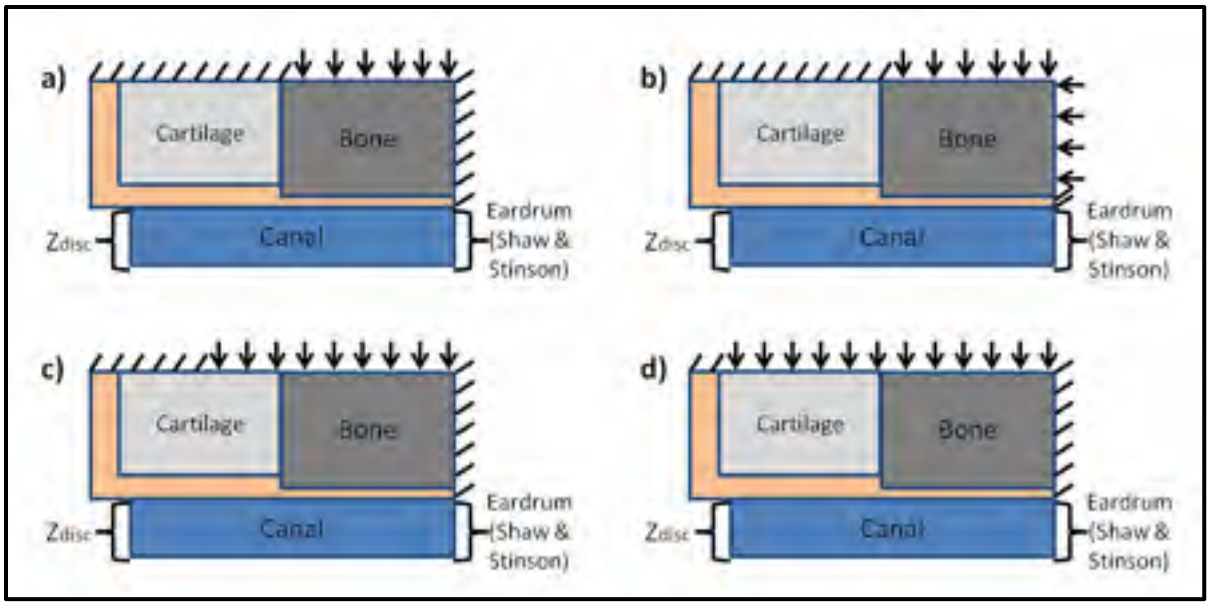

Figure 3.2: Overview of the four boundary and load conditions tested in the present study. Arrows indicate the locations at which the force was introduced normally on the surface. Inclined dashes indicate fixed boundaries. The brackets at the entrance and the end of the ear canal indicate impedance boundary conditions. The unmarked boundaries adjacent to the ear canal entrance (next to Z_{disc}) indicate free boundaries

For the present model, four boundary condition configurations were considered (see Figure 3.2). All configurations use fixed, free (ear canal entrance regions), impedance, and boundary load conditions. In the present study, the boundary load is always introduced normally and uniformly on either the bony and/or cartilaginous boundaries of the model (configurations a) to d)). In a preliminary study several other loading condition configurations have been examined. Among others, the boundary loads had been introduced tangentially to examine the effects of the exciting force vector orientation. The obtained numerical results, showed that purely normal force lead to the best results. Nevertheless, the examined loading conditions remain an idealization of the real stress vectors which act on the human tissues. The latter likely vary in terms of amplitude and direction along the tissue boundaries.

To model the open ear canal entrance, a locally reacting impedance boundary condition that corresponds to the radiation impedance of a baffled flat circular piston is applied (Shaw, 1976). In the occluded finite element model the latter boundary condition was replaced by a

free boundary condition. The tympanic membrane is assumed to terminate the cylindrical ear canal perpendicularly to its central axis and is modeled as a locally reacting specific acoustical impedance boundary condition (Shaw and Stinson, 1981; Hahn, 1985). This is a simplification, because it does not allow for the sound radiation that stems from the inertial movement of the ossicles to be considered.

3.3.4 Finite element modeling

The cartilage, bone, skin and earplug of the simplified external ear model represent solid domains and the ear canal a fluid filled cavity. Under the assumption of small deformations and a temporal dependency $e^{j\omega t}$ for all fields the wave propagation in the solid domains is governed by the classical linear elasto-dynamic equation

$$\hat{\sigma}_{ij}^{k}\left(\underline{\hat{u}}^{k}\right) + \omega^2 \rho_s^k \hat{u}_i^k = 0. \tag{3.1}$$

Here, $\hat{\sigma}_{ij}^{k}$, ω, ρ_s^k, and $\hat{u}_i^k$ correspond to the stress tensor, angular frequency, density, and displacement vector of a given domain k, respectively. Structural damping is introduced as a multiplier $(1 + j\eta_s^k)$ in the stiffness matrix. η_s^k corresponds to the isotropic structural loss factor (see Table 3.2) of a given domain k and j is the imaginary unit. On the other hand, the governing equation of the fluid domain is given by the Helmholtz equation

$$\Delta\hat{p} + k^2\hat{p} = 0 \tag{3.2}$$

where $\hat{p}$ denotes the sound pressure and $k = {\omega}/{c}$ is the wave number. Coupling between the solid and acoustical domains is introduced via the continuity of stress vectors $\hat{\sigma}_{ij}^{k} n_j = -\hat{p} n_i$ and normal displacements $\frac{\partial \hat{p}}{\partial n} = \rho_{air}\, \omega^2 \hat{u}_i^k n_i$ where n corresponds to the unit normal vector that points outward a solid domain k. The axi-symmetric coupled elasto-acoustic finite element system was solved using COMSOL Multiphysics (COMSOL®, Sweden). The material properties and boundary conditions outlined in sections 3.3.2 and 3.3.3 were applied

to the model domains. Subsequently, all domains were meshed according to a criterion of four elements per wavelength at 3 kHz to ensure that the minimum element size was satisfied in the entire frequency range. Quadratic triangular elements were used for all domains. The open and occluded models were solved separately. The open model consisted of 699 solid and 467 acoustic elements. The occluded models consisted of 866 solid and 344 acoustic elements (11.7mm occlusion).

3.3.5 Calculation of estimated transfer function levels and the numerical occlusion effects

The sound pressure level at the center of the tympanic membrane was computed for the open and occluded ear models, respectively, using the power spectral density (PSD) of the B-71 (©Radioear Corporation, PA, USA) bone transducer's RMS-force (obtained during the experimental study) as the spectra for the mechanical excitation. The frequency resolution of the analysis was twenty equally spaced points in each third octave band. These points were used to calculate the third-octave response in five bands (0.125 kHz, 0.25 kHz, 0.5 kHz, 1 kHz, and 2 kHz) through third octave integration which was carried out using an in-house MATLAB (MathWorks®, MA, USA) routine. Third-octave responses were obtained for the mean square pressure (p_{rms}) as well as for the input force (F_{rms}) to obtain the sound pressure level related to the excitation force which was employed to approximate the TFL:

$$TFL = 20\log_{10}\left(\frac{\left|\frac{p_{rms}}{Frms}\right|}{ref.}\right), ref.1\ \left[\frac{Pa}{N}\right] \tag{3.3}$$

The OEs were calculated by subtracting the open ear TFL from the occluded ear TFLs.

3.3.6 Experimental measurements

To better evaluate the finite element model, the obtained numerical results were compared to objective OE measurements. The experimental measurements outlined hereafter are part of a larger study that aims at comparing subjective and objective measurement methods for hearing protector attenuation and the OE (Nélisse et al., 2013). The described protocol was approved by the local ethics committee.

3.3.6.1 Subjects

Eighteen subjects aged 20 to 60 years volunteered to participate in this study. All subjects exhibited hearing thresholds < 25 dB HL at frequencies ranging from 125 to 8000Hz as specified in ANSI/ASA S.12-6.

3.3.6.2 Apparatus

All experimental measurements were carried out in a semi-anechoic room that respects the room requirements specified in ISO 8253-2 and ANSI/ASA S.12-6 for hearing protection device attenuation measurements. A Knowles FG-23329 miniature microphone (©KNOWLES Electronics, IL, USA) was used to measure the sound pressure level inside the subjects' open and occluded right ear canals and a 1-inch 40HF (©G.R.A.S. Sound & Vibration, Denmark) control microphone was placed 30 cm above each subject's head. A B-71 bone transducer (©Radioear Corporation, PA, USA) served as stimulation device at the right mastoid process. All stimulation signals were created using REATMaster (©Nelson Acoustics, TX, USA) and data acquisition was carried out in LabVIEW (©National Instruments, TX, USA). The Knowles miniature microphone and the 1-inch control microphone were connected to amplifiers that communicated with the REATMaster and LabVIEW components via a NI PXI 1033 chassis that was equipped with two 4461 data acquisition cards (©National Instruments, TX, USA). A summarizing overview of the used measurement setup is provided in Figure 3.3.

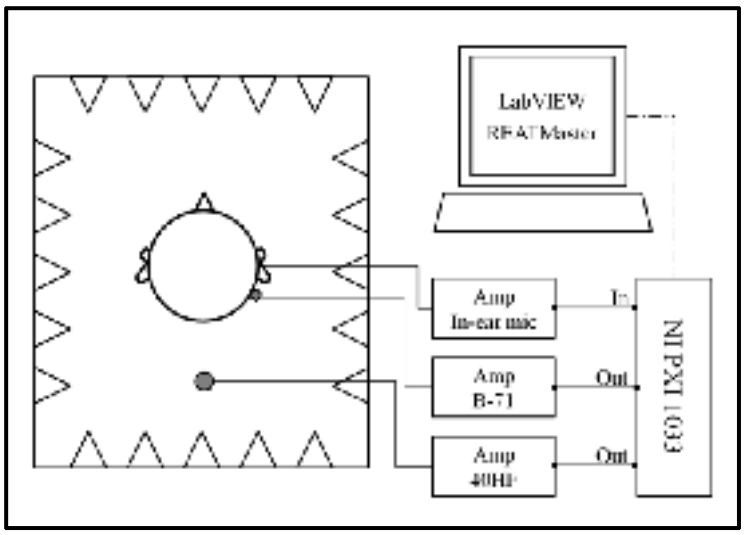

Figure 3.3: Top view of the experimental measurement setup used to determine the open and occluded TFLs and the OE subsequent to bone condition stimulation at the right ipsilateral mastoid process. Right hand side, top view (schematic) of the instrumented test subject inside the semi-anechoic room. Left hand side, data acquisition chain (schematic)

3.3.6.3 Protocol

Prior to measurement onset each participant was instrumented with a Knowles miniature microphone. The microphone was placed inside the right ear canal about midway between the medial earplug surface and the tympanic membrane (microphone insertion depth from ear canal entrance approximately 20.13 mm ± 2.18 mm [mean ± S.D.]). The bone transducer's flat circular excitation surface (surface area 175 mm^2) was securely attached to each subject's right mastoid process and held in place by an elastic headband (static force about 5 N). First, open ear measurements were carried out on the instrumented subjects. Third octave band limited noises were generated in 5 bands (125 Hz, 250 Hz, 500 Hz, 1000 Hz, and 2000 Hz). Ten second time recordings were used for each microphone and frequency band. No masking was performed during any of the tests. The stimulation magnitude of the bone transducer output was adjusted for the open ear until a sound pressure level reading was obtained at the

in-ear microphone at each frequency. The chosen stimulation amplitudes stayed the same for the open and occluded ear measurements and did not cause any noticeable discomfort for the participants. Upon completion of the open ear test, each subject was instrumented with custom molded silicone earplugs. Earplug molding was performed prior to experiment onset. It was not necessary to remove the in-ear miniature microphone during the experiment. For inexperienced subjects, the earplugs were fitted by the experimenter whereas experienced subjects user-fitted the custom modeled earplugs. The average earplug insertion depth, as measured with respect to the ear canal entrance, equaled 11.71 mm ± 1.33 mm (mean ± S.D.). Upon earplug insertion, the bone transducer measurements outlined above were repeated.

3.3.6.4 Experimental transfer function level approximation and occlusion effect calculation

All obtained time recordings were analyzed and post-processed using in-house MATLAB routines (MathWorks®, MA, USA). Each excitation frequency band (third octave band limited noises in bands: 125 Hz, 250 Hz, 500 Hz, 1000 Hz, and 2000 Hz) was analyzed independently. For each excitation frequency, the third octave band autospectra for the open and occluded ear mean square pressure (p_{rms}) measured at the in-ear microphone were normalized by the autospectrum of the B-71 (©Radioear Corporation, PA, USA) bone transducer's input force (F_{rms}) in order to approximate the open and occluded TFLs. To obtain the OE for each excitation frequency, the third octave band autospectra for the occluded and open ear SPLs were subtracted. This subtraction resulted in a frequency spectrum. The spectral value that corresponds to the excitation frequency equaled the OE value at this frequency.

3.4 Results

3.4.1 Transfer function level and occlusion effect prediction with bone conduction stimulation

Figure 3.4a and Figure 3.4b compare the TFLs of the open and occluded numerical models to the mean (± S.D.) experimental data. For the numerical models the boundary condition configurations outlined in section 3.3.3 were tested.

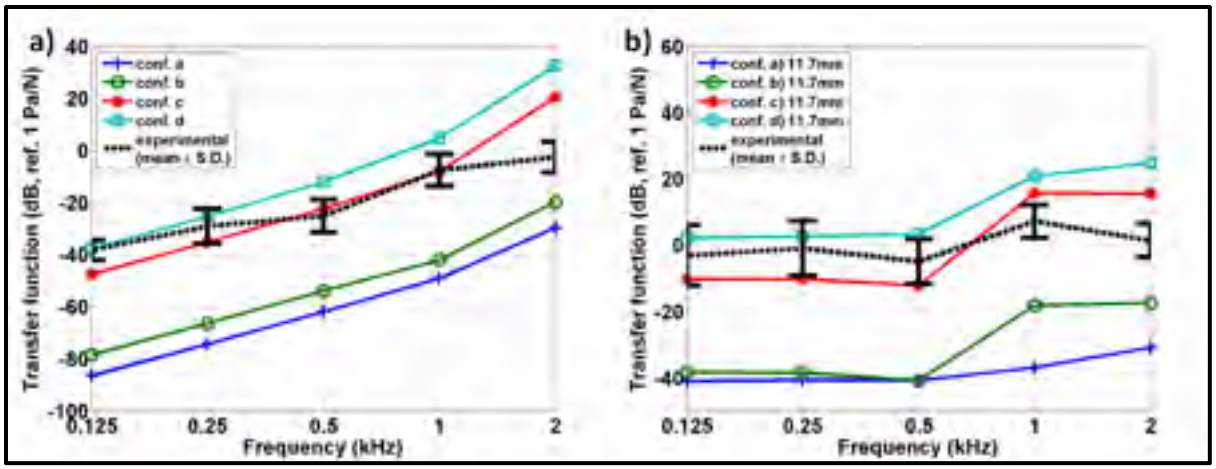

Figure 3.4: a) numerical open ear TFL predictions obtained for the four boundary condition configurations. b) numerical occluded ear TFLs obtained for each tested boundary condition configuration. In addition to the numerical results the experimental (mean ± S.D.) open and occluded TFLs are included for comparison (dashed lines)

In the open ear condition (Figure 3.4a) configurations a) and b) underestimate the mean experimental data by 40dB and 32dB on average. Configuration c) overestimates the experimental mean by 2dB on average. At frequencies below 0.5 kHz this configuration exhibits a smaller TFL and above 1 kHz a larger TFL as compared to the mean experimental data. Configuration d) overestimates the mean experimental data by on average 13dB. At 0.125 kHz the numerical (configuration d)) and experimental TFLs almost coincide (delta 0.6dB). Above 0.125 kHz the deviation magnitude between configuration d) and the experimental mean TFL increases steadily. Both, configurations c) and d) exhibit the largest

deviations from the experimental mean TFL at 2 kHz (23dB and 35dB). The slope of the TFL graphs is quite constant (offset-like) and little affected by the chosen boundary conditions.

For the occluded numerical model (see Figure 3.4b), configurations a) and b) result in TFLs that are much smaller than the experimental mean data (on average 38dB and 31dB). Configuration c) underestimates the mean experimental TFL for frequencies up to 0.5 kHz (on average 8dB) and overestimates the experimental data for higher frequencies (on average 11dB). The TFL falls close to the lower boundary of the experimental standard deviation for frequencies < 1 kHz. At 1 kHz and 2 kHz this configuration overestimates the upper experimental standard deviation by 3.6dB and 9.2dB, respectively. Configuration d) overestimates the mean experimental data at all frequencies (on average 11dB). The numerical TFL falls close to the upper limit of the experimental standard deviation for frequencies < 1 kHz. At 1 kHz and 2 kHz the numerical TFL exceeds the experimental mean plus one standard deviation by 8.7dB and 18.4dB, respectively. For configurations a) and b), the TFLs start to deviate at frequencies >0.5 kHz. The slope of the occluded numerical TFLs is influenced more strongly by the chosen boundary conditions than the open TFLs.

Figure 3.5 compares the numerical OEs obtained for the TFLs illustrated in Figure 3.4a and Figure 3.4b to the mean experimental OE. The mean ± S.D. of the numerical OEs stem from the insertion depth variability. Each earplug was tested at the mean as well as the mean ± one standard deviation insertion depths (10.4mm, 11.7mm, and 13mm).

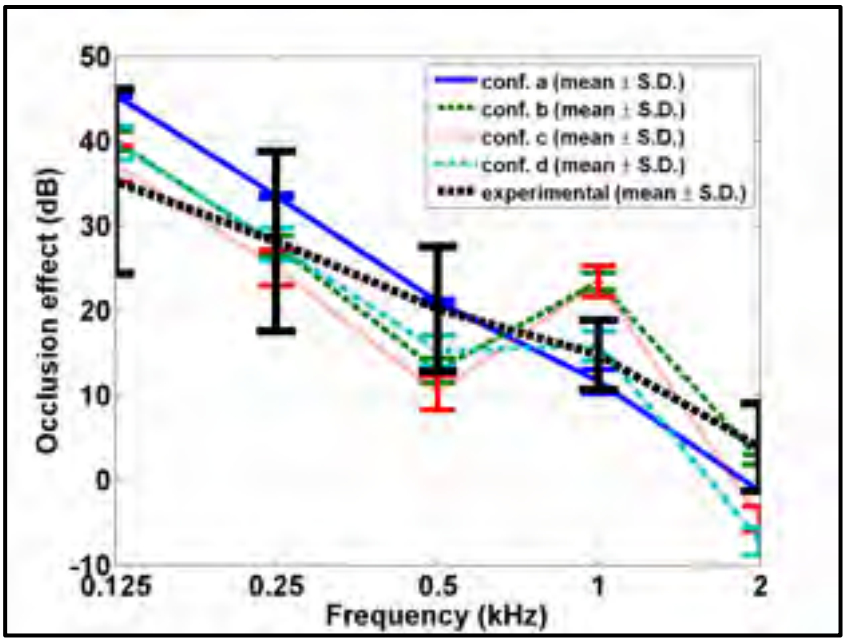

Figure 3.5: Numerical OE predictions (solid lines) obtained from the TFLs when only structure borne excitation is being considered. The OEs are provided for the experimental insertion depths 10.4mm, 11.7mm, and 13mm for all boundary condition configurations. The experimental OE (mean ± S.D.) is included for comparison (dashed error bar graph)

An important inter-individual OE variability is noticeable for the experimental data. At frequencies < 0.5 kHz all numerical configurations fall inside the range of one experimental standard deviation. Configuration a) causes the largest mean OE. Configurations b) and d) cause relatively similar OEs up to 0.5 kHz. They are smaller than the OE of configuration a) (on average 5.6dB) but larger than the OE of configuration c) (on average 2.6dB). At 0.5 kHz the mean OE of configuration a) and the experimental data almost coincide (delta 0.9dB) whereas all other configurations predict mean OEs that are 5dB to 10dB smaller than the mean experimental data. At 1 kHz only configuration d) predicts an OE that matches the mean experimental data whereas the remaining configurations either under or over predict the experimental mean OE. Lastly, at 2 kHz, configuration b) provides the most accurate mean OE simulation whereas all other configurations result in OE predictions that are smaller than the mean experimental value.

With respect to the insertion depth variability it can be seen that configuration a) is affected the least (on average 0.5dB S.D.) when the mean experimental insertion depth is varied by ± 1.3mm. The OEs of configurations b), c), and d) vary on average by 1.1dB, 1.9dB, and 1.8dB (S.D.) when the insertion depth is altered by ± 1.3mm.

3.4.2 The combined effect of airborne noise and structure borne excitation on transfer function levels and occlusion effects

The B-71 (©Radioear Corporation, PA, USA) bone transducer used for stimulation at the ipsilateral mastoid also emits airborne noise. This noise can potentially corrupt the sound pressure level measurements inside the open ear canal. To monitor this transmission pathway a reference microphone was placed at the ipsilateral tragus of Nélisse et al.'s setup (Nélisse et al., 2013). Figure 3.6 compares the sound pressure level readings (mean ± S.D.) obtained at the open ipsilateral tragus to the sound pressure levels inside the open ear canal.

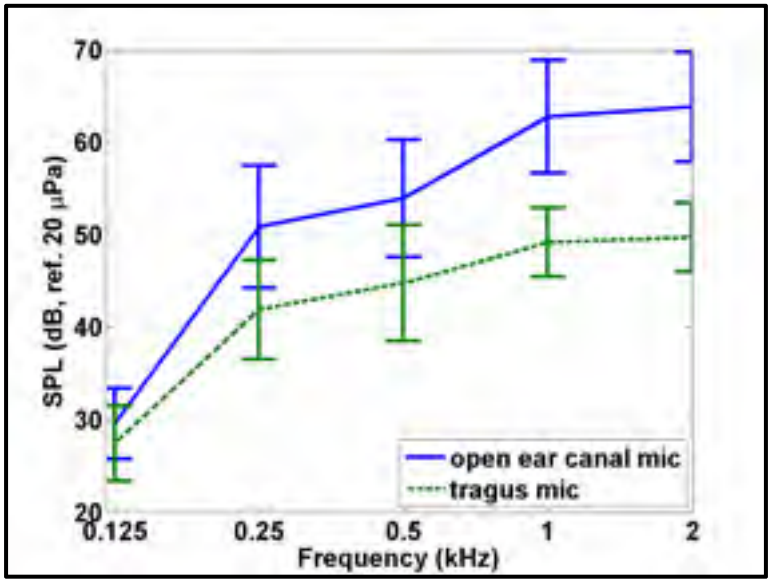

Figure 3.6: Comparison of the experimental sound pressure level readings obtained at the ipsilateral tragus (open ear) and inside the open ear canal (mean ± S.D.)

At 0.125 kHz the mean sound pressure levels recorded at the tragus and in-ear microphone are fairly similar (27.5dBSPL and 29.6dBSPL). At higher frequencies the mean sound pressure level of the in-ear microphone is on average 11.5dB larger than the mean sound pressure level of the tragus microphone. The standard deviations of the sound pressure levels, however, continue to overlap up to 0.5 kHz.

Figure 3.7 illustrates the TFLs of the open and occluded numerical models when both the structure borne excitation and the airborne excitation from the bone transducer are incoherently accounted for in the model. The mean square acoustic pressure associated with the airborne noise was derived from the mean sound pressure level reading at the open ear tragus microphone and applied as a loading at the open and occluded ear canal entrance. All boundary condition configurations described in section 3.3.3 were considered. The experimental (mean ± S.D.) TFLs are included for comparison.

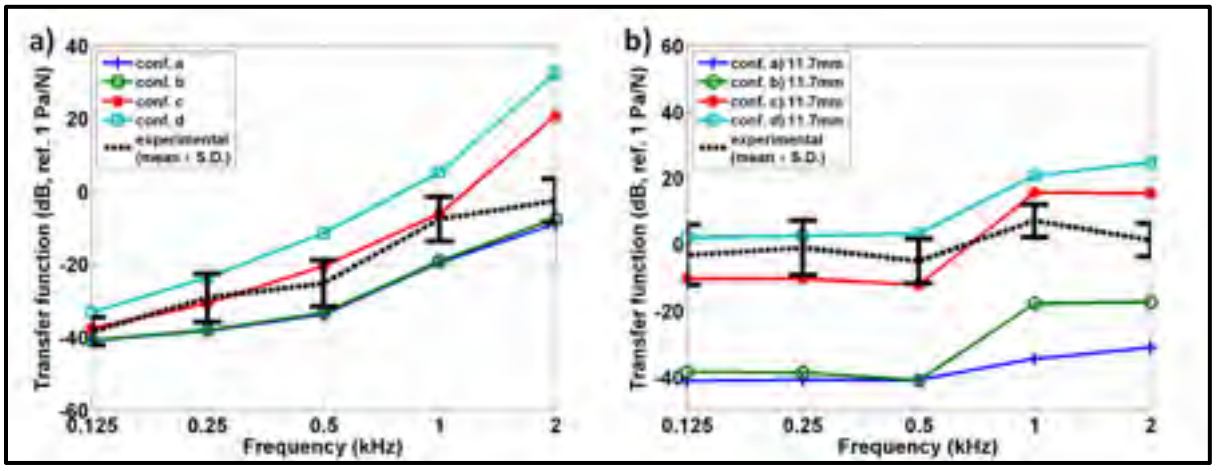

Figure 3.7: a) numerical open ear TFL predictions. b) numerical occluded ear TFLs. All boundary condition configurations were considered (solid lines) for the open and occluded model under both structure borne and airborne excitation from the bone transducer. In addition to the numerical results the experimental (mean ± S.D.) open and occluded TFLs are included for comparison (dashed error bar graphs)

Adding the airborne noise to the open numerical model increases the TFLs of boundary configurations a) and b) (see Figure 3.7a) by on average 32dB and 24dB. While these configurations were shown to underestimate the mean experimental TFL by on average 40dB

and 32dB they fall now close to the lower boundary of one experimental standard deviation (except for 1 kHz). The open ear TFL of configuration c) increases by 10dB, 4.6dB, 2dB, 2dB, and 0.2dB upon introduction of the airborne noise at the ear canal entrance. For configuration d) the open TFL increases the least at each frequency (4.6dB, 1.8dB, 0.7dB, 0.5dB, 0.01dB) when the airborne noise is added to the model. The occluded numerical model is not affected by the presence/absence of the airborne noise at the ear canal entrance hence the TFLs for all boundary condition configurations remain almost constant (compare Figure 3.7b and Figure 3.4b). A small increase of 2.5dB occurs at 1 kHz for configuration a).

Figure 3.8 compares the simulated and experimental OEs. The numerical OEs are provided as mean and standard deviation values because the three occlusion depths which correspond to the mean experimental insertion depth and its standard deviation (10.4mm, 11.7mm, and 13mm) were tested.

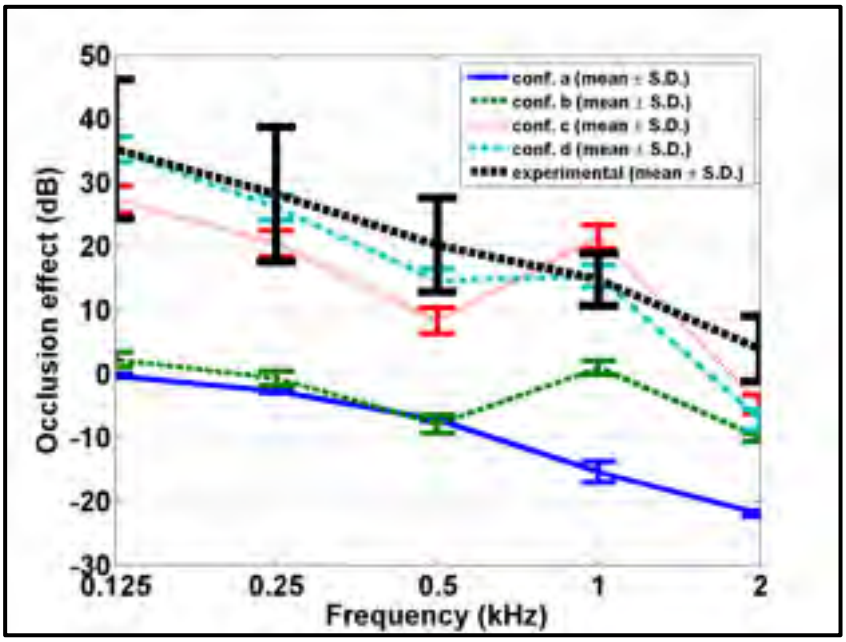

Figure 3.8: Numerical OE predictions (solid lines) obtained for both structure borne and airborne excitation from the bone transducer. The OEs are provided for the experimental insertion depths 11.7mm ± 1.3mm (mean ± S.D.) for all boundary condition configurations. The experimental OE (mean ± S.D.) is included for comparison (dashed error bar graph)

The OEs for configurations a) and b) fall completely outside the target zone established by the experimental OE data. The OEs for these configurations are practically inexistent at the lowest frequencies. Nevertheless, configuration b) provides an OE prediction similar to that of configuration d) at 2 kHz (delta 2.7dB). The OE magnitudes for configurations c) (up to 1 kHz) and d) (up to 0.5 kHz) also decrease due to the increased open ear TFLs. The slopes of the numerical OE (configuration c) and the mean experimental data are almost parallel for frequencies up to 0.5 kHz. While the OE for configuration d) is very close to the experimental mean value (except for 0.5 kHz and 2 kHz) the OE for configuration c) is closer to the lower limit (except at 1 kHz) of one experimental standard deviation. At 0.5 kHz, 1 kHz, and 2 kHz the OE for configuration c) exceeds the experimental mean ± one standard deviation by -4.5dB, 2.6dB, and -3.5dB. Configuration d) exceeds the experimental mean ± one standard deviation only at one frequency (2 kHz) by -5.9dB. Negative deviations indicate an underestimation and positive deviations indicate an overestimation.

When the insertion depth of the numerical earplug model is altered by ± 1.3mm the OEs continue to vary little. For configurations a), b), c), and d) the OE differences amount to (on average) 0.6dB, 1.1dB, 1.9dB, and 1.8dB (S.D.).

3.4.3 The role of earplug leaks in combination with airborne and structure borne excitation

Adequate fitting of the earplug is important to provide optimal attenuation. With respect to the OE, earplug fit is important, because it can potentially alter the magnitude of the TFL in the occluded ear. The latter becomes especially important when airborne noise is present. The insertion loss, an objective microphone-in-real-ear based measure of hearing protection device attenuation, also provides a qualitative indication of the acoustic seal. In their study, Nélisse et al. (2013) determined the insertion loss of the custom molded earplugs subsequent to pink noise excitation (90dB at the center of the head when head absent) from a loudspeaker. Figure 3.9 illustrates the experimental insertion loss (mean ± S.D.) at the center frequencies of the considered third-octave bands.

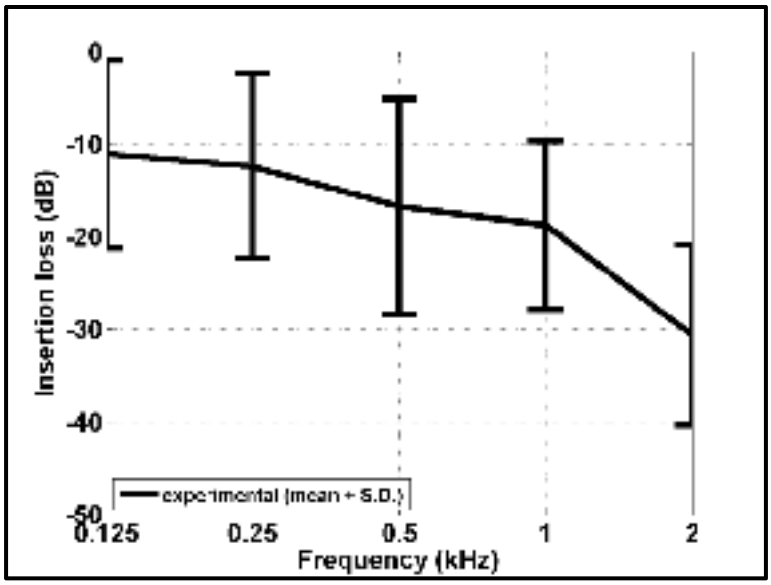

Figure 3.9: Experimental insertion loss data (mean ± S.D.) obtained for the custom molded earplugs (right ear only) under pink noise excitation from a loudspeaker

The insertion loss graph (Figure 3.9) shows the sound attenuation achieved with the custom molded earplugs at each examined center frequency. The experimental standard deviation (on average about 10dB), however, also indicates an important inter-subject variability and a possible presence of leaks in some of the test subjects' earplugs. These leaks could have been introduced in the experimental measurements by the thin in-ear microphone wire (diameter approximately 0.2mm) that ran between the circumference of the earplug and the ear canal walls. To account for this observation in the numerical model, leaks of varying diameters (0.2mm, 0.3mm, 0.4mm, and 0.5mm) were included along the centre axis of the earplug. Due to the small leak diameters, thermal and viscous effects have to be considered in these models. The leak length equaled the earplug length. Figure 3.10 illustrates the numerical TFLs of the occluded models (insertion depth 11.7mm) under the presence of earplug leaks of varying diameters, the airborne noise emitted from the bone transducer, and the structure borne excitation. All boundary conditions configurations outlined in section 3.3.3 were considered.

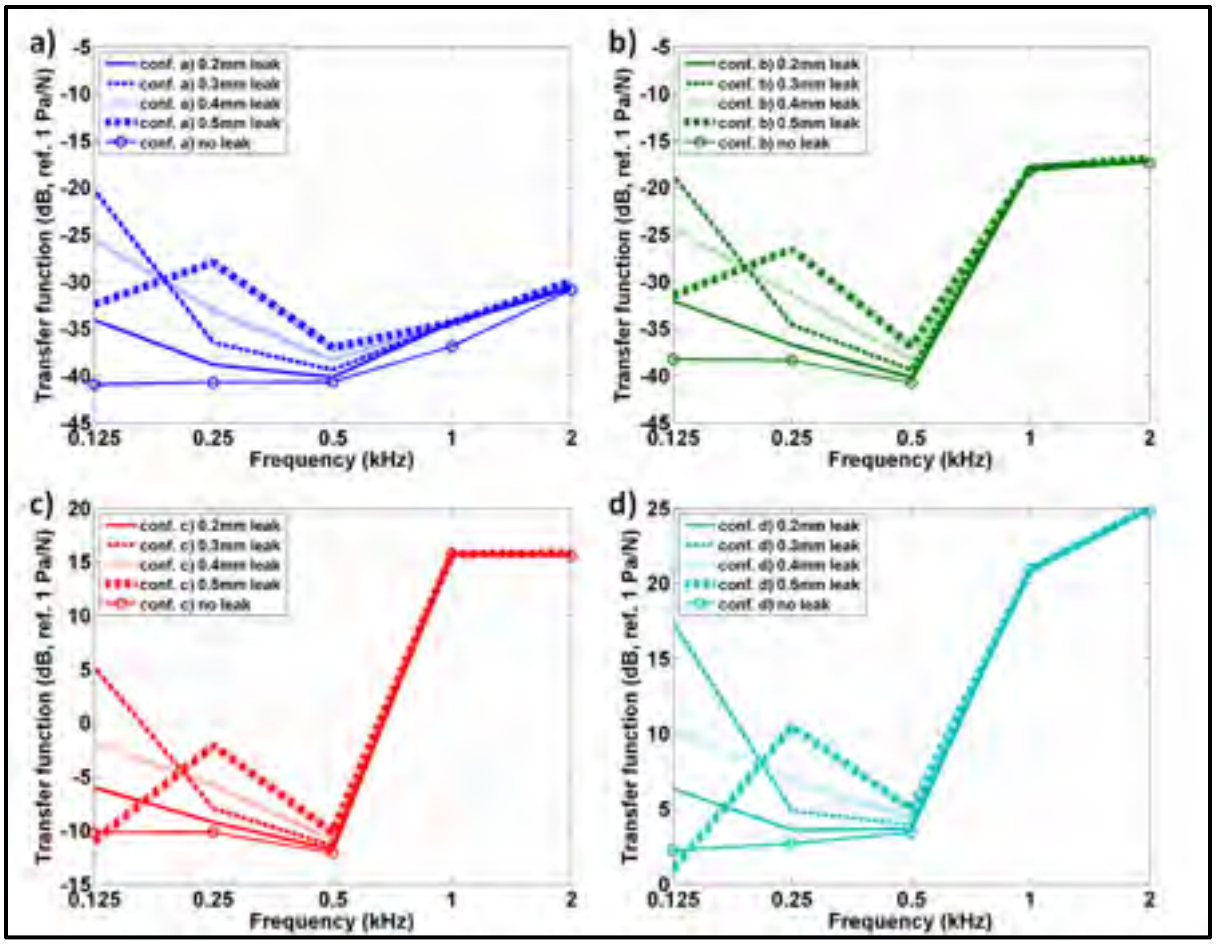

Figure 3.10: Numerical TFLs (occluded ear model only, 11.7mm) for earplug leak diameters ranging from 0.2mm to 0.5mm for configurations a), b), c) and d). Numerical TFLs obtained for both structure and airborne excitation from the bone transducer are depicted. For comparison the TFLs obtained for the leak free condition (solid lines with markers) are included

Compared to the leak free condition, the introduction of earplug leaks of varying diameters causes variations in the TFLs of the occluded ear models (configurations b)-d)) for frequencies up to 0.5 kHz. The TFLs of configuration a) continue to vary up to 1 kHz for all leak diameters. At higher frequencies the presence of leaks becomes negligible. The TFLs increase (with respect to the leak free TFL) when leaks are present for all boundary configurations. An exception to this observation occurs at 0.125 kHz for configurations c) (Figure 3.10c) and d) (Figure 3.10d) and a leak diameter of 0.5mm. Here, the TFLs decrease by about 1dB with respect to the occluded TFLs of the leak free earplug. At 0.125 kHz the

TFLs increase in the following leak diameter order: 0.5mm, 0.2mm, 0.4mm, and 0.3mm. This order applies to configurations c) and d) only. For configurations a) and b) the TFL increases in the leak diameter order: 0.2mm, 0.5mm, 0.4mm, and 0.3mm. Again the first leak diameter causes the smallest and the last diameter the largest increase in TFL. At 0.25 kHz and 0.5 kHz the TFLs increase with leak diameter for all boundary configurations. Lastly, for 1 kHz the TFLs for configuration a) increase by about 2.5dB for all leak diameters. For leak diameters 0.2mm, 0.3mm, and 0.4mm the largest TFL increase with respect to the leak-free earplug TFLs occurs at 0.125 kHz for all boundary condition configurations whereas for the leak diameter 0.5mm the largest TFL increase occurs at 0.25 kHz for all boundary condition configurations.

Figure 3.11 illustrates the resulting OE predictions (insertion depth 11.7mm) when leaks are present in the earplug models. For comparison the experimental OE (mean ± S.D.) was included.

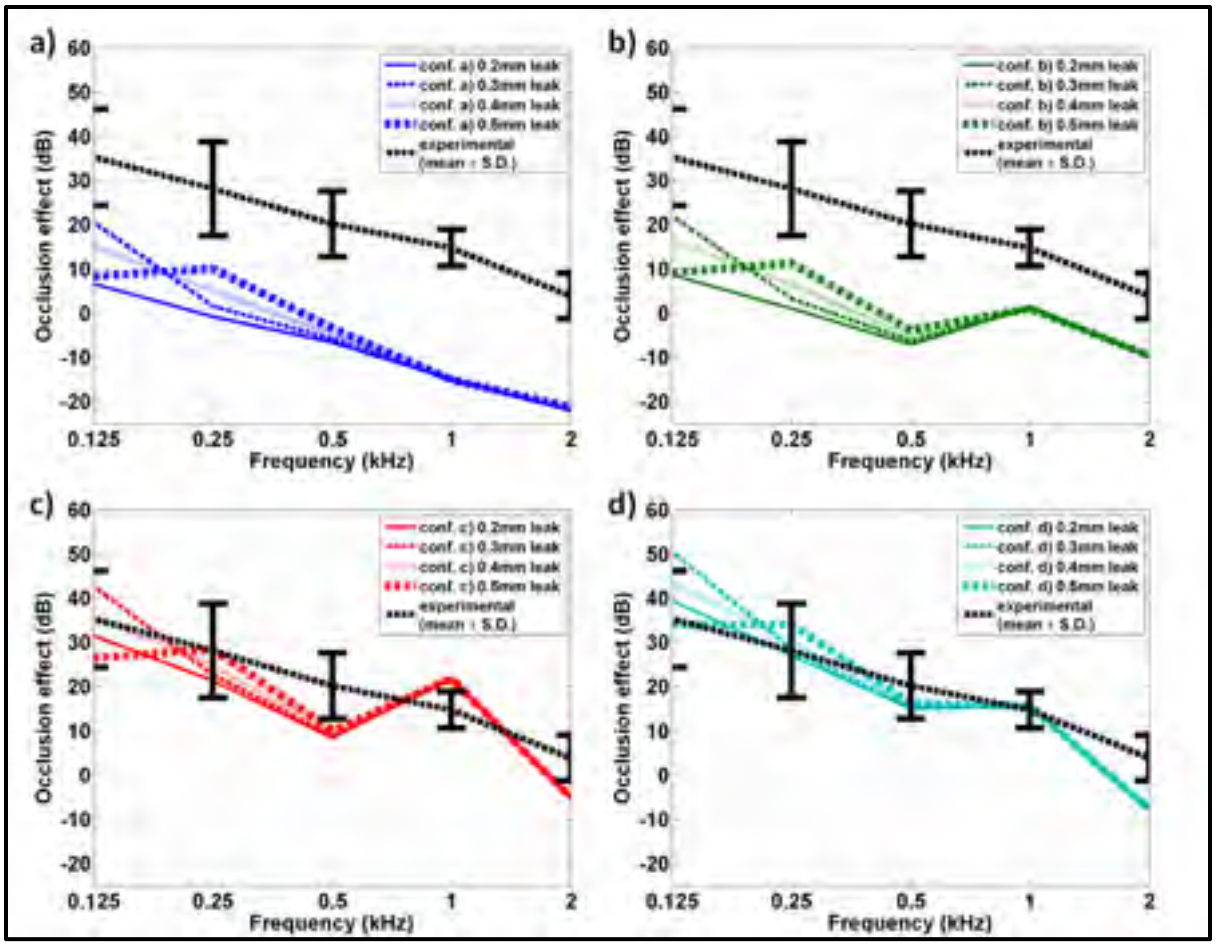

Figure 3.11: Numerical OE predictions (insertion 11.7mm) for earplug leak diameters ranging from 0.2mm to 0.5mm together with structure and airborne excitation from the bone transducer for configurations a), b), c) and d). For comparison the experimental OEs (mean ± S.D.) are included (dashed error bar plot)

The numerical OEs increase in the presence of earplug leaks (together with airborne noise and structure borne excitation). Configurations a) and b) continue to provide OE predictions that fall some 25dB (on average) below the mean experimental OE. Due to the increased occluded ear TFLs, however, these configurations now result in positive OE predictions at the lowest frequencies. For a leak diameter of 0.4mm configuration c) predicts the mean experimental OE at 0.125 kHz. This configuration also predicts the mean experimental OE at 0.25 kHz when a leak diameter of 0.5mm is present. Configuration d) predicts the mean experimental OE at 0.125 kHz (0.5mm leak diameter) and at 0.25 kHz (for leak diameters: 0.2mm, 0.3mm, and 0.4mm).

3.5 Discussion

3.5.1 Transfer function level and occlusion effect prediction with bone conduction stimulation

The large deviations between the mean experimental TFL and the numerical TFLs (open ear) observed for configurations a) and b) occur, because too little ear canal sound pressure is generated by the ear canal walls for these boundary and load condition configurations. When configurations c) and d) are used the ear canal sound pressure increases sufficiently to either match (configuration c)) or exceed (configuration d)) the mean experimental TFL at several frequencies. The increase in TFL magnitude originates from the introduction of the excitation force on both cartilaginous and bony portions of the numerical external ear model. This result is also in agreement with Stenfelt et al. (2003) who reported that sound transmission through the cartilaginous tissue of the external ear is the most important contributor to ear canal sound pressure for bone conduction. The slopes of the numerical open TFLs were found to vary little with the chosen boundary conditions. This is likely due to the acoustical properties of the open ear canal which remains unaltered in terms of geometry and boundary conditions. The rising slope indicates a convergence of the open TFLs towards the open ear's quarter wavelength resonance frequency which is located around 2.9 kHz. In this respect the relatively large deviation between the numerical TFLs and the mean experimental TFL at 2 kHz is noticed. Given that the numerical model's ear canal length approximately corresponds to the mean ear canal length of the test subjects, both numerical and experimental TFLs would be expected to converge similarly to the quarter wave length resonance thus exhibiting similar TFL values at 2 kHz. This deviation could indicate a limitation of the simplified numerical model at this frequency. For instance, such limitation could originate from the way in which the eardrum is modeled. Using an impedance boundary condition does not allow modeling of the ear canal sound pressure that results from the inertia of the ossicles coupled to the tympanic membrane. The latter is known to contribute to the ear canal sound pressure at the mid frequencies (Stenfelt and Goode, 2005; Stenfelt et al., 2002).

The TFLs of the occluded numerical models exhibit similar trends as the open ear's TFLs. While configurations a) and b) underestimate the experimental data, configurations c) and d) fall inside the experimental reference zone defined by the experimental mean and standard deviation. Again, this outcome can be attributed to the effect of the different boundary and load conditions and underlines the important contribution of the cartilaginous external ear tissue. Unlike the open ear TFLs, the slope of the occluded TFLs is influenced more strongly by the chosen boundary condition configuration. This can be attributed to the earplug model. The way in which the excitation force is introduced throughout the different configurations is critical to the vibro-acoustic behavior of the earplug and thus determines how much acoustical power gets exchanged between the medial earplug surface and the ear canal cavity.

The examined boundary conditions provide satisfactory (with respect to the experimental data) OE predictions for frequencies up to 0.5 kHz. The deviations that occur at 0.5 kHz, 1 kHz, and 2 kHz result from the TFL differences observed for the open and occluded TFLs. For instance, the deviations at 0.5 kHz, and 1 kHz for configuration c) are caused by over and underprediction of the occluded experimental TFL at these frequencies (the open TFLs are in very good agreement). Interestingly, although configuration a) underpredicts the open and occluded experimental TFLs the obtained OE is acceptable at all test frequencies and at 0.5 kHz even the mean experimental OE is obtained for this configuration.

3.5.2 The combined effect of airborne noise and structure borne excitation on transfer function levels and occlusion effects

When the airborne noise emission from the bone transducer is included in the numerical model, the open TFLs of configurations a) and b) were shown to increase considerably at all frequencies. This observation is due to the small amount of ear canal sound pressure that is generated by the ear canal walls for these configurations which results in a small signal to noise ratio. Thus, the new open TFLs correspond to the TFLs of the added airborne noise. The open TFL magnitudes of configurations c) and d) increase much less under the presence of bone transducer noise and above 1 kHz (configuration c)), and 0.5 kHz (configuration d))

the presence of airborne noise becomes negligible. This is due to better signal to noise ratios between the acoustical pressure that is radiated at the ear canal walls and the bone transducer noise for these configurations. The latter results are also in agreement with the experimental sound pressure level measurements at the ipsilateral tragus and in-ear microphone (Figure 3.6) which show that airborne noise corruption is more likely to occur at the lowest frequencies.

The occluded TFLs (all configurations) were shown to remain almost constant (except for a small increase at 1 kHz observed for configuration a)) because of the sound attenuation of the airborne noise through the earplug model.

The OE predictions mirror the observations described above in that the increased open ear TFLs in combination with the unaltered occluded TFLs cause the numerical OEs to decrease by the same magnitudes at which the open TFLs increase each frequency. For instance, the OE decrease at 0.125 kHz is more pronounced for configuration c) than for configuration d), because their open TFLs increase by different magnitudes subsequent to airborne noise introduction. Unlike before (section 3.4.1), however, configuration a) and b) do not continue to provide acceptable OE predictions. Configurations c) and d) (even more so), on the other hand, do.

3.5.3 The role of earplug leaks in combination with airborne and structure borne excitation

The introduction of earplug leaks of varying diameters and airborne noise was shown to alter the occluded TFLs at the low frequencies. Except for one leak diameter at 0.125 kHz (configurations c) and d)), the occluded TFLs increased subsequent to leak and noise introduction. The largest TFL increase occurred either at 0.125 kHz for leak diameters 0.2mm, 0.3mm, and 0.4mm or at 0.25 kHz for a leak diameter of 0.5mm. These results can be attributed to a Helmholtz resonator like behavior of the system earplug-ear canal. The Helmholtz resonator's neck (effective length and cross section) is formed by the earplug leak,

and the occluded ear canal represents the cavity volume. The resonance frequencies (analytical solution) of the considered orifice diameters (0.2mm to 0.5mm) occur at 0.12 kHz, 0.179 kHz, 0.238 kHz, and 0.297 kHz, respectively. These analytical results help to explain the TFL increase at 0.125 kHz for the 0.2mm diameter. Nevertheless, they also suggest that for 0.3mm, and 0.4mm the largest TFL increase should occur at 0.25kHz (e.g. 0.2 kHz third octave band was not considered). This deviation from the analytical solution can be explained through the boundary conditions of the leaking earplug and the occluded ear canal cavity. The analytical solution of the Helmholtz resonator assumes rigid boundaries which is not the case in the model of the cavity. This was verified with a simulation case in which the impedance boundary condition of the eardrum was replaced by sound hard boundary. This caused the system's rigidity to increase and the numerical TFL peaks to converge towards the analytical solutions. Additionally, the Helmholtz resonator formed by the system earplug-cavity also explains the TFL magnitude order as a function of leak diameter at 0.125 kHz. For instance, one might expect the 0.5mm leak to cause the largest TFL increase at 0.125 kHz. Due to the Helmholtz resonance, however, the 0.2mm diameter surpasses the 0.5mm orifice diameter at this frequency.

The OE predictions increase (with respect to section 3.4.2) at low frequencies when earplug leaks, airborne noise, and structure borne excitation are present. This increase is due to the leak induced TFL increase in the occluded ears. Similarly to the condition when only airborne noise is considered, the OE predictions of configurations a), and b) underestimate the experimental OEs for all leak diameters. Configurations c), and d) continue to provide satisfying OE predictions. The deviations between the numerical and experimental results vary both as a function of frequency and leak diameter.

3.6 Conclusions

An axi-symmetric linear elasto-acoustic finite element model of the human external ear was developed for simulation of the TFLs and the bone conduction OE. All computations were carried out using COMSOL Multiphysics (COMSOL®, Sweden) and the obtained results

were compared to experimental data (both TFL and OE) that were measured in a healthy human reference group. The numerical model provides TFL predictions (open and occluded) which can be consistent with the experimental data for frequencies up to 2 kHz. The obtained numerical precision in terms of TFL magnitude is strongly influenced by the chosen boundary conditions. In this respect it could be verified that the excitation of the cartilage tissue is crucial to the ear canal TFL as was suggested by Stenfelt et al. (2003). The slope of the open TFLs is influenced only little by the boundary conditions. The occluded TFL slopes are more sensitive to the chosen boundary condition configuration.

Although some boundary configurations provide unsatisfying TFL magnitudes the obtained OEs can be in good agreement with the experimental measurements. When only structure borne excitation is considered configurations a), b), c), and d) provide satisfying OE predictions for frequencies < 0.5 kHz. At 1 kHz, configurations a) and d) provide the most accurate (with respect to the experimental data) OE predictions. Lastly, at 2kHz configuration b) provides the most accurate OE prediction. The deviation magnitudes between the experimental mean OE and the tested configurations vary with frequency. The uncertainty regarding the earplug insertion depth was found to be of secondary importance, in the present study, to explain the numerical and experimental OE deviations.

Noise corruption from the bone transducer might have occurred at the lowest frequencies in some test subjects. Thus, this airborne noise component was included incoherently in the numerical model. The open TFL magnitudes increased subsequent to the introduction of airborne noise. For configurations that result in very little structure borne ear canal sound pressure, the resulting TFLs correspond to the airborne noise TFL. For boundary configurations that induce sufficient structure borne ear canal sound pressure, the TFLs increase only at the low frequencies. When leak free earplug models are used the occluded TFLs remain unaltered subsequently to airborne noise introduction. The presence of airborne noise improves the OE prediction for configuration d) which, together with configuration c), provides satisfying OEs.

In addition to airborne noise, leaks might have occurred at the lowest frequencies in some test subjects due to the insertion of the in-ear microphone wire. When both leaks and airborne noise are included in the numerical model, the occluded TFLs increase at the lowest frequencies. The magnitude by which the occluded TFLs increase as a function of frequency is influenced by the leak diameter. The system earplug-cavity exhibits Helmholtz resonator like behavior. The presence of both leaks and airborne noise causes the OE predictions to increase at the low frequencies (with respect to airborne noise). The deviation magnitudes between the numerical and experimental data vary with frequency, boundary configuration, and leak diameter with configurations c) and d) providing the best overall numerical results.

The present study shows that in order to predict average experimental TFLs and OEs, a model considering average external ear geometry, appropriate boundary conditions, airborne noise and earplug leaks can be implemented. While the numerical results obtained in this study are promising, care must be taken with respect to model limitations and simplifications. These include the chosen material properties and behavioral law as well as a truncated model of the external ear as opposed to a model of the entire head. Only four boundary condition configurations have been tested in the present study. Other configurations might even be more suited than the ones examined here. Lastly, it could be beneficial to consider more than five test frequencies in a future study.

3.7 Acknowledgements

The authors gratefully acknowledge the IRSST for funding this work. Additionally, the authors would like to thank C. Le Cocq (ÉTS) and J. Boutin (IRSST) for their very valuable contribution during the experimental measurements.

CHAPTER 4

ARTICLE 3: AN AXI-SYMMETRIC MODEL TO STUDY THE EARPLUG CONTRIBUTION TO THE BONE CONDUCTION OCCLUSION EFFECT

Martin K. Brummund [a)]

Department of Mechanical Engineering, École de technologie supérieure,

1100 rue Notre-Dame Ouest, Montréal, Québec, H3C 1K3, Canada,

Franck Sgard

IRSST, Direction scientifique

505 Boulevard de Maisonneuve Ouest, Montréal, Québec, H3A 3C2, Canada

Yvan Petit [b)] and Frédéric Laville

Department of Mechanical Engineering, École de technologie supérieure

1100 rue Notre-Dame Ouest, Montréal, Québec, Canada, H3C 1K3

Hugues Nélisse

IRSST, Service de la recherche

505 Boulevard de Maisonneuve Ouest, Montréal, Québec, Canada, H3A 3C2

Submitted for publication to:

Acta Acustica united with Acustica on July 17, 2014

[a)] Electronic address: martin.brummund.1@ens.etsmtl.ca

[b)] Also at Research Centre, Hôpital du Sacré-Cœur de Montréal, 5400 Boulevard Gouin Ouest, Montréal, Québec, Canada, H4J 1C5

4.1 Abstract

An axi-symmetric linear elasto-acoustic finite element (FE) model of an occluded human external ear is proposed to simulate the bone conduction occlusion effect (OE). The model consists of a cylindrical ear canal cavity surrounded by layers of biological tissues (skin, cartilage and bone) in which an earplug is inserted. Geometrical and material properties are taken from the literature. OEs are predicted for foam and silicone earplug FE-models using COMSOL Multiphysics (COMSOL®, Sweden).

The FE-model is shown to predict the experimental OE measured in two healthy human reference groups wearing foam or silicone earplugs, satisfactorily. Deviations between model and experiment are of similar magnitudes as for previous electro-acoustical OE models.

Comparison of the axi-symmetric FE-model with two existing gold standard electro-acoustical OE models showed (i) minor differences for shallow occlusion and (ii) a large underestimation for frequencies <1kHz, but a good agreement above 1kHz, for deep insertion depth. OE differences between silicone and foam earplug types (similar insertion depths, close to bony meatus) were observed experimentally and confirmed with the FE-model. Power balance computations in the ear canal and the earplug (both FE-models) indicate an insertion depth dependent contribution of the earplug type to the OE magnitude.

4.2 Introduction

The contribution of the outer ear path to bone conduction hearing has been shown to be negligible in the open ear (e.g. Stenfelt and Goode, 2005). Upon occlusion with a hearing protection device (e.g. earplug), however, this pathway dominates bone conduction hearing for frequencies below 1kHz (Stenfelt et al., 2003). This causes a perceived low frequency sound increase that alters the perception of the wearer's voice and amplifies physiological noises (Berger et al., 2003). This phenomenon is known as occlusion effect (OE) (Békésy,

1941; Goldstein and Hayes, 1965; Huizing, 1960; Tonndorf, 1966). It is defined as the sound pressure level difference in the ear canal with and without the protection device in place.

To qualitatively explain the OE two models have been established. At the low frequencies, Tonndorf (1966) states that the open ear canal acts as a high pass filter element. Occlusion of the ear canal removes the high pass filter effect and emphasizes the low frequencies. At the mid frequencies, Huizing (1960) scientifically elaborated that the open and occluded ear canals correspond to open and closed pipes of varying lengths. Consequently, the occlusion effect can be attributed to a frequency shift in the resonance frequency of the occluded ear canal.

To quantitatively explain the OE, numerous experimental studies have been conducted. Research findings indicate (but are not limited to) that the low frequency ear canal sound pressure level under bone conduction excitation mainly originates from the sound transmission through the cartilaginous external ear tissue (Stenfelt et al., 2003). Occlusion of the auditory meatus alters the ear canal sound pressure level depending on occlusion depth and frequency (e.g. Stenfelt and Reinfeldt, 2007). At the low frequencies, the OE typically reaches 20dB to 30dB (Schroeter and Poesselt, 1986). Its magnitude varies strongly between subjects (Stenfelt and Reinfeldt, 2007) and is influenced by the presence of earplug leaks. Additionally, the OE is influenced by the occlusion volume (Berger and Kerivan, 1983; Watson and Gales, 1943). Both small (e.g. deeply inserted earplugs) and large occlusion volumes (e.g. spacious circumaural earmuffs) are associated with small OE whereas the OE is large for occlusion at the ear canal entrance (Berger et al., 2003). The decreasing OE magnitude with increasing earplug insertion depth has been attributed to several mechanisms. They include (i) a gradual reduction of the radiating surface of the ear canal walls (Tonndorf, 1972), (ii) a progressive immobilization of the eardrum (Tonndorf, 1972), (iii) less sound energy being radiated by the stiffer bony tissue of the medial external ear compared to the softer cartilaginous tissue (Berger and Kerivan, 1983), and (iv) a gradual stiffening of the remaining unoccluded ear canal walls (Berger and Kerivan, 1983).

Very few studies can be found in the literature that have examined how different earplug types influence the OE for similar insertion depths (Lee, 2011; Nélisse et al., 2013). Lee and Casali (2011) reported that the chosen earplug type influenced OEs for deep occlusion (11mm) and the authors concluded that the earplug design variables (e.g. material properties) ought to be studied in more detail to reduce the OE.

Finite element (FE) modeling could contribute to better understand how different earplug types influence the OE. Axi-symmetric models can be generated using existing averaged geometrical data of the external ear and their implementation is less tedious as 3D reconstruction of an anatomically correct geometry. Additionally, axi-symmetric models require little computational resources which facilitate the implementation of sensitivity analyses with respect, for instance, to earplug's material properties. The latter could contribute to help identifying and eventually optimizing key material properties. Moreover, simplified numerical models can be useful for the design and implementation of geometrically equivalent artificial external ear test fixtures to study the OE in a standardized and objective manner (e.g. Brummund et al., 2013).

The objective of the present work is threefold. First, the OEs of foam and silicone earplugs are simulated using an axi-symmetric linear elasto-acoustic FE model of the human external ear. The numerical OEs are compared to experimental reference data measured in two healthy reference groups using a custom molded silicone earplug and a foam earplug to validate the numerical model. Second, the numerical OEs obtained with the axi-symmetric FE model are compared to two existing gold standard OE models to further validate the proposed axi-symmetric FE model in terms of its material properties as well as its boundary and load conditions. Third, existing earplug type related OE differences are discussed using power balance computations between the exchanged and dissipated time averaged acoustic powers in the occluded ear canal cavity as well as in the earplug.

4.3 Methodology

4.3.1 Geometrical layout of the axi-symmetric external ear model

Figure 4.1 illustrates the geometrical layout used in the present study. The ear canal and earplug are represented as straight cylinders of identical cross-sectional areas (see dimension L2 in Figure 4.1). The ear canal walls are formed by a cylindrical skin layer which is surrounded by a cylindrical cartilage layer in the lateral outer ear (close to ear canal opening) and a cylindrical bone layer in the medial outer ear (close to the eardrum). In the literature different cartilage to bone tissue volume ratios around the ear canal have been reported (e.g. Alvord and Farmer, 1997; Lucente et al., 1995; Oliveira and Hoeker, 2003; Stenfelt et al., 2003). The present model assumes that half of the ear canal is backed by cartilaginous tissue and the other half by bony tissue. To account for the thicker skin tissue of the cartilaginous ear canal wall (e.g. Lucente et al., 1995), the skin tissue of the lateral ear canal wall is slightly thicker than that of the medial half. The anatomical landmarks of the pinna are not accounted for in the present model, mainly to preserve the axi-symmetry of the system. The ear canal entrance region geometry is constructed from a protruding outward extension of the cartilage tissue that backs the lateral ear canal and the skin tissue on the ear canal walls.

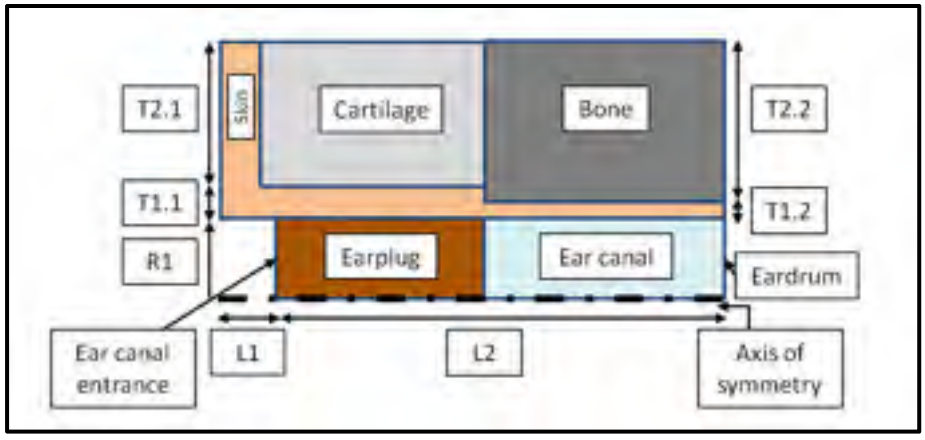

Figure 4.1: Geometrical layout of the axi-symmetric FE model including the ear canal, earplug, cartilaginous tissue, skin tissue and bony tissue. The axis of symmetry is indicated through a dash-dotted line. All model identifiers are provided in Table 4.1

The external ear dimensions vary between subjects. Prior to this study, the model's sensitivity to these dimensions was examined within naturally occurring upper and lower limits using a two-level sensitivity analysis. All upper and lower levels of the ear dimensions were taken from the literature. Table 4.1 summarizes the geometrical parameter range considered during this preliminary sensitivity analysis.

Table 4.1: Geometrical parameter range studied during the sensitivity analysis concerning the external ear geometry

		Dimension [mm]		
Identifier	Dimension name	Lower level	Upper level	Comments
L1	Protrusion at canal entrance	2	5	70% skin, 30% cartilage
L2	Ear canal length	25	37	50% cartilage backed, 50% bone backed
R1	Ear canal radius	3	4.2	
T1.1	Lateral canal wall thickness	0.5	1	Medial wall 80% thinner than lateral wall
T1.2	Medial canal wall thickness	0.1	0.2	
T2.1	Lateral skin and cartilage thickness	10	20	
T2.2	Medial bone tissue thickness	10.4	20.8	

The protrusion at the ear canal entrance (L1) was considered at 2 mm and at 5 mm length. At both levels the ratio of cartilage to skin was kept constant. The 2 mm length resulted from average thickness data of the auricular cutis, subcutis and cartilage (Danter et al., 1996). The upper level (see Table 4.1) for dimension L1 was hypothesized. The ear canal length was considered at the maximum valuereported by Stinson and Lawton (Stinson and Lawton, 1989). The lower level value corresponded to average ear canal length data reported in the literature (e.g. Alvord and Farmer, 1997; Johansen, 1975). Stinson and Lawton's (1989) individual data were used in the present study to define the lower and upper levels for the ear canal radii. The resulting radii varied between 3 mm and 4.2 mm. At the high level, the

lateral skin thickness and the medial skin thickness equaled 1 mm and 0.2 mm, respectively (Lucente et al., 1995). At the low level the lateral skin thickness was reduced to 0.5 mm (Lucente et al., 1995) and the medial skin thickness reduced to 0.1mm, because the ear canal wall thickness ratio was assumed to be constant. Besides, Jahn and Santos-Sacchi (Jahn and Santos-Sacchi, 2001) stated that the bone backed ear canal skin thickness could be as little as 15 µm to 30µm (for the epidermal layer). Lastly, the cartilage tissue that backs the ear canal was considered at a thickness of 20 mm (upper level) and at a thickness of 10mm (lower level). Consequently, the bone tissue thickness varied between 10.4mm and 20.8mm to account for the constant thickness ratios of the lateral and medial ear canal walls.

A two-level factorial design was implemented in STATGRAPHICS Centurion XVI (©StatPoint Technologies, VA, USA). The geometrical parameters outlined in Table 4.1 were defined as +1-levels and -1-levels. Due to the abovementioned fixed ratios between some of the geometrical parameters (e.g. lateral and medial ear canal wall) the resulting two-level factorial design consisted of a total of five parameters (2^5, resolution V+). The obtained run sheet was imported as input parameters into COMSOL Multiphysics (COMSOL®, Sweden) for numerical simulation. The transfer function levels of the open and occluded ear models (both silicone and foam earplugs) served as response variables and where analyzed at five third octave band center frequencies (0.125 kHz, 0.25 kHz, 0.5 kHz, 1 kHz and 2 kHz), which also correspond to the four test center frequencies of the experimental study (see section 4.3.6). The obtained numerical results were re-imported into STAGRAPHICS (©StatPoint Technologies, VA, USA) for multi-response optimization. One geometrical configuration could be identified that provided satisfying OE predictions for both earplug test groups independently of the chosen boundary and load conditions. This configuration was selected for the present study. Table 4.2 summarizes the dimensions of the selected configuration.

Table 4.2: Overview of the geometrical dimensions used in the axi-symmetric external ear model subsequent to the implementation the geometrical sensitivity analysis

Identifier	Dimension name	Value [mm]	Comments
L1	Protrusion at canal entrance	2	70% skin 30% cartilage
L2	Ear canal length	25	50% cartilage backed 50% bone backed
R1	Ear canal radius	4.2	n/a
T1.1	Lateral canal wall thickness	0.5	n/a
T1.2	Medial canal wall thickness	0.1	n/a
T2.1	Lateral skin and cartilage thickness	20	n/a
T2.2	Medial bone tissue thickness	20.4	n/a

4.3.2 Material properties of the external ear tissues and the earplug models

The implementation of a linear elasto-acoustic finite element model of the external ear requires the assessment of Young's moduli, densities, loss factors and Poisson's ratios of the bony, cartilaginous and skin tissues, respectively. Usually, these tissue domains exhibit viscoelastic, non-linear, anisotropic material behavior and their properties vary as a function of age and gender. While the assumption of linear stress-strain behavior seems reasonable for small tissue deformations (Fung, 1993), the hypothesis of isotropic elastic material characteristics introduces a simplification. Such simplification seems presently inevitable due to a lack of material data in terms of anisotropy, homogeneity, parameter frequency dependency and pre-stress state. For the present model, the linear elastic material properties of Brummund et al. (2014) are being utilized. These material properties have repeatedly shown to yield satisfying numerical results when compared to experimental data. Nevertheless, further research is necessary to accurately determine the error introduced by the abovementioned simplifications. Table 4.3 summarizes the material properties of the bony, cartilaginous and skin tissue domains used in this work. The speed of sound and density of the air inside ear canal cavity are equal to 343.2 m/s and 1.2 kg/m^3 respectively.

Table 4.3: Material properties used for modeling of the external ear tissues

		Density [kg/m^3]	Young's mod. [MPa]	Poisson's ratio	Loss factor
Bone	Value	1714	11316	0.3	0.01
	Anatomical site	Mean over skull	Mean over temporal bone	Mean over temporal bone	Assumed
	Reference	Delille et al. (2007)	Delille et al. (2007)	Peterson and Dechow (2003)	n/a
Cartilage	Value	1080	7.2	0.26	0.05
	Anatomical site	Human articular	Human septum	Human septum	Assumed
	Reference	Cox and Peacock (1979)	Grellmann et al. (2006)	Grellmann et al. (2006)	n/a
Skin	Value	1100	0.5	0.4	0.1
	Anatomical site	Average skin density	Breast skin model	Assumed	Assumed
	Reference	Duck (1990)	Sarvazyan et al. (1995)	n/a	n/a

Two cylindrical earplug models were used to occlude the ear canal. Both earplug models are kept flush with respect to the ear canal entrance and are assumed to fit the ear canal without deforming the ear canal walls upon insertion. This assumption seems reasonable for soft foam and custom molded earplugs. Additionally, the earplug seal is assumed to be free of any leaks and the earplug models are hypothesized to exhibit linear elastic, isotropic material behavior. First, a silicone earplug of known material properties (Sgard et al., 2010) is considered at one insertion depth (11.7 mm). This insertion depth corresponds to the experimental mean insertion depth (see section 4.3.6) which was determined with respect to the ear canal entrance by the experimenter. Note that due the earplug design and its molding procedure (e.g. silicone flows into a rubber pouch of constant dimensions) deep occlusion to the second bend is not possible with this earplug. Second, a foam earplug is used to occlude the ear canal at four occlusion depths (7 mm, 9.2 mm, 11.1 mm, 22 mm). Here, four occlusion depths are used, because more reference data are available for this earplug type. The shallow (7mm, 9.2mm) and deep occlusion (22mm) conditions correspond to the

occlusion depths of Stenfelt and Reinfeldt's (2007) as well as of Schroeter and Poesselt's (1986) models which serve as reference for the present study. The 11.1 mm occlusion depth corresponds to the mean experimental occlusion depth of the present study which was determined with respect to the ear canal entrance. The foam earplug's material properties were drawn from the literature (James, 2006). James (2006) determined the material properties for several compressive radial strain conditions (6%, 18%, and 30%). In the present study, the 30% radial strain and 10mm earplug length are being used, because 30 percent radial strain corresponds best to the ear canal radius of the simplified model (see Table 4.2) and the earplug length approximately corresponds to the experimental insertion depth used in the experimental part of this study. Table 4.4 summarizes the used material properties.

Table 4.4: Material properties of earplugs used in the present study to occlude the external ear model

	Density [kg/m^3]	Young's mod. [MPa]	Poisson's ratio	Loss factor	Reference
Silicone plug	1050	0.85	0.48	0.1	(Sgard et al., 2010)
Foam plug (30% radial strain 10mm length)	220	0.1 Long term modulus	0.1	0.5 (assumed)	(James, 2006)

4.3.3 Boundary and load conditions

Ideally, the connections that exist between the external ear boundaries and their adjacent tissue domains ought to be expressed using transfer impedance boundary conditions. Their assessment, however, has been shown to be challenging (Viallet et al., 2013). In the present study more conventional boundary conditions have been used as a first approximation. The chosen boundary condition configuration is illustrated in Figure 4.2.

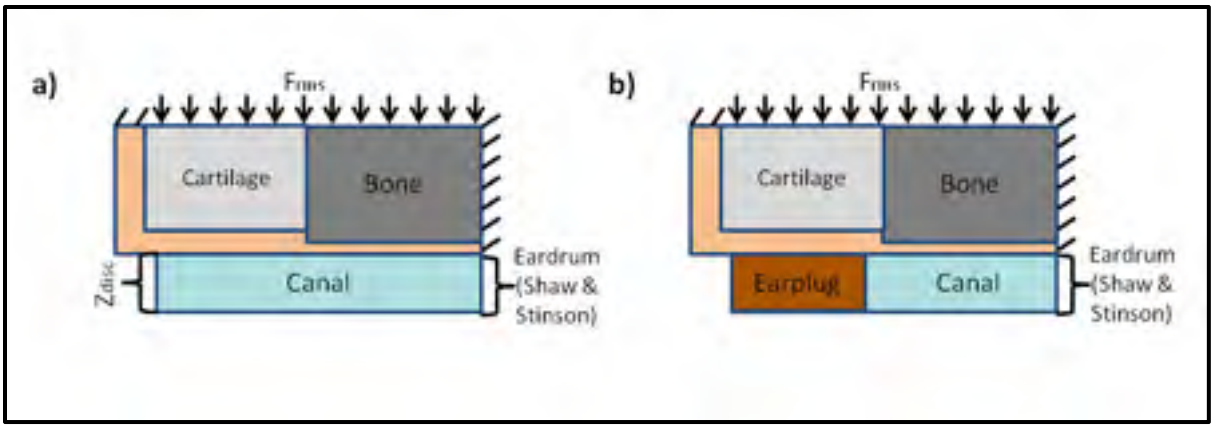

Figure 4.2: Boundary and load conditions employed in the present study for the open (a) and occluded (b) external ear model. Arrows indicate boundaries at which loading was introduced in normal direction. Brackets denote impedance boundary conditions used to model the eardrum and the ear canal entrance (open ear only). Unmarked boundaries indicate free boundary conditions

The horizontal boundary of the ear canal entrance region and the medial, vertical boundaries of the bone and skin tissue are considered as fixed in the present model to express the rigid connection between the tympanic portion of the temporal bone (location of the bony ear canal) and other portions of the temporal bone (e.g. squamous portion). A structure borne mechanical boundary load (F_{rms}) is introduced normally and uniformly on the horizontal boundaries of the cartilage and bone tissues. It must be noted that this loading condition represents an idealization of the real stress vectors which act on the human tissues, which likely vary in terms of amplitude, phase and direction along the tissue boundaries. A locally reacting impedance boundary condition that corresponds to the radiation impedance of a baffled flat circular piston is used to model the open ear canal entrance. A second locally reacting specific acoustical impedance boundary condition (Hahn, 1985; Shaw and Stinson, 1981) is used to model the tympanic membrane. It is applied on the medial vertical boundary of the ear canal. It should be noted that expressing the eardrum through an impedance boundary condition does not allow for the sound radiation that stems from the inertial movement of the ossicles to be considered. The latter has been shown to influence bone conduction sound in the mid-frequencies (around 1-3 kHz) (Stenfelt and Goode, 2005; Stenfelt et al., 2002).

4.3.4 Finite element modeling

Assuming small deformations and a temporal dependency $e^{j\omega t}$ for all fields, the wave propagation in the cartilage, bone, and skin tissue domains is governed by the linear elasto-dynamic equation

$$\hat{\sigma}_{ij}^{k}\left(\underline{\hat{u}}^{k}\right) + \omega^2 \rho_s^k \hat{u}_i^k = 0 \tag{4.1}$$

j, ω, $\hat{\sigma}_{ij}^{k}$, , ρ_s^k, and $\hat{u}_i^k$ correspond to the imaginary unit, angular frequency, stress tensor, density, and displacement vector of a given domain k, respectively. Structural damping is accounted for through a multiplier $(1 + j\eta_s^k)$ in the stiffness matrix where η_s^k corresponds to the isotropic structural loss factor (see Table 4.3) of a given domain k. The ear canal sound pressure is governed by the Helmholtz equation

$$\Delta\hat{p} + k^2\hat{p} = 0 \tag{4.2}$$

$\hat{p}$ denotes the sound pressure and $k = {\omega}/{c}$ is the wavenumber, c is the sound speed in the ear canal. Coupling between the solid and acoustical domains is introduced via the continuity of stress vectors $\hat{\sigma}_{ij}^{k} n_j = -\hat{p} n_i$ and normal displacements $\frac{\partial \hat{p}}{\partial n} = \rho_{air}\, \omega^2 \hat{u}_i^k n_i$ where n corresponds to the unit normal vector that points outward a solid domain k.

The solid domains and the ear canal are meshed according to a convergence criterion of four elements per wavelength at 3 kHz using quadratic triangular elements. Open and occluded models are solved separately. The open model consists of 979 solid and 730 acoustic quadratic triangular elements. The occluded models consists of 1136 solid and 673 acoustic elements (silicone earplug and 11.7mm occlusion) as well as 1968 solid and 775 acoustic elements (foam earplug and 11.1mm occlusion). For the 7mm, 9.2mm and 22mm occlusion depths with the foam earplug 1871, 1939, 2764, solid and 788, 756, 212 acoustic elements are used, respectively.

4.3.5 Computation of the numerical occlusion effects and exchanged powers

The power spectral density (PSD) of the bone transducer's RMS-force was used to mechanically excite the open and occluded models, respectively. The open and occluded models were solved for the sound pressure level at the center of the tympanic membrane. The frequency resolution equaled twenty evenly spaced points in each third octave band. Third octave integration was carried out in MATLAB (MathWorks®, MA, USA) to obtain the third octave responses for the mean square pressure at the center of the eardrum. The OEs were obtained through subtraction of the occluded and open ear mean square pressure at the center of the eardrum.

In the present study, the time averaged acoustic powers that are exchanged between the ear canal walls and the ear canal (open and occluded models) and between the inner earplug surface and the ear canal (occluded models) are calculated using (Pierce, 1991)

$$\bar{W}_{exc,i} = \frac{1}{2}\Re\left[\int_{S_i} \hat{p}\hat{v}_n^* dS\right], \tag{4.3}$$

where $\hat{p}$ corresponds to the complex acoustic pressure, $\hat{v}_n^*$ is the complex conjugate of the acoustical normal particle velocity and S_i is the contact surface between a solid and a fluid domain. To determine the time averaged power that is dissipated at the tympanic membrane whose area is referred to as $S_{eardrum}$ (open and occluded models), $\hat{v}_n^*$ can be expressed in terms of the acoustic impedance of the eardrum $\hat{Z}_{eardrum}$. The dissipated power then reads

$$\bar{W}_{diss,eardrum} = \frac{1}{2}\Re\left[\int_{S_{eardrum}} \frac{|\hat{p}|^2}{\hat{Z}_{eardrum}^*} dS\right]. \tag{4.4}$$

In addition to these powers, the time averaged powers that are exchanged at the ear canal walls in contact with the earplug and the time averaged dissipated power inside the earplug volume are calculated. The time average power that is exchanged at an interface surface S_i of two solids can be calculated using

$$\bar{W}_{exc,i} = -\frac{1}{2}\Re\left[\int_{S_i}(\hat{\sigma}_{ij}\hat{v}_i^*)n_j\, dS\right], \tag{4.5}$$

where $\hat{\sigma}_{ij}$, $\hat{v}_i^*$, n_j correspond to the stress tensor, the complex conjugate of the solid particle velocity vector and the normal vector. The time averaged dissipated power due to structural damping inside a solid volume V_i can be calculated using

$$\bar{W}_{exc,i} = \frac{1}{2}\Re\left[-i\omega\int_{V_i}\hat{\sigma}_{ij}\hat{\varepsilon}_{ij}^*\, dV\right]. \tag{4.6}$$

Here, $\hat{\sigma}_{ij}$ and $\hat{\varepsilon}_{ij}^*$ correspond to the stress tensor and the complex conjugate of the strain tensor.

4.3.6 Experimental measurements

The experimental procedure summarized hereafter is part of a larger study that aims at comparing subjective and objective measurement methods for hearing protector attenuation and the OE (Nélisse et al., 2013). A total of 37 subjects aged 20 to 60 years volunteered to participate in this study. All subjects were found to have hearing thresholds < 25 dB HL in the frequency range 0.125 kHz to 8 kHz (ANSI, 2008). The test subjects were divided into two groups. For the first group (18 subjects) custom molded earplugs served as occlusion device. For the second group a foam earplug served as occlusion device. The apparatus and experimental protocol were identical for both groups. Thus, the outlined steps apply to the silicone earplug group and to the foam earplug group.

All measurements were conducted inside a semi-anechoic room suited for measurement of hearing protection device attenuation (ANSI, 2008; ISO, 1992). Two Knowles FG-23329 miniature microphones (©KNOWLES Electronics, IL, USA) were used to measure the sound pressure levels inside the right ear canal (open and occluded) and at the ispilateral tragus. The tragus microphone mainly served to monitor the bone transducer's airborne noise emission. A 1-inch 40HF (©G.R.A.S. Sound & Vibration, Denmark) control microphone was placed

30 cm above each subject's head. The stimulus was provided using a B-71 bone transducer (©Radioear Corporation, PA, USA). The bone transducer was securely attached (static force about 5N) to each subject's right mastoid process for ipsilateral stimulation.

Prior to experiment onset each subject was instrumented with the miniature microphones and the bone transducer. Additionally, the custom-made earplugs were molded for the participants of the silicone group. Third octave band limited noises were generated in the bands 0.125 kHz, 0.25 kHz, 0.5 kHz, 1 kHz and 2 kHz. Ten second time recordings were performed in each band at each microphone. The stimulation magnitude of the bone transducer was adjusted at each frequency until a sound pressure level reading was obtained at the ear canal microphone. This magnitude remained constant for open and occluded measurements in each participant and did not result in any discomfort. Upon completion of the open ear measurements the test subjects were either equipped with a custom molded silicone earplug (insertion depth with respect to ear canal entrance: 11.7mm ± 1.3mm [mean ± S.D.]) or a foam earplug (insertion depth with respect to ear canal entrance: 11.1mm ± 2.6mm [mean ± S.D.]) depending on their test group. Experienced participants user fitted their earplug, whereas inexperienced participant received an experimenter fit. Upon earplug insertion the abovementioned protocol was repeated.

Obtained time recordings were analyzed separately for each third octave band. The OE was determined through subtraction of the occluded and open sound pressure levels (SPLs).

4.4 Results and discussion

4.4.1 Occlusion effect predictions for foam and silicone earplugs

Figure 4.3a and Figure 4.3b illustrate the numerical OE predictions obtained for the foam (11.1 mm insertion) and the silicone (11.7 mm insertion) earplug models. The experimental OEs (mean ± S.D.) are included for comparison.

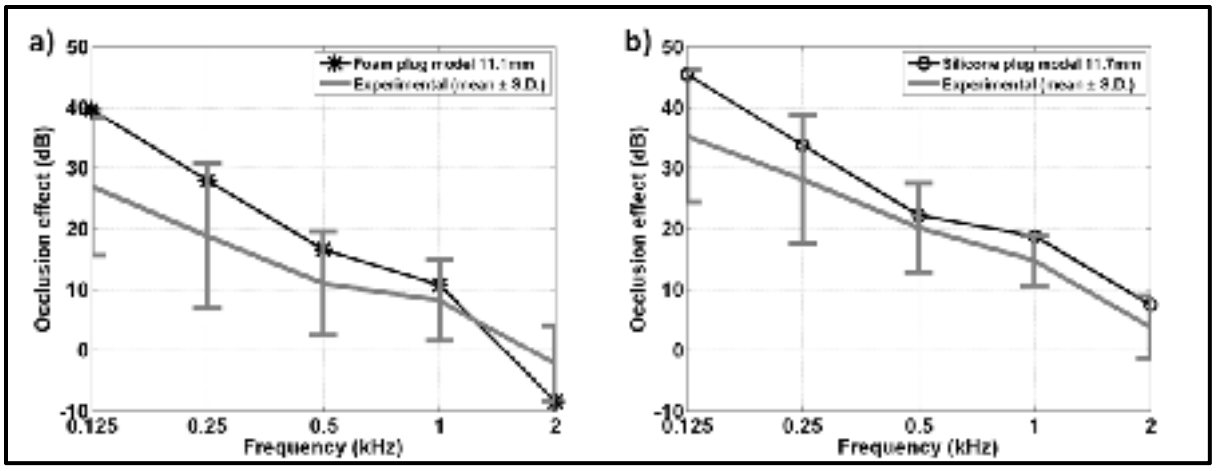

Figure 4.3: Comparison of numerical OE predictions and experimental OE measurements. a) foam earplug occlusion device inserted 11.1 mm into the ear canal with respect to the ear canal entrance in both numerical and experimental conditions. b) silicone earplug occlusion device at 11.7 mm insertion with respect to the ear canal entrance

At frequencies up to 1 kHz the numerical OE obtained for the foam earplug model (Figure 4.3a) overestimates the experimental mean value by 13 dB, 9 dB, 6 dB and 3 dB, respectively. At 2 kHz the numerical model under predicts the experimental mean OE by 6 dB. The numerical OE falls inside the range of the mean ± one standard deviation of the experimental data, albeit close to the lower boundary at 0.125 kHz and 2 kHz.

The numerical OE obtained for the silicone earplug (Figure 4.3b) overestimates the mean experimental data obtained for this earplug at 0.125 kHz and 0.25 kHz by 10 dB and 6 dB, respectively. The smallest deviation between the numerical and experimental data is obtained at 0.5 kHz (2 dB). At 1 kHz and 2 kHz the numerical model over predicts the mean experimental OE by 3 dB and 4 dB, respectively. The numerical OE obtained for the silicone earplug falls inside the range defined by the mean ± one experimental standard deviation at all frequencies. At 0.125 kHz, 1 kHz and 2 kHz, however, the predicted numerical OE is close to the upper boundary.

Similar deviations were obtained by Stenfelt and Reinfeldt (2007) who implemented a lumped element OE model. The authors compared the OE predictions to median

experimental OE data obtained for occlusion with a foam earplug (7 mm insertion). The model overestimated the experimental ear canal sound pressure level OE for frequencies up to 1kHz by about 10 dB (0.125 kHz), 3 dB (0.25 kHz), 5 dB (0.5 kHz), and 3 dB (1 kHz). At 2 kHz Stenfelt and Reinfeldt's (2007) model coincides with the experimental OE.

In the present study, two factors could explain the low frequency deviation between the numerical and experimental OEs of both earplug types. First, the numerical model does not account for earplug leaks. Earplug leaks of sufficient diameter could reduce the occluded transfer function levels and hence reduce the numerical occlusion effect. Second, a low signal to noise ratio due to the presence of airborne sound emission from the bone transducer could have contributed to increase the experimental open ear transfer function level in the present study. Some evidence for the presence of earplug leaks in the present study is provided by the insertion loss data (Figure 4.4a) which exhibit a large inter-subject variability throughout the entire frequency range for both earplug models. Additionally, at low frequency the sound pressure level (SPL) at the open in-ear microphone is very similar to the reference microphone SPL at the ipsilateral tragus which could indicate the presence of airborne sound emission from the bone transducer. As the SPL at the reference microphone only changed a little at the low frequencies upon occlusion it is unlikely that the measured SPL at the tragus microphone leaked out from the open ear canal for the BC stimulus.

Figure 4.4a and Figure 4.4b illustrate the experimental insertion loss data and the sound pressure level at the in-ear and ipsilateral tragus microphones. Only the foam earplug group is depicted here, but similar results were obtained for the silicone earplug.

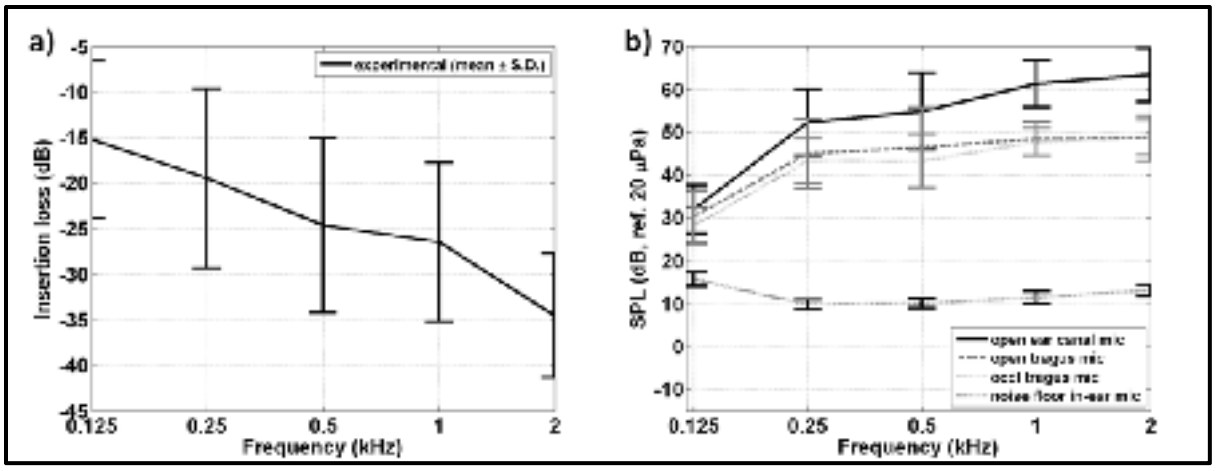

Figure 4.4: a) insertion loss data (mean ± S.D.) measured for foam earplug test subjects for a mean earplug insertion depth of 11.1mm. b) sound pressure level data (mean ± S.D.) obtained for the open ear and occluded ear measurements of the foam earplug test subjects. The solid black line corresponds to the sound pressure level at the open in-ear microphone. The dashed grey line indicates the sound pressure level at the ipsilateral tragus reference microphone (open ear). The dotted grey line indicates the sound pressure level at the ipsilateral tragus reference microphone (occluded ear). The dotted black line represents the noise floor of the in-ear microphone (open ear)

Stenfelt and Reinfeldt (2007) argue that the inter-subject variability observed at low frequency in their experimental data can be attributed to low microphone sensitivity. In the present study this explanation seems unlikely as the noise floor of the in-ear microphone lies well below the measured open ear SPL at the in-ear microphone (see Figure 4.4b).

Deviations between the numerical and experimental OEs in the present study that occur at higher frequencies could be due to differences with respect to the model geometry and the external ear geometries of the examined healthy reference groups. For instance, large geometrical variability with respect to the ear canal length can cause shifts in the quarter wavelength resonance of the open ear canal (up to 0.7 kHz when the ear canal length changes from 27 mm to 37 mm). Some evidence for this explanation is supported by the fact that the numerical model better fits the mean experimental OE of the silicone earplug group as compared to the foam earplug group. As different test subjects were used for each group it might be possible that the simplified external ear geometry better fits the average geometry

of the former test group. Assessing the contribution of interindividual external ear geometry differences is presently not possible due to a lack of data.

Furthermore, model assumptions might contribute to explain the deviations which occur at the mid and higher frequencies. For instance, the impedance boundary condition used to model the tympanic membrane does not account for sound pressure that originates from inertial movement of the ossicles which has been shown to influence BC sound in the mid frequencies (1-3kHz) (Stenfelt and Goode, 2005; Stenfelt et al., 2002). Other model limitations of importance include inaccuracies with respect to the chosen material properties (e.g. earplug, ear tissues) and boundary conditions, the assumption of linear elastic material behavior as well as modeling of the external ear as compared to the entire head.

4.4.2 Comparison of modeling results with existing lumped OE models

Figure 4.5a and Figure 4.5b compare the OE predictions obtained with the present model to Stenfelt and Reinfeldt's (Stenfelt and Reinfeldt, 2007) as well as Schroeter and Poesselt's (1986) OE predictions which were taken from the literature. These models are referred to as "Stenfelt model" and "Schroeter model" for convenience. The following paragraphs provide a brief summary of both models. More detailed information can be found in (Stenfelt and Reinfeldt, 2007) and (Schroeter and Poesselt, 1986).

Stenfelt's model is a lumped element ear canal model with variable cross sectional area (four acoustic impedances which are based on the average ear canal area data from Stinson and Lawton (1989) to predict the objective earplug occlusion effect, among others. The ear canal is approximately 29 mm long. The acoustical radiation impedance of the open ear canal entrance as well as the mechanical impedance of the eardrum and middle ear in this model were taken from Hudde and Engel (1998). The earplug occlusion device is modeled as an infinite impedance that can be introduced at variable insertion depths. The Stenfelt model uses two coupled volume velocity sources that are located in the cartilaginous and bony portions of the ear canal. The sources are tuned with the help of experimental ear canal sound

pressure measurements (Stenfelt et al., 2003) and can be scaled to the unoccluded ear canal wall area in order to simulate varying occlusion depths.

Schroeter's model is an acoustical transmission line of 21 mm ear canal length (center of eardrum) and 7.5 mm ear canal diameter. It aims at predicting the objective occlusion effect of a foam earplug, among others. Schroeter's model uses an adapted version of the middle ear model of Shaw and Stinson (1981) which includes a volume velocity source to model middle ear inertia (not considered here). A second volume velocity source is placed in the middle of the unoccluded ear canal to model external ear bone conduction (used in present comparison). The gain of this source can be adjusted to simulate varying insertion depths in the cartilaginous meatus (bony occlusion not considered). The magnitudes of the middle ear and ear canal volume velocity sources in Schroeter's model were calculated from experimental threshold sound pressure level data. The radiation impedance of the open ear and the mean occlusion impedance for the intra-aural earplugs used in Schroeter's model were measured experimentally using a special artificial test fixture.

To facilitate comparing the OE predictions obtained with the reference models, the present model is adapted in terms of its geometry and boundary conditions, when possible.

To reproduce Stenfelt's configuration as closely as possible, the ear canal length of the present model is extended to match the 29mm ear canal length of Stenfelt's model. The four variable mean ear canal cross sections of Stenfelt's model are not considered since the present model uses a constant cross-section cylinder. A variable cross-section cylinder could definitely be implemented in future work to improve the realism of the proposed model. Instead, a constant mean radius of 3.7 mm is used. This radius corresponds to the mean radius of Stinson and Lawton's (1989) average ear canal area curve. Additionally, the acoustical radiation impedance as well as the eardrum and middle ear model of Hudde and Engel (1998) are applied to the present model.

Regarding the comparison with Schroeter's model, the ear canal length of the present model is reduced to 21 mm and the ear canal radius is reduced to 3.75 mm.

The occlusion device used for all comparisons is the foam earplug type described in Table 4.4 which is inserted 7 mm, 22 mm and 9.2 mm into the ear canal depending on the reference model.

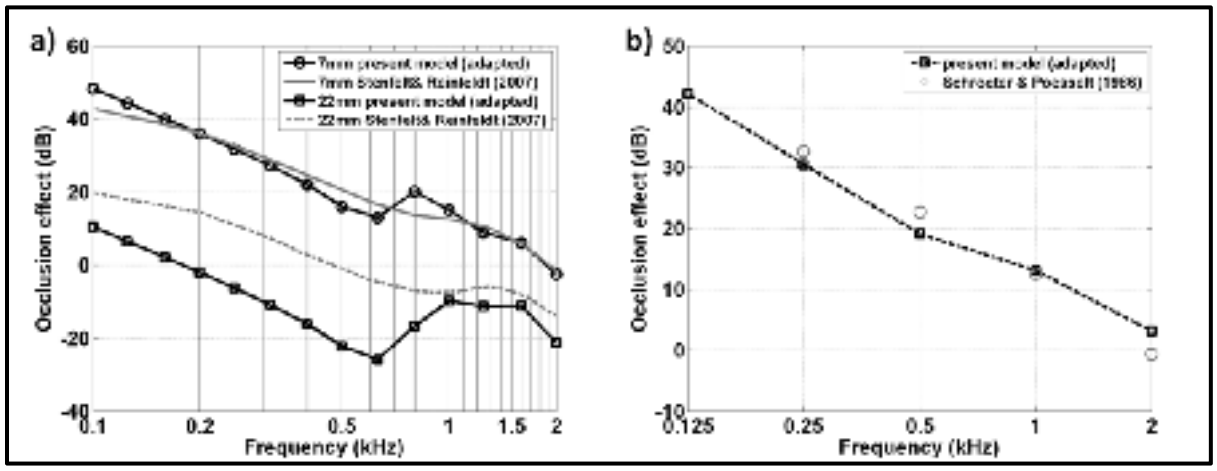

Figure 4.5: a) comparison of OE predictions obtained with the FE model to OE predictions obtained by Stenfelt and Reinfeldt (2007) at shallow (7 mm) and deep (22 mm) earplug insertion. b) comparison of OE prediction obtained with the FE model to prediction obtained by Schroeter and Poesselt (1986) at one occlusion depth (9.2 mm)

Except for smalls deviation around 0.125 kHz (on average 5 dB) and at 0.8 kHz (6 dB) the numerical OE prediction for the 7 mm occlusion agrees very well with the simulation result of Stenfelt's model (Figure 4.5a). Similarly, the OE prediction obtained for the present model is in very good agreement with the simulation result obtained by Schroeter's model for the 9.2mm occlusion (Figure 4.5b).

The OE deviations that exist between the present model and the reference models at shallow occlusion, and in part at deep occlusion (see subsequent paragraph), originate from modeling differences. For instance, Stenfelt models the earplug as an infinite acoustical impedance. In terms of geometry, Stenfelt's model also differs from the present model as the authors use the

average ear canal area function of variable cross sectional area measured by Stinson and Lawton (1989). Schroeter's model mainly differs from the present approach in terms of the chosen open ear radiation impedance (measured in Schroeter's work versus calculated using a baffled piston model in this work) and the way the earplug is modeled (occlusion impedance in Schroeter's work versus linear-elastic solid domain in this work)

At 22 mm earplug insertion the proposed model results in a considerably smaller OE (about 10 dB around 0.125 kHz and up to 20 dB around 0.5 kHz) than Stenfelt's model for frequencies up to 1 kHz. Above 1 kHz, both models are in good agreement. For frequencies below 1 kHz and 22 mm occlusion, the present model predicts a small OE. This was to be expected since the earplug is inserted very deeply into the ear canal . The OE predicted by Stenfelt's is much larger). Note that Stenfelt and Reinfeldt (2007) report that their simulated OE magnitude was about 5 dB too large compared to their experimental OE data, for frequencies between 0.3 kHz and 0.7 kHz and deep occlusion. Nevertheless, their OE prediction remains closer to the experimental data than the present model between 0.3kHz and 0.7kHz. Overall these results suggest that the OE prediction obtained with the present model at 22 mm occlusion for frequencies < 1kHz might be some 10 to 15 dB too small in magnitude compared to both the experimental and simulation data by Stenfelt and Reinfeldt (2007). This outcome could indicate a limitation of the present model at deep insertion with respect to literature data. Nevertheless, it would be desirable to compare the present model to further experimental data in the future. An important factor that might contribute to explain the deviations observed at deep occlusion is the earplug insertion depth itself. Berger (2013) underlined the importance of monitoring this parameter. A difference between an insertion of 50-60% and 80%-100% of the total earplug length can induce real ear attenuation differences of the order of 10 dB for foam earplugs. For frequencies up to 1 kHz the present model proves to be very sensitive to the chosen earplug insertion depth. Calculations for a 18 mm insertion depth (not shown in Figure 4.5) reveal an average OE increase of 12 dB at these frequencies compared to the 22 mm insertion, confirming Berger experimental results. Additionally, Tufts (2013) reported similar trends as Berger (2013) for the real ear attenuation of custom molded earplugs. Unfortunately, in Stenfelt and Reinfeldt (2007)

details on how the 22 mm earplug insertion was achieved and which earplug type was used as occluding device were not provided. An error of a few millimetres about this insertion depth could explain the differences with Stenfelt's results. Another factor that is crucial to explain the deviations at low frequencies for the 22 mm occlusion is the way in which the excitation is accounted for in the models. The interrelated volume velocity source in the bony ear canal (open ear) of Stenfelt's model generates about 10% of the volume velocity that is generated by the volume velocity in the cartilaginous ear canal at the lowest frequencies. In the present model, however, the time averaged acoustical power that is exchanged between the bony ear canal and the ear canal cavity only amounts to about 0.05% of the power exchanged between the cartilaginous ear canal wall and the ear canal cavity. The latter is, among others, due to the chosen material properties of the external ear tissues and the chosen boundary and load conditions.

The increase in OE above 1 kHz observed for the present model might mainly be due to the presence of two radiating modes for the foam earplug which exist around 1.4 kHz and 1.6 kHz. While Stenfelt's model also predicts a small, much less pronounced bump around 1.6 kHz the aforementioned explanation does not apply as the authors modeled the earplug as infinite impedance. Nevertheless, to tune their coupled volume sources Stenfelt et al. used experimental ear canal sound pressure level data (Stenfelt et al., 2003). Hence, the small bump observed in Stenfelt's OE prediction could be due to a radiating mode of the occlusion device used in Stenfelt et al. (2003). Due to a lack of data (material properties and insertion depth) of the class cover used in (Stenfelt et al., 2003) it is presently not possible to further investigate this possibility. The results obtained around 1.6 kHz should be interpreted cautiously.

4.4.3 Comparison of the exchanged and dissipated powers in the occluded numerical models

Power balances provide a valuable means to further investigate the OE differences that exist between both earplug types. The latter differences could be observed both experimentally

and numerically. In the following, the term time averaged power is denoted as power for convenience. Figure 4.6 illustrates a scatter plot of the dissipated powers (mean values in each band up to 1 kHz) at the tympanic membranes of the occluded external ear models (diamond markers refer to right hand ordinate). Additionally, bar charts (referring to left hand ordinate) are included in Figure 4.6 to indicate how much of the dissipated power (in percent) in each band can be attributed to power that gets exchanged between earplug surface and the ear canal and between the ear canal walls and the ear canal, respectively.

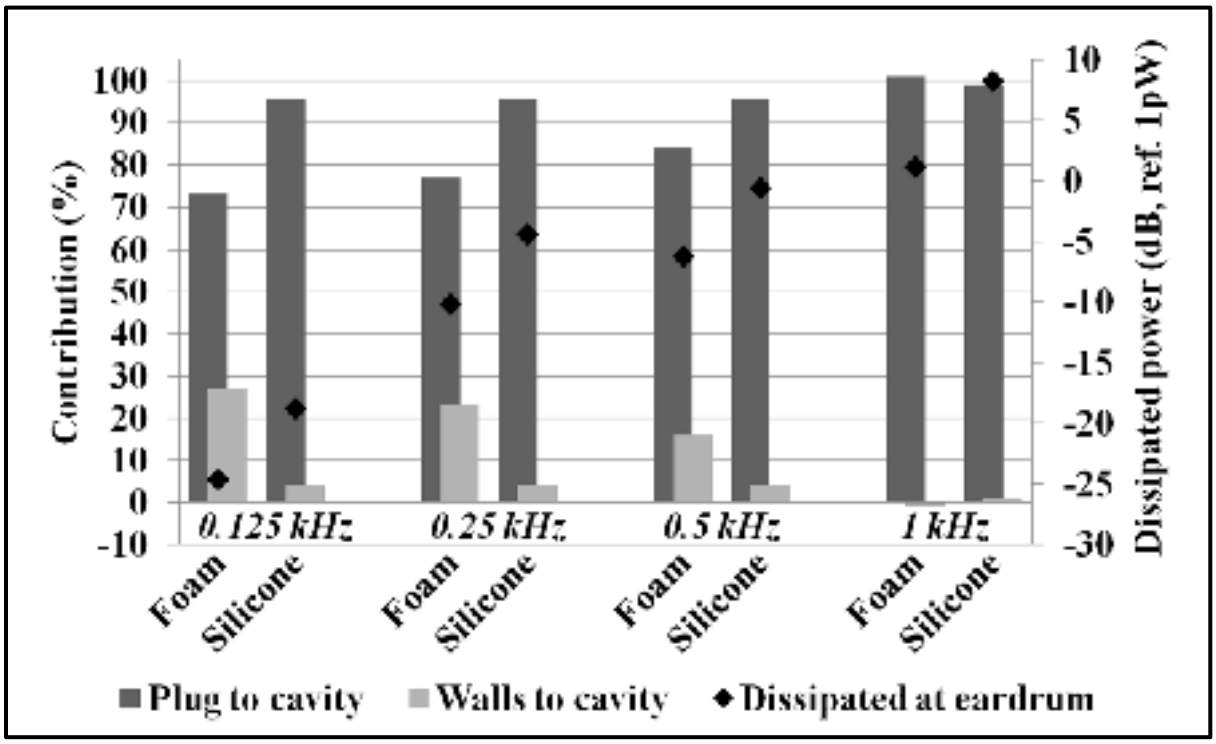

Figure 4.6: Occluded ear canal cavity power balance computation for foam (11.1 mm insertion) and silicone (11.7 mm insertion) earplugs for frequencies up to 1 kHz. Diamond markers refer to right hand ordinate and vertical bars refer to left hand ordinate. At 0.25 kHz about -10 dB of power gets dissipated (right hand ordinate) at the eardrum (black diamond marker) when the *foam* earplug numerical model is used. Of these -10 dB, 77% stem from the medial earplug surface (dark grey bar, left hand ordinate) and 23% stem from the unoccluded ear canal walls (light grey bar, left hand ordinate)

The power dissipated at the tympanic membrane (PDTM) (black diamond markers in Figure 4.6) in the case of the silicone earplug exceeds that in the case of the foam earplug by on

average 6 dB for frequencies up to 1 kHz. For both earplug types the PDTMs are mainly due to the power that gets exchanged between the medial earplug surface and the ear canal cavity (dark grey bars). The contribution of the ear canal walls (light grey bars) in contact with the ear canal cavity is seen to be of secondary importance. At 1 kHz, the PDTMs of both models are almost entirely equal to the power exchanged at the medial earplug surface in contact with the ear canal. For the silicone earplug, 99% of the PDTM stems from the medial earplug surface and only 1% originates from the ear canal walls at 1 kHz. The power exchanged at medial earplug surface of the foam earplug exceeds the PDTM by 1 dB at 1 kHz. Thus, the bar chart indicates a contribution of 101%. The excess power is exchanged at the unoccluded ear canal walls via a negative power flow from the ear canal cavity into the ear canal walls. The latter is indicated through a -1% percent contribution.

The inner earplug surfaces are seen to contribute more to the PDTMs than the ear canal walls in contact with the air cavity for both earplug types. The contribution of the ear canal walls to the PDTMs varies as a function of earplug type (about 4% for silicone earplug and about 22% for foam earplug below 1 kHz, respectively). In this respect it is noteworthy that even though the ear canal wall contribution in percent differs between both earplug models, the exchanged power levels in dB at the ear canal walls are quite similar for both earplug groups (not depicted in Figure 4.6). For instance, up to 0.5 kHz the differences in exchanged power level at ear canal wall between both earplug models amount to about 1.5 dB and to about 4 dB at 1 kHz. This result is likely due to the circumstance that the unoccluded ear canal wall areas are very similar for both occluded models, because the earplug insertion depths are very similar. In comparison, the power level differences (in dB) of the exchanged powers at the inner earplug surfaces are more distinct (about 7 dB up to 1 kHz). The latter observation is relevant, because it provides some evidence that the PDTM differences of the occluded models are primarily due to the chosen earplug model at the considered occlusion depths.

Previous research has shown that the OE magnitude is strongly linked to the sound radiation of the ear canal walls and that the OE decreases as a function of earplug insertion depth partly because (i) the radiating surface of the ear canal walls gradually reduces (Tonndorf,

1972) and because (ii) less sound energy is radiated by the stiffer bony tissue of the medial external ear compared to the softer cartilaginous tissue (Berger and Kerivan, 1983). Thus, it is likely that the present findings are strongly influenced by the chosen earplug insertion depths (11.1 mm foam, 11.7 mm silicone) which occlude the cartilaginous ear canal almost entirely (cartilaginous ear canal length 12.5 mm). In other words the observed contribution of the earplug model to the OE magnitude might be insertion depth dependent.

For instance, the contribution of the bony ear canal to the OE is much smaller than the contribution of the cartilaginous ear canal in the present model (e.g. Figure 4.5a shallow vs. deep occlusion) and it is possible that differences in the amount of exchanged power at the medial earplug surface could become sufficiently crucial (relative to the power exchanged at the unoccluded bony ear canal walls) to influence the OE magnitude when medium occlusion is used.

In this respect it is also important to note the experimental observations made by Lee (2011) who statistically compared the OEs obtained for a foam earplug and a medical balloon type earplug at two insertion depths (2 mm and 11 mm) in one third octave band centered at 0.5 kHz. Lee (2011) reported statistically significant effects of the earplug type on the occlusion effect at 11 mm insertion. At 2 mm insertion, the author observed only a small, statistically insignificant, difference between both earplug types. Additionally, Brummund et al. (2014) used power balances to explain a numerical OE inversion between 1.1 kHz and 1.8 kHz. The authors reported that at medium (15 mm) and deep (22 mm) occlusion the power exchange at the medial earplug surface is the primary contributor to the PDTM, whereas at shallow (7 mm) occlusion more power is transferred from the ear canal walls than from the medial earplug surface in contact with the ear canal.

Interestingly, when the occlusion depths of the silicone and foam earplug (present model) are very shallow (2 mm) the differences in PDTM decrease to only about 1.5 dB at all frequencies (consequently OE differences also amount to 1.5 dB) and the unoccluded ear canal walls primarily contribute to the DPTM at all frequencies and for both earplug models.

These latter findings provide further evidence that the contribution of the earplug model to the observed OE magnitude is insertion depth dependent. Nevertheless, obtained results must be interpreted very cautiously as presently no experimental data (apart from the results provided by Lee (2011) for the medical balloon and foam earplugs) are available to validate these model findings at shallow occlusion.

Figure 4.7 illustrates the power balance for the 2 kHz band (not depicted in Figure 4.6). This band is treated separately, because the sign of the power flow changes within the third octave band and two zones can be distinguished.

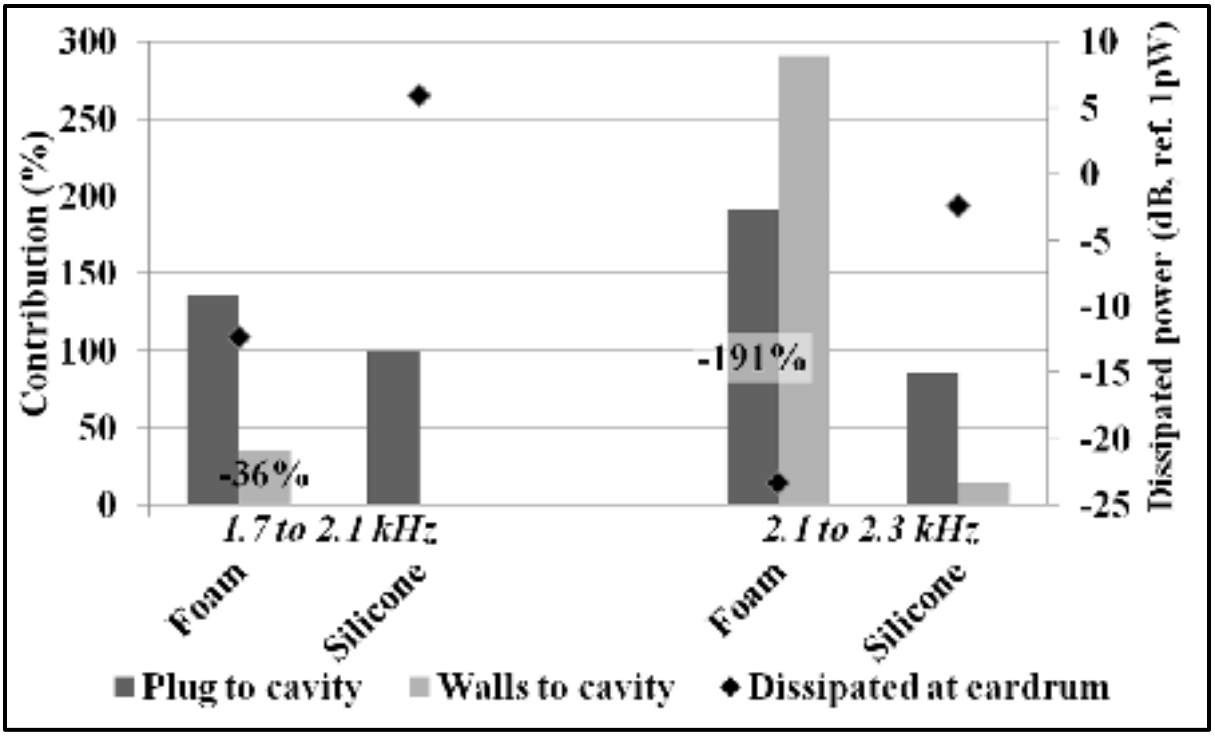

Figure 4.7: Occluded ear canal cavity power balance computation for foam (11.1 mm insertion) and silicone (11.7 mm insertion) earplugs for the 2 kHz third octave band. Diamond markers refer to right hand ordinate and vertical bars refer to left hand ordinate. In this third octave band the power flow changes its sign and two zones can be distinguished. An example on how to read this figure can be found in the caption of Figure 4.6

For frequencies up 2.1 kHz the PDTM of the silicone earplug model is 100% due to the power that is exchanged between the inner earplug surface and the ear canal. In contrast, the

power exchanged at the inner earplug surface of the foam earplug exceeds the PDTM by 36%. This excess power flows from the ear canal cavity into the canal walls (-36%). At frequencies > 2.1 kHz, the power exchanged at the ear canal walls (foam earplug condition) exceeds the PDTM considerably and the excess power flows from the ear canal into the earplug (-191%). The inner surface of the silicone earplug continues to contribute the most (86%) to the PDTM at frequencies > 2.1 kHz. The remaining 14% stem from the ear canal walls. Lastly, in the 2 kHz third octave band, the eardrum dissipates on average 19 dB more power in the case of the silicone model than in the case of the foam earplug model.

Figure 4.6 and Figure 4.7 indicate that the silicone earplug exchanges more power with the ear canal than the foam earplug. To better explain this observation, additional power balances for the two earplug types have been computed and are illustrated in Figure 4.8.

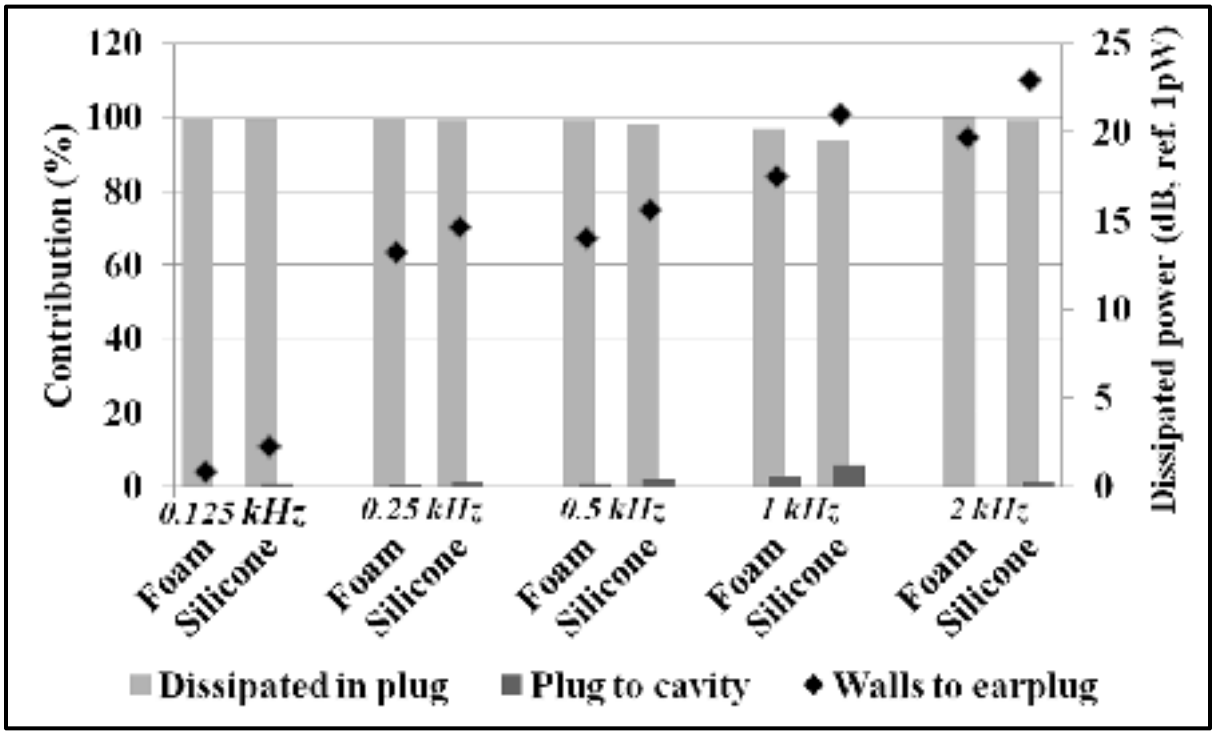

Figure 4.8: Power balance computation inside foam (11.1 mm insertion) and silicone (11.7 mm insertion) earplugs for frequencies up to 2 kHz. Diamond markers refer to right hand ordinate and vertical bars refer to left hand ordinate. An example on how to read this figure can be found in the caption of Figure 4.6

The power that is exchanged between the ear canal walls in contact with the earplug (black diamond markers refer to right hand ordinate) varies as a function of earplug type. For frequencies up to 1 kHz, the silicone earplug receives about 1.5 dB more power from the ear canal wall than the foam earplug. At 1 kHz and 2 kHz this difference increases to about 3.5 dB, again, the silicone earplug receives more power from the ear canal walls than the foam earplug. One possible explanation for this result could be a smaller impedance mismatch for the silicone material which allows more power to flow into the earplug.

Figure 4.8 furthermore indicates that, for both earplug types, the majority of the input power from the ear canal walls in contact with the earplug is dissipated inside the earplug volumes (light gray bars in Figure 4.8) at all frequencies. Secondly, the foam earplug is seen to dissipate slightly more of the input power from the ear canal walls than the silicone earplug especially at 1 kHz. These results are most likely attributable to the material properties used in the numerical models. For instance, the difference in power dissipation at 1 kHz could be due to the larger loss factor (which was assumed in the present study) of the foam earplug which dampens the resonance frequency of this earplug (11.1 mm earplug length) around 1.2 kHz. The silicone earplug (11.7 mm earplug length) also exhibits a resonance frequency around 1.4 kHz. Due to the smaller loss factor used in the silicone earplug model this resonance would be dampened less. At frequencies below 1 kHz, the rigidity of the earplug might likely have influenced the observed results whereas above 1 kHz, the mass of the earplug might be of importance to explain the results illustrated in Figure 4.8.

4.5 Conclusions

An axi-symmetric linear elasto-acoustic FE model of the human external ear was developed to predict the bone conduction OE. All computations were carried out using COMSOL Multiphysics (COMSOL®, Sweden). The proposed model compares well with experimental data measured in two healthy human reference groups and two commonly used earplug types. Observed deviations between the experimental and numerical data are similar to those obtained with previous OE models (Stenfelt and Reinfeldt, 2007). In the present study low

frequency deviations from the experimental data are likely a combined result of earplug leaks and weak sound emission from the bone transducer during the experimental data collection. Mid and high frequency deviations between the numerical and experimental data are more likely due to geometrical differences between the implemented FE model and the test subjects' ear geometries.

With respect to Stenfelt and Reinfeldt's (2007) as well as Schroeter and Poesselt's (1986) reference OE models, the proposed model exhibits only minor differences for shallow earplug insertion depth. The latter are due to differences in the model layouts (e.g. earplug impedances and open ear radiation impedance) and ear canal geometry (e.g. variable ear canal cross sections). At deep occlusion and frequencies below 1 kHz, the present model predicts a considerably smaller OE than Stenfelt and Reinfeldt's (2007) model which could originate from the uncertainty with respect to the earplug insertion depth and the excitation used in the present model. Further experimental data should be obtained to further investigate this deviation. The model excitation should also be adjusted, if necessary. Above 1 kHz the OE prediction obtained with the present model increases and is close to Stenfelt and Reinfeldt's (2007) OE prediction. In the present model this increase in OE is likely due to the presence of two radiating modes in the foam earplug. While Stenfelt's model also exhibits a small increase in OE around these frequencies, the aforementioned explanation does not apply, as these authors did not model the foam earplug, but used an infinite impedance instead.

OE differences were observed both experimentally and numerically for the earplug types considered in this study. In the present study, power balances showed that in the case of the silicone earplug more power gets exchanged and dissipated in the occluded ear canal cavity than when the foam earplug is used, thus, causing a larger OE. The reason for the larger power exchange at the earplug - ear canal interface of the silicone plug could be shown to originate from a larger power exchange at the interface ear canal wall – earplug (likely due to a smaller impedance mismatch) in combination with slightly less power dissipation inside the silicone earplug body. Nevertheless, the observed OE differences seem to depend on the

chosen occlusion depth. While the earplug type was found to contribute to the OE magnitude at medium occlusion (e.g. occlusion of almost the entire cartilaginous canal) the earplug type is of little importance at shallow occlusion. The latter finding is in agreement with the results obtained by Lee (2011) and likely originates from the important contribution of the cartilaginous ear canal walls to the OE magnitude (e.g. Berger and Kerivan, 1983; Stenfelt et al., 2003). The cartilaginous ear canal transfers the majority of power to the ear canal at shallow occlusion and the medial earplug surface is of secondary importance. At medium and deep occlusion, however, the medial earplug surface transfers most of the power to the ear canal, because the contribution of the bony ear canal is much smaller both with respect to the medial earplug surface and the cartilaginous ear canal. Similar results were also reported by Brummund et al. (2014) between 1.1 kHz and 1.8 kHz.

The obtained results therefore suggest that an improved earplug design should aim at reducing the power exchange between the ear canal wall and the earplug circumference and increase the power dissipation inside the earplug through adequate material selection. Furthermore, in order for these improvements to be effective the earplug should occlude most of the cartilaginous ear canal. In the future such a design could contribute to provide earplug users with a passive solution to reduce the earplug OE.

While the present results are very promising, care should be taken with respect to model simplifications that might have contributed to the obtained numerical results. Model limitations include, among others, the chosen material properties and behavioral laws, the excitation, as well as a truncated model of the external ear as opposed to a model of the entire head. Additionally it could be beneficial to consider more than five third octave bands in a future study and to repeat the power balance computation for other earplug models and insertion depths.

4.6 Acknowledgements

The authors gratefully acknowledge the IRSST for funding this work. Additionally, the authors would like to thank C. Le Cocq (ÉTS) and J. Boutin (IRSST) for their very valuable contribution during the experimental measurements.

CHAPTER 5

IMPLEMENTATION OF A SIMPLIFIED, ARTIFICIAL EXTERNAL EAR TEST FIXTURE FOR MEASUREMENT OF THE EARPLUG INDUCED AUDITORY OCCLUSION EFFECT

5.0 Preliminary note

As was mentioned in section 0.2.2, objective 4 consisted in testing the general feasibility to implement an artificial occlusion effect test fixture. To date no commercially available ATF allows for measuring the occlusion effect.

Objective 4 has not yet been the subject of a fourth journal article, but obtained results have been published in the conference proceeding of the International Congress on Acoustics 2013 (Brummund et al., 2013) during which the results were also presented orally. The present chapter aims at providing details on the implementation of the experimental prototype and to present preliminary experimental results.

5.1 Introduction

Hearing protection devices such as earplugs represent a frequently used short term solution for occupational hearing conservation. Nevertheless, research has also shown that workers often only tend to wear provided earplugs for limited amounts of time (Berger, 2000) due to physical and auditory discomfort. One important source of auditory discomfort is the occlusion effect. The occlusion effect is a low frequency phenomenon that occurs upon earplug insertion. It causes an uncomfortable, hollow-sounding distortion of the perception of the wearer's own voice and an amplification of physiological noises. Therefore, the occlusion effect can impede the communication between workers as well as their auditory perception. These and other reasons lead to a reduction in earplug wearing time which leaves the workers prone to developing professional hearing loss.

Many studies (e.g., Békésy, 1941; Berger and Kerivan, 1983; Goldstein and Hayes, 1965; Huizing, 1960; Stenfelt et al., 2003) have examined the occlusion effect experimentally using both subjective (Real Ear Attenuation at Threshold) and objective (ear canal sound pressure measurement) measurement techniques during which the structure borne excitation is achieved via ipsilateral mastoid, forehead or incisor excitation. The results of these experimental studies have permitted to distinguish different bone conduction pathways and to understand how structure borne sound propagates in the external ear. On the other hand, only little is known about the contribution of the earplug (e.g. occlusion magnitude varies as a function of occlusion depth or volume (Békésy, 1941; Berger et al., 2003)) and its defining characteristics (e.g. geometry, material properties). With the exception of an experimental study by Lee (2011) no research could be found that examined the influence of the earplug type on occlusion effect measurements.

One difficulty with occlusion effect measurements is the large inter-subject variability of the obtained results; the reasons for which can be diverse. For instance, while it is challenging to insert an earplug to a given occlusion depth, this occlusion depth is often defined with respect to the ear canal entrance (e.g. the tragus). This eventually results in varying relative occlusion depths (ratio of ear canal length to occlusion depth) that are due to inter-subject differences in ear canal length and cause varying occlusion effect magnitudes. Besides the variability in ear canal length other geometrical characteristics of the external ear can be of importance as well. The ratio of how much of the ear canal is effectively backed by soft tissue (the main source of ear canal sound pressure in the occluded ear (Naunton, 1963; Stenfelt et al., 2003) as compared to bony tissue can potentially alter the amount of sound power radiated into the ear canal independently of occlusion depth variability. Lastly, air borne noise emission of the bone transducer can, depending on microphone sensitivity and noise floor, increase the ear canal sound pressure level in the open ear and therefore reduce the obtained occlusion effect.

A simplified artificial test fixture of the external ear can help to bridge some of the abovementioned gaps and contribute to better assess and design earplugs. Furthermore, such an artificial model can serve to validate existing numerical occlusion effect models

(Brummund et al. 2011; Brummund et al., 2011a; Sgard et al., 2012). This work describes the implementation of a cylindrical artificial test fixture of the human outer ear. It comprises the auditory canal as well as the bony, cartilaginous, and skin tissues that are made up of rigid polyurethane foam and two different types of silicones, respectively. In the following, the implementation of the test fixture is outlined.

5.2 Methodology

5.2.1 Implementation of the artificial axi-symmetric external ear

The geometry of the synthetic external ear model closely resembles the shape of the simplified axi-symmetric finite element models proposed in (Brummund et al., 2014a, 2014b; Brummund et al., 2011). Minor geometrical adjustments (e.g. ear canal diameter), however, had to be carried out to enable the use of standardized measurement equipment, such as the IEC 60711 coupler to measure the sound pressure level inside the ear canal. In Figure 5.1, a schematic of the unoccluded synthetic external ear model is depicted.

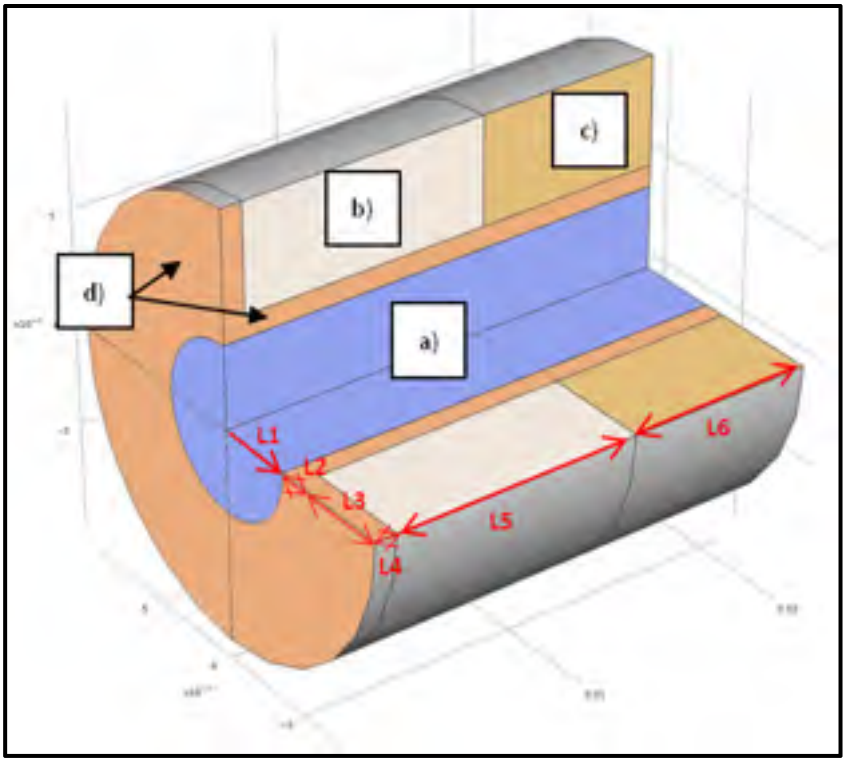

Figure 5.1: Schematic of the designed (built and assembled in-house) artificial external ear model, its domains and its dimensions. a) ear canal, b) soft tissue domain, c) bony tissue, d) skin tissue at ear canal entrance and on ear canal walls. For further reference see also Table 5.1

The synthetic external ear model comprises the ear canal, the soft tissue, the bony tissue as well as the skin tissue that covers the ear canal entrance region and the ear canal walls. In Table 5.1 the geometrical features of the synthetic external ear model are summarized (for reference see Figure 5.1).

Table 5.1: Dimensions of the synthetic ear model

Dimension name	Value [mm]
Radius ear canal (L1)	3.75
Wall skin thickness (L2)	2
Radial tissue thickness (L3)	8.05
Length skin (L4)	7.7
Length cartilage (L5)	19
Length bone (L6)	15

To mimic the bony tissue, solid rigid polyurethane foam (SAWBONES®, Pacific Research Laboratories, WA, USA) is used (ASTM F-1839-08). The cartilaginous and skin tissues are made up of two types of silicone. For the cartilage, V-340 silicone (hardness shore A = 55) is used. For the skin tissue at the ear canal entrance and on the ear canal walls, RTV 1556 (hardness shore A = 30) is employed. During the fabrication process, the first 5mm of a precut sawbone cylinder was tightly pressed (polyurethane foam external diameter > bore hole diameter) into the central bore hole of a slip-on flange (class 600, ANSI/AMSE 16.5 slip-on flange). Afterwards, a cylindrical insert (ABS material) whose radius equals the ear canal radius *plus* the ear canal skin (L1 + L2) was inserted into the precut central bore hole of the sawbone cylinder. A batch of V-340 silicone was mixed and casted in the subassembly described before. After completion of the curing process, the ABS insert was removed. Next, a second insert (ABS material) of the radius of the ear canal (L1) was introduced concentrically into the polyurethane and V-340 subassembly. A batch of the low viscosity RTV 1556 silicone was mixed and injected using a syringe to represent the ear canal walls and ear canal entrance. After completion of the curing process, the second insert was removed. During the silicone injection, specimens of each silicone type were also casted and subsequently analyzed to determine the material properties of the utilized batch. These data can later serve as input variables in a axi-symmetric FE-model to model the experimental setup for (i) numerical validation and (ii) to study the earplug occlusion effect using a mixed-experimental-numerical approach.

5.2.2 Assembly of the entire test apparatus

A square steel plate (30cm x 30cm) (see Figure 5.2a)) is tightly screwed into a double layered gypsum drywall until flush. The drywall separates a semi-anechoic and a reverberant room. A class 600, ANSI/AMSE 16.5 slip-on flange (see Figure 5.2b)) is tightly screwed to the rear side of the steel plate (in between the drywalls). To decouple the flange and the plate, acoustical sealing rubber is applied. The simplified synthetic axi-symmetric model of the human external ear (see Figure 5.2c)) described above is pressed (bony part) and molded (soft and skin tissue domains) directly into the central bore hole of the slip-on flange following the procedure described in the preceding paragraph. All acoustical sound pressure level measurements are carried out using an IEC 60711 ear simulator (see Figure 5.2d)). The coupler is pressed against the rear side of the synthetic model's ear canal. It is held in place with the help of a sticky modeling clay that also serves to isolate the coupler against extraneous noise. A SmartShaker™ K2007E01 mini-shaker is used to introduce a structure borne excitation along the central axis, on the circumference of the bony tissue domain (see Figure 5.2f)). To connect the mini-shaker to the bony tissue, a cage (see Figure 5.2e)) was developed. The cage consists of two parallel discs which are rigidly connected through four screws. The anterior disc exhibits a bore hole whose internal diameter is slightly smaller than the outer diameter of the bony part of the artificial ear model. This anterior disc is press-fitted around the bony tissue. The spacing between the discs and the lengths of the screws were chosen so that the IEC coupler (see Figure 5.2d)) can be placed concentrically with respect to the cage (see Figure 5.2e)) without touching it. The cage is connected to the mini-shaker via a fifth screw that allows for the vibration of the mini-shaker (see Figure 5.2f)) to be transmitted to the bony part of the artificial ear model (see Figure 5.2c)).

A prototype of the artificial external ear has been molded, in-house, into the slip-on flange (Figure 5.3). All remaining parts, with the exception of the IEC 60711 coupler and the mini-shaker, have been built in-house and assembled according to Figure 5.2. The obtained artificial external ear measurement apparatus was installed in the drywall that separates a semi-anechoic and a reverberant room. In the following, selected images are presented to

illustrate the development process of the synthetic external ear (Figure 5.3) which constitutes an integral part of the proposed occlusion effect measurement apparatus.

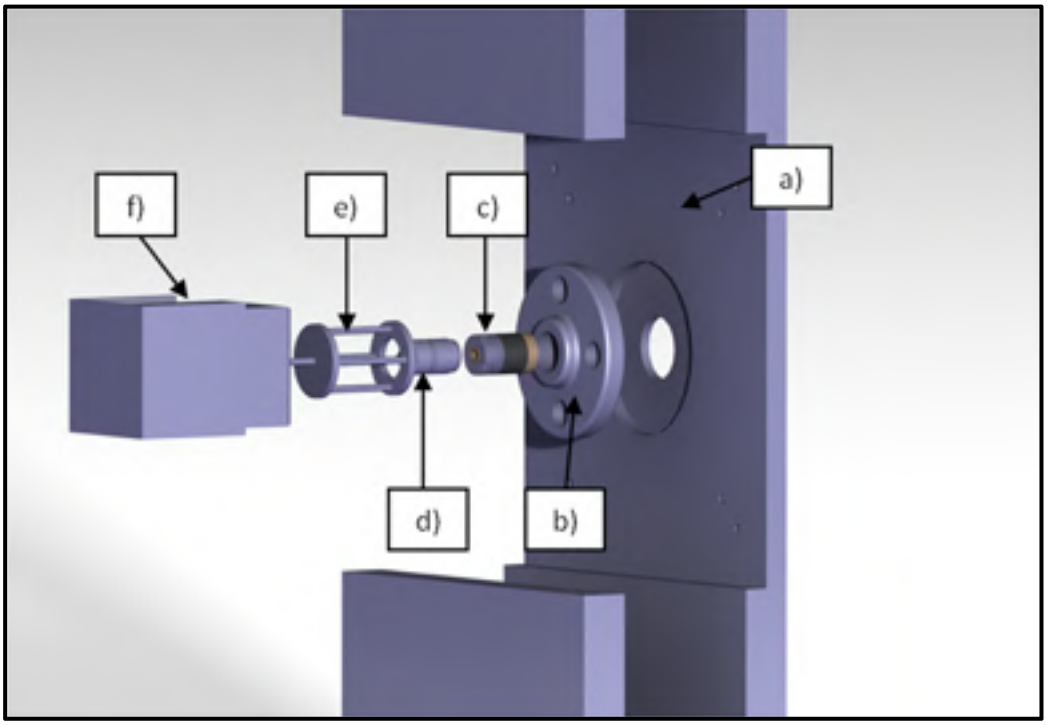

Figure 5.2: Schematic of the assembled test apparatus. a) square steel plate, b) slip-on flange, c) artificial external ear, d) IEC 60711 coupler, e) cage for transmission of mechanical excitation, f) mini-shaker K2007E01

Figure 5.3: Summarizing overview of the development process of the artificial external ear model. a) Back view: Polyurethane cylinder, to mimic bony tissue, (beige) is press-fitted into slip-on flange (black). Anterior disc of excitation cage is press-fitted around bony tissue b) Front view: Polyurethane cylinder after press-fitting into slip-on flange. Remaining volume of central bore hole in slip-on flange to be filled with two different types of silicone to mimic soft and skin tissues. c) Front view: After injection of the first silicone that is used to mimic the soft tissue, the silicone is cured overnight (grey). The insert (white) delimits the soft tissue cylinder and is removed after completion of the curing process. d) Front view: Final result after molding of soft tissue cylinder and removal of the insert. e) Front view: A second insert (white) is placed concentrically in the soft/bony tissue subassembly. Its diameter is chosen so that the second silicone, used to mimic the skin tissue, can fill the remaining volume that corresponds to the ear canal walls and the skin tissue around the ear canal entrance. f) Front view: following the molding and curing of the skin tissue domain, the second ABS insert is removed. An earplug can be inserted into the finalized artificial external ear model

5.2.3 Working principle of the occlusion effect test fixture

Figure 5.4 illustrates a subassembly of the apparatus described in the previous section. The depicted components include the slip-on flange, the artificial external ear, the IEC-60711

coupler, as well as the cage for transmission of the mechanical excitation (see also Figure 5.2 components b-e).

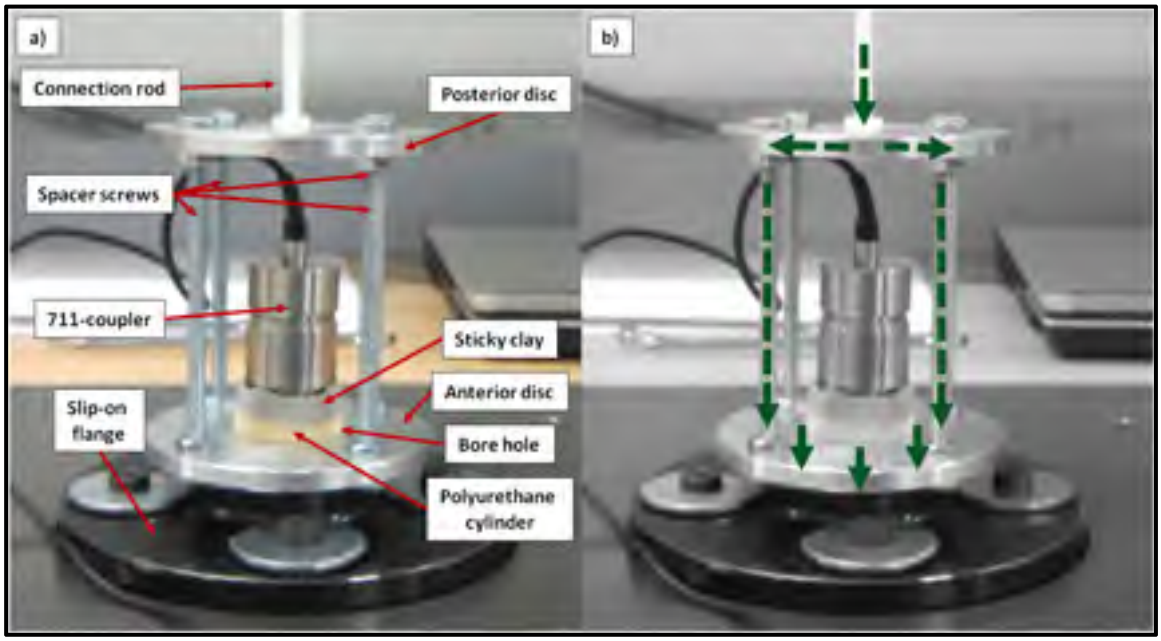

Figure 5.4: Function principle of test fixture a) components important for structure borne sound transmission. b) schematic of the structure borne transmission

To experimentally measure an occlusion effect, the mechanical excitation from the mini-shaker (not depicted in Figure 5.4) is transmitted into the transmission cage via the connection rod. The excitation is then transmitted to the anterior disc via the four spacer screws. The press fitted anterior disc's bore hole transmits the mechanical shear stimulation into the polyurethane cylinder used to mimic the temporal bone. Afterwards, the stimulus propagates into the silicone domains used to mimic the cartilage and skin and causes a vibration of the ear canal walls as well as a sound radiation into the test fixture's ear canal. The latter is measured with the help of the 60711 style coupler (Figure 5.5).

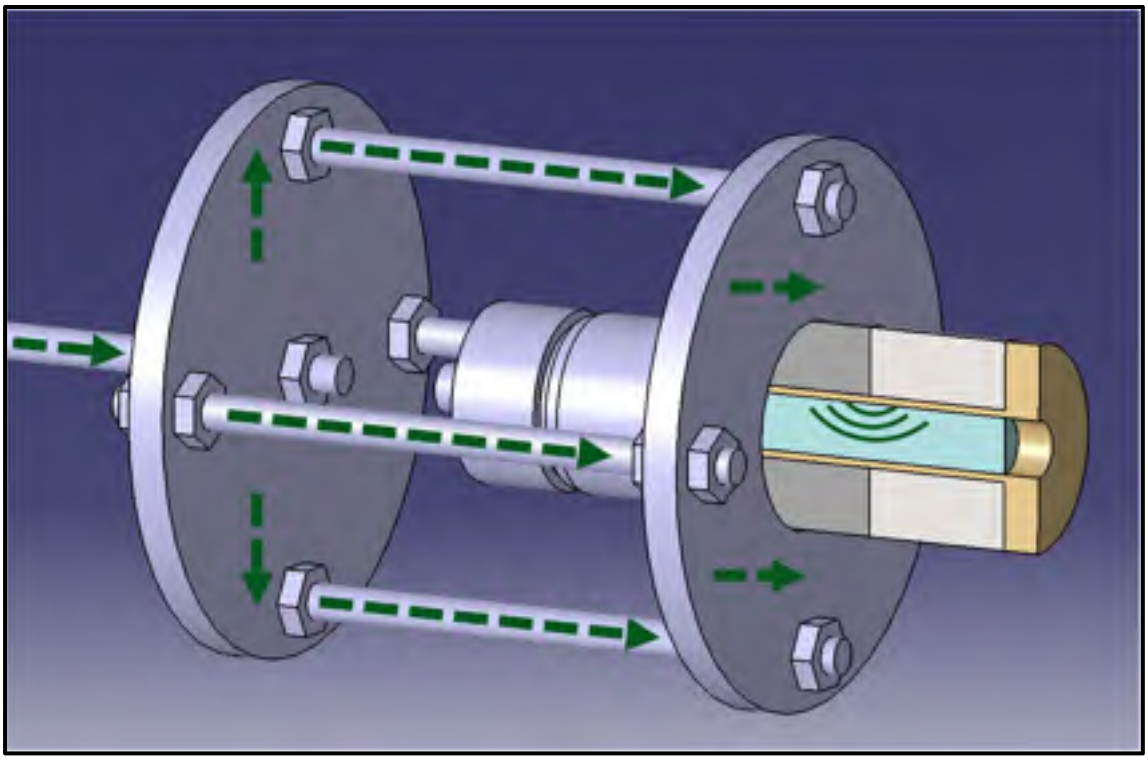

Figure 5.5: Schematic representation of the structure borne sound transmission in the synthetic external ear and sound radiation into the open ear canal

The implementation of a structure borne excitation is very challenging in the present prototype mainly because it was attempted to keep the test fixture axisymmetric both in terms of geometry and the stimulation. In the future this axisymmetry will be beneficial for the implementation of a test fixture equivalent numerical FE-model, which together with the test fixture could be used to further study the occlusion effect. The bone transducers typically used during experimental occlusion effect measurements (e.g. Nélisse et al., 2013; Stenfelt and Reinfeldt, 2007) cause a compressional excitation at the point of attachment. These bone transducers, however, cannot be employed to here, because they do not fulfill the axisymmetry requirement mentioned above. One possible solution to this problem includes applying the bone transducer to the medial horizontal boundary of the artificial ear. This scenario, however, has to be rejected, because the sound would directly radiate into the ear canal. Additionally, the artificial tympanic membrane couldn't be used. The latter limitation, however, is of secondary importance, because a miniature microphone could be inserted via

the ear canal entrance to replace the 60711 style coupler. Impulse hammers exhibit similar disadvantages as bone transducers as they result in a point excitation (non-axisymmetric). Additionally, impulse hammers are difficult to manipulate in terms of excitation repeatability and it is challenging to avoid rebounding with an impulse hammer. Piezoelectric sensors could be applied symmetrically around the circumference of the polyurethane cylinder. This excitation method, however, was rejected for the present study due to several considerations. First, the polyurethane cylinder exhibits a relatively small radius and no flat contact surface thus the piezo sensors ought to be small. Second, it is difficult to excite such a sensor at the frequencies considered in this work, because the sensor's frequency range that exhibits a flat transfer behavior is located at much higher frequencies than the ones considered here. Lowering the sensor's resonance frequency by adding mass (e.g. a clamp) could solve this problem it is, however, challenging to implement and control in terms of the adequate clamping force.

Small mechanical shakers like the one used in the present setup are appealing, because they can be placed at some distance away from the artificial ear and the artificial eardrum thus leaving enough physical space to insulate the test fixture against airborne noise emission from the excitation device. Nevertheless, mechanical shakers commonly only provide one point of attachment for the stinger which, again, makes it challenging to implement an axisymmetric stimulation. Using multiple mini-shakers in parallel on the other hand is quite cumbersome and cost inefficient. To overcome this limitation it was attempted in the present study to design a coupling cage to distribute the point excitation axisymmetrically on the circumference of the polyurethane cylinder. One important limitation of the chosen excitation method, however, includes the fact that a shear stimulation is generated which represents a simplification of the stress vectors which act upon the external ear tissues and which does not correspond to the compressional excitation caused by bone transducers.

5.2.4 The role airborne noise corruption

During the operation of the experimental prototype the transmission cage also radiates airborne noise. This noise could corrupt the sound pressure level reading obtained at the 60711 style coupler. For instance, the airborne noise artifacts could bypass the sticky clay (see Figure 5.4) and pollute the sound pressure level at the 60711 artificial ear. It is thus necessary to determine whether the signal obtained at the 60711 style coupler is truly due to structure borne sound transmission.

To test for airborne noise corruption, the experimental setup was operated as illustrated in Figure 5.2 (shaker setup). The airborne noise generated by the transmission cage was recorded with the help of a ¼ - inch B&K 4961 microphone (Brüel & Kjær, Denmark) which was placed adjacent to the IEC 60711 coupler.

Afterwards the recording was fed into a loudspeaker which was placed about 15 cm behind the 60711-coupler. The loudspeaker served to reproduce the airborne noise field at similar sound pressure levels as the shaker setup. Note, that the sound field reproduced by the loudspeaker which excites the set-up is an approximation of that created by the radiation of the shaker. The mini-shaker, the connection rod, the posterior disc as well as the four spacer screws were removed during this experiment. The anterior disc could not be removed as it was rigidly attached to the polyurethane cylinder. Barymat (AcoustiGuard™, ON, Canada) acoustic foam was placed on the anterior disc as shielding. Figure 5.6 illustrates the outlined test.

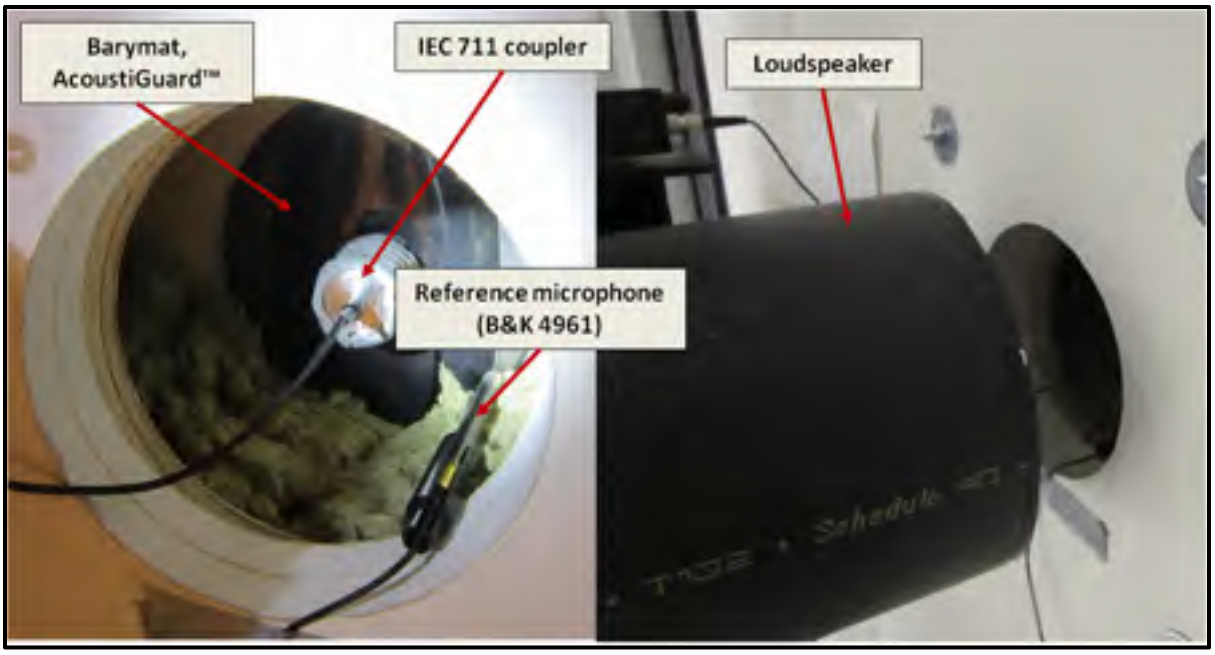

Figure 5.6: Experimental setup used to reproduce the airborne noise sound field emitted by the transmission cage

5.3 Preliminary results and discussion

5.3.1 Sound field reproducibility

Figure 5.7 illustrates the sound pressure level readings at the reference microphone when the experimental apparatus is operated normally using the mini-shaker and when the recorded airborne noise sound field is reproduced using the loudspeaker.

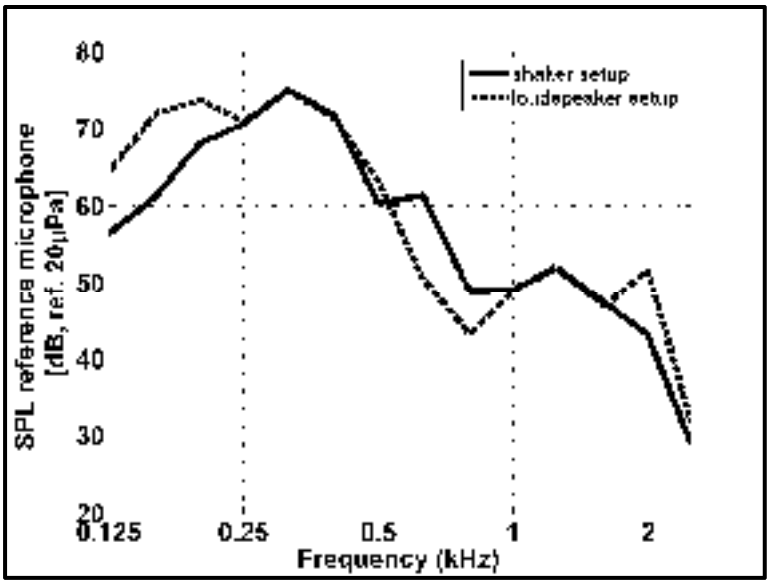

Figure 5.7: Sound pressure level readings obtained at the ¼-inch *reference microphone* subsequent to excitation with the shaker setup (solid line) and the loudspeaker setup (dashed line). Third octave band filter applied

Even though the acoustic fields generated by the shaker and the loudspeaker setup are not identical, feeding the airborne noise field recording into the loudspeaker resulted in similar sound pressure level measured at the reference microphone (Figure 5.7). For frequencies up to 0.25 kHz the loudspeaker setup caused about 10 dB more sound pressure level. Between 0.5 kHz and 1 kHz the loudspeaker setup resulted in about 5 dB less sound pressure level at the reference microphone. Lastly, around 2 kHz the loudspeaker setup causes about 8 dB more sound pressure level at the reference microphone as compared to the shaker setup. In addition to differences in the generated acoustic fields (shaker and loudspeaker), the sound pressure level deviations could also be due to the loudspeaker placement (see Figure 5.6) which might have excited part of the dry wall installation that houses the test fixture. Furthermore, the reference microphone had to be removed subsequent to completion of the measurements with the shaker setup in order to disconnect the posterior disc and the connection rods of the excitation cage (see Figure 5.6). The microphone location might have been slightly different after it had been put back in place

5.3.2 Analysis of transmission pathways

Figure 5.8 illustrates the sound pressure level readings obtained at the 60711 style coupler when the test fixture is operated in the shaker setup and in the loudspeaker setup, respectively.

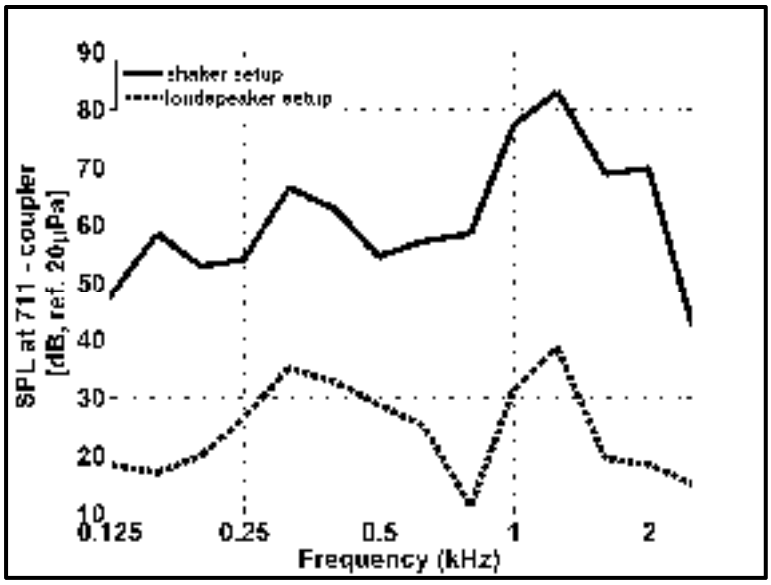

Figure 5.8: Sound pressure level readings obtained at the *IEC 60711-coupler* subsequent to excitation with the shaker setup (solid line) and the loudspeaker setup (dashed line). Third octave band filter applied

When the shaker setup is used the sound pressure level at the IEC 60711 coupler is some 30 dB larger as compared to the condition where the loudspeaker setup is used. The smallest deviation between sound pressure level readings obtained at the IEC 60711 ear simulator equals 25 dB. This deviation occurs at 0.25 kHz. At 1.25 kHz a resonance peak can be observed for the shaker setup. This resonance frequency corresponds to the quarter wavelength resonance of the open ear. Usually this resonance frequency would be expected to occur at higher frequencies. In the present study this deviation is partly due to the 60711 style coupler. This coupler is usually used in commercially available ATFs (e.g. (G.R.A.S. Sound & Vibration, Denmark) whose ear canals are shorter than the human ear canal. To

compensate for this difference in length the 60711-coupler exhibits an air-filled cavity behind the protective microphone cover. Additionally, the ear canal length of the present artificial external ear is too long (compare Table 5.1). Together these added lengths explain the low frequency shift of the open ear's resonance frequency.

Comparison of the sound pressure level readings obtained at the ear simulator for the shaker and loudspeaker setups demonstrates that the contribution of airborne noise artifacts is negligible in the proposed occlusion effect test fixture.

5.3.3 Measured occlusion effect

Figure 5.9 illustrates the occlusion effect measurements obtained for a foam earplug which was inserted flush with respect to the ear canal entrance (insertion depth about 20 mm). Pink noise served as stimulus for this experiment. The pink noise was presented at 90 dB output level using a Larson Davis SRC 20 (Larson Davis, USA) signal generator (frequency range 50 Hz to 5000 Hz).

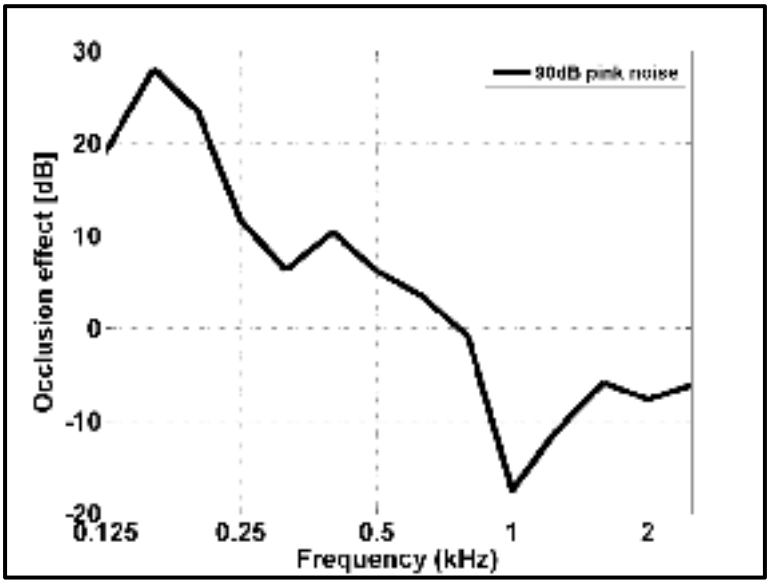

Figure 5.9: Third octave band Occlusion effect measurement of a foam earplug (insertion depth about 20 mm) for pink noise excitation (90 dB)

At the lowest frequencies, the occlusion effect magnitude presented in Figure 5.9 equals about 20-30 dB. This magnitude is in good agreement with experimental measurements in healthy human subjects (e.g. Schroeter and Poesselt, 1986). The occlusion effect magnitudes decreases with frequency and becomes negative around 0.8 kHz. An occlusion effect minimum occurs at 1 kHz. Similar trends can also be found in healthy human test subjects (e.g. Stenfelt and Reinfeldt, 2007). Nevertheless, the zero crossing and the occlusion effect minimum would be expected to occur at higher frequencies. For instance for a foam earplug (insertion depth about 15mm) and ipsilateral mastoid stimulation Stenfelt and Reinfeldt (2007) observe a zero crossing at 2 kHz and an occlusion effect minimum at 5 kHz. The authors attribute the latter minimum to airborne noise radiation from the bone transducer.

The deviations between the data of this study and the experimental measurements on human subjects can in part be explained due to the erroneous ear canal length of the synthetic ear which caused a low frequency shift of the quarter wavelength resonance. Other factors that contribute to the observed deviations include the way in which the artificial external ear test fixture is excited and resonances in the excitation mechanism (e.g. in the excitation cage).

For frequencies up to 2.5 kHz it could be shown that airborne noise corruption did not contribute to the sound pressure level readings at the 60711-coupler (see Figure 5.8) thus it is unlikely that the minimum observed at 1 kHz is due to airborne noise radiation in the present study. The minimum at 1 kHz of the present study could be explained by the presence of the open ear canal resonance peak around 1.25 kHz (see Figure 5.8). Further research is, however, necessary to understand the contribution of the occluded ear to the observed minimum.

5.3.4 Linearity analysis

To test for the linearity of the obtained occlusion effect, the pink noise stimulus was presented at 100 dB and 110 dB in addition to the 90 dB level. The occlusion device (foam

earplug) and insertion depth remained constant for all tests. In Figure 5.10 the obtained results are illustrated.

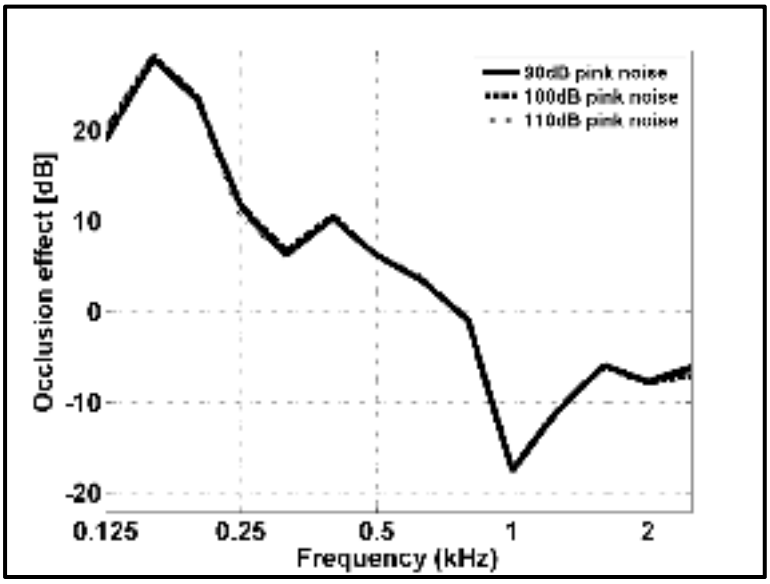

Figure 5.10: Occlusion effect measurements of a foam earplug (constant insertion depth about 20mm) for pink noise excitation at three difference levels (90dB, 100dB, 110dB). Third octave band filter applied

The obtained results demonstrate that the measured occlusion effect remains almost constant when the pink noise levels are increased. The proposed occlusion effect test fixture thus behaves linearly with respect to these pink noise excitation levels.

5.4 Conclusions and future work

The present study demonstrated the general feasibility to implement a functional artificial occlusion effect test fixture. To the best of our knowledge, no such test fixture has been described in the accessible literature.

In the proposed setup, the sound pressure level reading and thus the occlusion effect measurements are due to structure borne sound transmission. The contribution of airborne noise corruption is negligible.

The present study suggests that it is generally possible to use a simplified external ear geometry for the implementation of an occlusion effect test fixture. Nevertheless, deviations between the occlusion effects measured with the artificial ear and those measured in healthy human subjects persist. In a future study it would be desirable to implement an occlusion effect test fixture of complex geometry to better account for the earplug deformations that occur upon insertion into the S-shaped ear canal. In addition, the manner in which the artificial external ear is excited should be reviewed to render the excitation more realistic and in order to reduce the test fixture's physical dimensions.

The obtained occlusion effect measurements exhibit similar trends as comparable measurements obtained in healthy human subjects in terms of occlusion effect magnitude and slope. Nevertheless, deviations were observed also with respect to the zero crossing, occlusion effect minimum and the quarter wavelength resonance of the open ear. In the present study these deviations originate at least in part from the erroneous synthetic ear canal length an combination with the added length of the IEC 60711-coupler. In the future an error free model ought to be implemented. To remove the contribution of the added coupler length a series of filter could be envisioned. The authors are currently working on these problems.

In a future version of this test fixture prototype, it would also be desirable to use even more realistic material properties. Nevertheless, prior to the implementation, experimental measurements ought to be completed to more accurately determine the material properties of the external ear tissues considered here.

5.5 Acknowledgements

The authors gratefully acknowledge the IRSST for funding this work. Additionally, the authors would like to thank J. Boutin (IRSST) for his very valuable contribution during the experimental measurements.

CHAPTER 6

SYNTHESIS AND CONCLUSIONS

This chapter aims at providing a synthesis of the main results obtained during this work in the context of the general and specific research objectives. The scientific and technological contributions as well as limitations of the present work are presented and critically discussed. Future recommendations are presented based on the currently existing limitations. Lastly, a brief general conclusion is presented.

6.1 Synopsis of the research problematic as well as the general and specific objectives of the present study

- Hearing protection devices such as earplugs and ear muffs represent a frequently used short term solution to protect workers from harmful noise exposure and from developing professional hearing loss.
- Despite auditory health benefits of hearing protectors, workers often only tend to wear hearing protection for limited amounts of time, if at all.
- While several reasons for hearing protector underutilization and non-use can be identified, problems that pertain to hindered workplace communication are of primary importance. In this context the occlusion effect becomes important as it causes the HPD wearer to perceive his/her own voice as being amplified and distorted and it also amplifies physiological noises upon earplug insertion.
- To improve the shortcomings (e.g. limited auditory comfort due to the occlusion effect) observed in currently existing HPDs a research collaboration between the IRSST and the ÉTS has been launched. The present study is part of this collaboration and aims at studying the earplug induced occlusion effect through the development of novel numerical models and experimental methods.
- To achieve this general objective four specific research objectives were defined. They include:

- The development of a 3D finite element model of the human external ear of complex geometry (objective 1) to simulate the occlusion effect.
- The development of an axisymmetric finite element model of the human external ear (objective 2) to predict the occlusion effect.
- Numerically studying the occlusion effects differences, if any, of two commonly used earplug types (objective 3).
- The design and implementation of an artificial occlusion effect test fixture to experimentally measure the occlusion effect (objective 4).

6.2 Article 1: Contributions, limitations and future recommendations

The technological and scientific contributions of this article include:

- A first 3D coupled linear elasto-acoustic external ear model was implemented through geometrical reconstruction of a human external ear of complex geometry including substructures such as the ear canal walls and the mastoid process (e.g. realistic bone conduction stimulation) on the basis of anatomical photographs.
- Compilation of isotropic linear elastic material properties to model the human external ear tissues (bone, skin, cartilage) on the basis of an extensive literature review. While several limitations apply (see further below) the obtained numerical results suggest that these material properties are suitable for numerical occlusion effect simulation.
- Analysis of the influence of the temporal bone's boundary conditions indicates that the occlusion effect is influenced little when either fixed or free boundary conditions are used. The predicted transfer function level magnitudes, however, increase remarkably when free boundary conditions are used instead of fixed boundary conditions.
- Prediction of open and occluded transfer function levels and occlusion effects of a silicone earplug at several insertion depths following mechanical stimulation at the ipsilateral mastoid process. It could be shown that the occlusion effect decreases as a function of earplug insertion depth (e.g. coherent with literature). Overall obtained

occlusion effect magnitudes are in good agreement with those observed in human subjects. At deep insertion the earplug material properties might have contributed to a relatively large, but acceptable, occlusion effect prediction.

- Investigation of the bone conduction occlusion effect of a silicone earplug using power balances to explain how the ear canal walls and the medial earplug contribute to observed occlusion effect magnitudes at varying occlusion depths between 1 kHz and 2 kHz. Results indicate that for shallow occlusion the unoccluded ear canal walls contribute the most to the obtained occlusion effect. At medium and deep earplug insertion the medial earplug surface contributes more to the obtained occlusion effect than the unoccluded ear canal walls.
- Comparison and discussion of the predicted occlusion effects of a silicone and a foam earplug (medium insertion depth) with experimental data kindly provided by Stenfelt and Reinfeldt (2007) shows that the present model provides satisfactory occlusion effect predictions (e.g. results fall inside or close to the experimental reference zone). Deviation magnitudes vary as a function of frequency. Reasons for these deviations include the possible presence of earplug leaks, uncertainty with respect to the occlusion depth, differences in terms of the external geometry, among others (see also limitations further below).
- The investigation of Tonndorf's (1966) qualitative low frequency occlusion effect (high pass filter effect) model using power balances and Huizing's (1960) qualitative mid frequency resonance frequency shift model using predicted transfer function levels inside the ear canal. With respect to Tonndorf's (1966) model a high pass filter effect like behavior of the open external ear could be demonstrated (e.g. power radiated at the open ear canal entrance relative to power exchanged at the ear canal walls). Furthermore, it could be shown that the removed high pass filter effect is not primarily influenced by the absence of sound radiation at the ear canal entrance, but rather by in an increase in the power flowing from the ear canal walls into the ear canal cavity. The latter increase was demonstrated to result from an increase of the input impedance seen by the ear canal walls that results from the insertion of the occlusion device which replaces the radiation impedance boundary condition of the

open ear. With respect to Huizing's (1960) model an open ear canal quarter wavelength resonance could be observed in the transfer function level prediction. Upon occlusion this resonance shifted towards the higher frequencies thus confirming Huzing's (1960) model.

The limitations of this article and future recommendations include:

- Limitations that pertain to the model geometry such as modeling of the temporal bone as compared to the entire head.
    - In a future study further 3D models should be implemented to study occlusion effect differences that are related to geometry. Nevertheless existing anatomical data are sparse.
- Limitations in terms of the material properties of the external ear tissues. While the assumption of linear elasticity seems reasonable, isotropy represents a simplification of the external ear tissues. In reality, the latter are anisotropic and viscoelastic and influenced by factors such as age and gender.
    - Future research is necessary to improve the current lack of data in terms of anisotropy, homogeneity, pres-stress state and frequency dependence of the biological tissues considered. The material properties and behavioral laws of the earplugs should be reviewed also (e.g. deep insertion for silicone earplug provided relatively large occlusion effect magnitude) and the foam earplug should be modeled as a porous, viscoelastic domain in the future.
- Limitations that relate to the chosen boundary conditions.
    - In the future, the connections that exist between the external ear boundaries and their adjacent tissue domains ought, ideally, to be expressed using transfer impedance boundary conditions instead of more conventional boundary conditions (e.g. free, clamped). The eardrum and middle ear impedance ought to be replaced by a more realistic model, because the impedance boundary condition does not allow considering sound pressure due to middle ear inertia.

6.3 Article 2: Contributions, limitations and future recommendations

The technological and scientific contributions of this article include:

- A first axisymmetric coupled linear elasto-acoustic finite element model of the human external ear was implemented (including the ear canal and its surrounding skin, cartilage and bone tissues) for simulation of the bone conduction occlusion effect.
- Compilation of ear canal, skin, cartilage and bone dimensions on the basis of an extensive literature review that serves as average external ear data in this work.
- Investigation of four different boundary and load condition configurations and their contribution to open and occluded transfer function levels and occlusion effects. Three scenarios were considered for each of the four configurations:
    - When only structure borne excitation is present (e.g. no leaking, no airborne noise), obtained results indicate that the boundary and load conditions are of secondary importance for the occlusion effect. The transfer function level magnitudes, however, are strongly influenced by the chosen boundary and load conditions. The transfer function levels can be predicted more accurately with respect to experimental measurements in human subjects when both the bone and cartilage tissue are stimulated. Note that several limitations apply. They are discussed further below.
    - Adding airborne noise incoherently at the ear canal entrance (e.g. simultaneous structure borne and airborne stimulation) mainly affects the open ear transfer function levels of configurations in which only the bony tissue is excited. The occluded ear transfer function levels for all configurations are unaffected by be the presence/absence of airborne noise due to the sound attenuation through the earplug model. Due to the increased open ear transfer function levels only those boundary condition configurations continue to provide satisfying occlusion effect predictions that excite both the bone and the cartilage tissue. Several limitations apply and are discussed further below.

- The presence of airborne, structure borne (added incoherently) excitation and small earplug leaks affects the occluded transfer function level predictions of all considered configurations at the low frequencies. The frequency at which maximum increase in transfer function levels occurs is influenced by the resonance frequency of the system earplug leak / ear canal which form a Helmholtz resonator like structure.

The limitations of this article and future recommendations include:

- Limitations that pertain to the model geometry mainly include using a truncated model of the external ear as opposed to a model of the entire head. The latter, however, cannot be implemented axisymmetrically. The chosen earplug leak diameters are presently very small.
  - In the future larger earplug leak diameters should be considered in order to observe a decrease in the occlusion effect magnitude similar to venting in hearing aids.
- Limitations in terms of the material properties of the external ear tissues and the earplugs. The same tissue and earplug material properties as in article one are used. Thus, the reader is kindly referred to section 6.2 where a detailed discussion of the limitations with respect to the material properties is provided along with future recommendations.
- Limitations that relate to the chosen boundary and load conditions. The most important limitation in this respect includes the model excitation. Here, the excitation force is applied normally and uniformly, because it provided the best numerical results (e.g. compared to tangential excitation). This loading condition represents an idealization of the real stress vectors which likely vary in terms of magnitude and direction throughout the tissues. Furthermore, the bone transducer's RMS-force used for stimulation was calibrated using an artificial mastoid. The obtained RMS-force force, thus, applies to the mastoid process and it likely changes in magnitude once it reaches the external ear region considered in this work. Adding the airborne noise incoherently is another simplification which is presently inevitable for a lack of data

on the phase differences between both stimuli. Generally, airborne noise corruption form the bone transducer has been shown to be problematic at the higher frequencies. The low frequency noise corruption observed in this work might be related to the experimental setup. Other limitations of importance include using conventional boundary conditions such as free and clamped conditions which should ideally be replaced by transfer impedance boundary conditions. Using an eardrum and middle ear impedance model does not allow considering the sound pressure due to middle inertia. Nevertheless, it is challenging to implement a more realistic eardrum and middle ear model due to the axisymmetric layout of the model.

- For a future study several recommendations can be identified. The force introduced in the model needs to be determined more accurately. The latter is also of importance to more accurately study the combined effect of airborne noise and structure borne excitation. Overall, the contribution of the airborne noise should be reinvestigated. In the future occlusion effect measurements with forehead bone transducer placement could be carried out in order to better avoid airborne noise corruption. Additional boundary and load configurations, other than the four considered here, should be investigated as they might provide more accurate results. To overcome the limitations that are related to using an impedance model of the eardrum and middle ear, an additional volume velocity could be added to the impedance boundary condition as was proposed by Schroeter and Poesselt (1986).

6.4 Article 3: Contributions, limitations and future recommendations

The technological and scientific contributions of this article include:

- A two level factorial design and multi-response optimization were implemented to investigate the sensitivity to the external ear dimensions in an axisymmetric coupled elasto-acoustic finite element. The upper and lower limits for the ear dimensions (e.g. ear canal length, radius, ear canal wall skin thickness) used during this work were compiled based on an extensive literature review. One axisymmetric geometrical

configuration was found that provides satisfactory occlusion effect predictions (mean values) for two independent experimental reference groups that use a foam and a silicone earplug, respectively.

- The axisymmetric model was compared to two existing gold standard electro-acoustical occlusion effect models for further validation. It was found that at shallow insertion the axisymmetric finite element model results in minor deviations with respect to both reference models. At deep occlusion the finite element model predicted a smaller occlusion effect than the reference model at the low frequencies (only one reference model considered deep occlusion). Reasons for these deviations include differences with respect to the model geometries, incertitude regarding the insertion depth, differences with respect to the amount of power that is exchanged between the bony ear canal wall and the ear canal cavity. The latter is also affected by the excitation and the material properties of the external ear tissues (e.g. behavioral laws, uniformity of excitation, excitation magnitude).
- Occlusion effect differences were observed both experimentally (measurements in healthy human subjects) as well as numerically using the axisymmetric external ear model.
- Obtained occlusion effect differences were further investigated using power balance computations in the ear canal cavity (unoccluded ear canal walls, ear drum, medial earplug surface) as well as in the earplug model (occluded ear canal walls, dissipation in earplug body, medial earplug surface). Obtained results indicate that for medium insertion the occlusion effect differences are mainly due to differences in the amounts of power that are exchanged between the medial earplug and the ear canal cavity for a foam and a silicone earplug. At medium insertion the contribution of the unoccluded ear canal walls to the occlusion effect magnitude was found to be of secondary importance. On the one hand, the difference in exchanged power at the medial earplug surface could be shown to originate from the amount of power that is exchanged between the occluded ear canal walls in contact with the earplug circumference (e.g. smaller impedance mismatch causes more power to flow into the silicone earplug model as compared to the foam earplug model) and earplug body. On

the other hand, the body of the foam earplug could be shown to dissipate more of the injected power than the body of the silicone earplug. This difference was most pronounced at the earplug modes (e.g. due to different loss factors).

- The contribution of the earplug model to the occlusion effect magnitude, however, could also be shown to be insertion depth dependent. While the earplug model contributes to the occlusion effect at shallow occlusion (occlusion down to the bony meatus) it is of little importance at shallow earplug insertion. The latter being due to the circumstance that the unoccluded ear canal walls contribute the most to the dissipated power at the eardrum for shallow occlusion (also refer to section 6.2).

The limitations of this article and future recommendations include:

- The geometrical layout used in article is the same as the baseline geometry of article 2 (dimensions differed though). Hence, the same limitations that applied to the geometry of article 2 apply here. The reader is kindly referred to section 6.3 where a detailed description of the limitations concerning the geometry is provided along with recommendations for a future study.
- The material properties as well as one boundary and loading condition (normal uniform excitation of the bone and cartilage circumference) of article 2 were used in this work. The reader is kindly referred to sections 6.2 and 6.3 where a detailed discussion with respect to the limitations of the material properties and boundary and load conditions can be found along with future recommendations.
- Limitations that relate to the power balance computations in the ear canal cavity and the earplug.
    - In the future, additional experimental occlusion effect data is required to further validate the model findings. While the present model predictions confirm research findings by Lee (2011), Lee (2011) considered a foam and a medical balloon type earplug), further occlusion effect measurements with the foam and silicone earplug ought to be implemented for shallow and deep occlusion. Nevertheless, in the case of the silicone earplug both shallow and very deep occlusion might be difficult to achieve as the earplug silicone flows

into a rubber pouch of constant length. Additionally it could be beneficial to consider more than five third octave bands in a future study.

6.5 Chapter 5: Contributions, limitations and future recommendations

The technological and scientific contributions of the work presented in this chapter include:

- A synthetic axisymmetric external ear model which includes the bony, cartilaginous and skin tissues (ear canal wall and entrance) as well as the ear canal was implemented. A simple method to press and cast the artificial ear components into a standardized slip-on flange (serves to hold the artificial ear) was presented. This method is easy to use and versatile in the sense that the slip-on flange can easily be replaced in the global assembly when other artificial ears (e.g. geometry, material properties) ought to be investigated.
- Solid rigid polyurethane foam to mimic the bone tissue and two types of silicone to mimic the cartilage and skin tissues could be identified on the basis of a comprehensive literature review.
- An assembly method for the artificial test fixture (e.g. artificial external ear, slip-on flange, baffles, excitation cage) was presented that permits (i) holding the artificial external ear, (ii) shielding the open ear canal entrance against noise artifacts from the mechanical shaker, (iii) applying conventional boundary conditions to the artificial external ear (e.g. ear canal entrance tissue free, clamped boundary condition around the skin and cartilage silicone). With respect to the boundary conditions several limitations apply (please see further below).
- A method to axisymmetrically excite the artificial ear on its bony portion was presented. The mechanical shear excitation is achieved using a small shaker that is connected to a coupling cage that rigidly attaches to the bony portion of the artificial ear. The coupling cage is designed so that standardized measurement equipment (e.g. IEC-60711 artificial ear) can be attached to the back side of the ear canal to measure the ear canal sound pressure level.

- Preliminary results obtained with the shear excitation method in combination with the proposed artificial ear and the global assembly of the test rig showed that an earplug occlusion effect can be measured with the proposed test fixture.

The limitations of the work presented in this chapter and future recommendations include:

- Limitations that pertain to the model geometry such as the constant thickness of the ear canal walls. Usually, the ear canal wall thickness decreases closer the eardrum. The present prototype exhibits an ear canal that is too long due a mistake during the fabrication. Additionally, the artificial eardrum (IEC 60711 style coupler) adds some length to the model's ear canal.
    - In a future version of the artificial external ear an ear canal wall of variable thickness should be implemented. The ear canal length must be shortened and the added length of the coupler ought to be corrected for instance through a series of filters. It would also be beneficial to implement and artificial external ear of complex geometry.
- Limitations in terms of the material properties of the polyurethane foam and the silicones.
    - While the chosen materials (together with the excitation) permit measuring and occlusion effect they must ultimately be replaced by material properties that are more similar to the human external ear tissues in a future version. Nevertheless, prior to doing so experimental measurements must be carried out to determine the material properties of the external ear tissues considered here.
- Limitations that relate to the imposed boundary conditions. The preliminary test fixture clamps the circumference of the cartilage domain and part of the bone domain and the excitation is introduced only on a small part of the bone circumference. The results presented in articles 2 and 3 (see sections 6.3 and 6.4), however, suggest that other boundary conditions are more suited especially to predict the open and occluded transfer function levels.

  - In a future version it would be desirable to implement a boundary condition (mechanical loading discussed further below) configuration that corresponds more to the ones presented in articles 2 and 3. Note, however, that it is very challenging to implement, for instance, a mechanical compressional excitation of the entire circumference of the bone and cartilage domains experimentally.
- Limitations with respect to the mechanical shear excitation.
  - In a future version of the text fixture the mechanical excitation should be applied to the entire bony and cartilaginous circumference and the mechanical excitation should be rendered more realistic. Bone transducers which are routinely used for occlusion effect measurements in human subjects cause a compressional point excitation either at the mastoid process or the forehead. In section 5.2.3 several different approaches to excite the artificial ear were discussed (e.g. including bone transducers). While the chosen stimulation method is not very realistic it satisfies the condition that the stimulation must be axisymmetric. This condition was defined in order to facilitate the implementation of a test fixture equivalent numerical model that could be used in the future to study the earplug occlusion effect both experimentally and numerically.

6.6 General conclusion

In the present study two novel numerical human external ear models of complex and simplified geometrical complexity were developed to (i) predict the earplug occlusion effect and to (ii) investigate the contribution of the earplug type to the occlusion effect magnitude. Additionally, the feasibility to implement an axisymmetric artificial external ear test fixture to measure the earplug occlusion effect was demonstrated.

The results obtained with the numerical models suggest that finite element modeling of the human external ear and the earplug induced occlusion effect represents a valuable and versatile numerical tool to further study and explain the occlusion effect.

One of the most fundamental outcomes of the present study includes the finding that the occlusion effect magnitude at medium insertion is earplug type dependent. While this result is in agreement with the experimental data reported by Lee et al. (2011) the present study provides an explanation of the predicted occlusion effect differences using power balance computations. Together with the results obtained by Lee et al. (2011) the experimental and numerical occlusion effect results, thus, provide further evidence that the earplug design could be optimized in order to reduce the earplug occlusion effect. Another important outcome of the present study is that future research is necessary in order to improve the limitations of the proposed models that apply to their geometrical layout, the employed material properties and the chosen boundary and load conditions.

The novel test rig presented in this work provides preliminary proof of the general feasibility to (i) implement an artificial external ear, to (ii) stimulate the external ear via structure borne excitation and to (iii) measure and earplug occlusion effect. In the future a test fixture similar to the one presented in this study has the potential to provide a useful experimental method to further investigate the earplug occlusion effect in a standardized and objective manner. Nevertheless, future research is necessary to improve currently existing limitations especially with respect to the mechanical stimulation as well as the geometrical layout, the chosen material properties and the boundary conditions.

Overall, the numerical models and artificial external ear test fixture presented in this work seem promising to complement existing modelling and measuring techniques to further study the occlusion effect and, in the long run, to guide the design and implementation of a passive low occlusion effect hearing protection device.

LIST OF BIBLIOGRAPHICAL REFERENCES

Allen, G. and C. Fernandez. 1960. « The mechanism of bone conduction ». *Ann. Otol. Rhinol. Laryngol.*, Vol. 69, n° 1, p. 5–28.

Alvord, L.S. and B.L. Farmer. 1997. « Anatomy and orientation of the human external ear ». *J Am Acad Audiol.*, Vol. 8, n° 6, p. 383–390.

ANSI. 2008. « *Methods for Measuring the Real-Ear Attenuation of Hearing Protectors* ». S12.6-2008. Washington D.C., USA: American National Standards Institute, 34 p.

Bàràny, E. 1938. « A contribution to the physiology of bone conduction ». *Acta Oto-Laryngologica*, Vol. 26, n° Suppl.26, p. 1–223.

Békésy, G. 1932. « Zur Theorie des Hörens bei der Schallaufnahme durch Knochenleitung ». *Ann. Physik*, Vol. 13, p. 111–136.

Békésy, G. 1941. « About acoustic transmission by bone conduction ». *Z. Hals Nasen Ohrenheik.*, Vol. 47, p. 430–442.

Békésy, G. 1941. « Ueber die Schallausbreitung bei Knochenleitung ». *Z. Hals Nasen Ohrenheilk.*, Vol. 47, p. 430–442.

Berger, E.H. 2013. « "Calibrating" the insertion depth of roll-down foam earplugs ». In *Proceedings of ICA 2013*. (Montreal, QC, Canada, June 2-7 2013), p. 1-9.

Berger, E. H. 2000. « Hearing Protection Device Utilization Around the World ». *Spectrum*, Vol. 17, n° Suppl. 1, p. 18.

Berger, E. H. and J. E. Kerivan. 1983. « Influence of physiological noise and the occlusion effect on the measurement of real-ear attenuation at threshold ». *J. Acoust. Soc. Am.*, Vol. 74, n° 1, p. 81–94.

Berger, E.H., L.H. Royster and D.P. Driscoll. 2003. *The noise manual,* Revised Fifth edition. Fairfax, VA: AIHA Press, 796.

Brinkman, W., E. Marres and J. Tolk. 1965. « The mechanism of bone conduction ». *Acta Otolaryngol.*, Vol. 59, p. 109–115.

Brummund, M.K., F. Sgard, Y. Petit and F. Laville. 2014. « Three-dimensional finite element modeling of the human external ear: simulation study of the bone conduction occlusion effect ». *J. Acoust. Soc. Am.*, Vol. 135, n° 3, p. 1433–1444.

Brummund, M.K., F. Sgard, Y. Petit, F. Laville and H. Nélisse. 2014a. « Prediction of the bone conduction occlusion effect using a two-dimensional axi-symmetric finite element model ». *J. Acoust. Soc. Am.*, submitted.

Brummund, M.K., F. Sgard, Y. Petit, F. Laville, and H. Nélisse. 2014b. « An axi-symmetric model to study the earplug contribution to the bone conduction occlusion effect ». *Acta Acustica United with Acustica*, submitted.

Brummund, M.K., F. Sgard, Y. Petit and F. Laville. 2012. « On the influence of the material properties of the external ear on occlusion effect simulations ». In *Proceedings Canadian Acoustics*. (Banff, Canada, Oct. 10-12 2012), p. 110-111.

Brummund, M.K., F. Sgard, Y. Petit, F. Laville and J. Boutin. 2013. « Implementation of a simplified, artificial external ear test fixture for measurement of the earplug induced auditory occlusion effect ». In Proceedings *ICA 2013 Montreal*. (Montreal, QC, Canada, June 2-7 2013), p. 1-7.

Brummund, M, Y. Petit, F. Sgard and F. Laville. 2011. « Development of a 3D finite element model of the human external ear for simulation of the auditory occlusion effect ». In *Proceedings Canadian Acoustics*. (Quebec City, Canada, Oct. 12-14 2011), p. 94-95.

Brummund, M., F. Sgard, Y. Petit and F. Laville. 2011. « A simplified axi-symmetric finite element model of the human outer ear to determine the earplug induced auditory occlusion effect ». In *Proceedings 162nd Meeting Acoustical Society of America*. (San Diego, CA, USA, Oct. 31 - Nov 04 2011), p.2469.

Cox, R.W. and M.A. Peacock. 1979. « The growth of elastic cartilage ». *J. Anat.*, Vol. 128, n° 1, p. 207–213.

Danter, J., R. Siegert and H. Weerda. 1996. « Ultrasonographische Haut- und Knorpeldickenmessungen an gesunden und rekonstruierten Ohren mit einem 20-MHz-Ultraschallgerät. (Ultrasound measurement of skin and cartilage thickness in healthy and reconstructed ears with a 20-MHz ultrasound device) ». *Laryngo-Rhino-Otol*, Vol. 75, n° 02, p. 91–94.

Delille, R., D. Lesueur, P. Potier, P. Drazetic and E. Markiewicz. 2007. « Experimental study of the bone behaviour of the human skull bone for the development of a physical head model ». *Int. J. Crashworthiness*, Vol. 12, n° 2, p. 101–108.

Duck, F.A. 1990. *Physical properties of tissue. A comprehensive reference book,* London: Academic Press. 346 p.

Franke, E.K., H.E. v.Gierke, F.M. Grossman and W.W. v.Wittern. 1952. « The Jaw Motions Relative to the Skull and Their Influence on Hearing by Bone Conduction ». *The Journal of the Acoustical Society of America*, Vol. 24, n° 2, p. 142–146.

Fung, Y.C. 1993. *Biomechanics: Mechanical Properties of Living Tissues,* 2nd ed. Berlin: Springer-Verlag. 568 p.

Gelfand, S.A. 2010. *Hearing. An introduction to Psychological and Physiological Acoustics,* 5th ed. Essex UK: Informa Healthcare. 311 p.

Goldstein, D.P. and C.S. Hayes. 1965. « The occlusion effect in bone conduction hearing ». *J. of speech and hearing research*, Vol. 8, p. 137–148.

Grellmann, W., A. Berghaus, E.J. Haberland, Y. Jamali, K. Holweg, K. Reincke and C. Bierögel. 2006. « Determination of strength and deformation behavior of human cartilage for the definition of significant parameters ». *J. Biomed Mater Res A.*, Vol. 78, n° 1, p. 168–174.

Guild, S.R. 1936. « Hearing by bone conduction ». *Ann. Otol. Rhinol. Lar.*, Vol. 45, p. 736–754.

Hahn, K.S. 1985. « The Effect of Variation in EarCanal Skin Parameters on the Beahavior of an Ear-Earplug Model ». BSc. thesis, University of Toronto, 53 p.

Hansen, M.O. 1998. Occlusion effects, Part II : A study of the occlusion effect mechanism and the influence of the earmould properties. PhD thesis, Technical University of Denmark, Lyngby, Denmark, 113 p.

Hansen, M.O.. 1997. Occlusion effects: Part I: Hearing aid users experiences of the occlusion effect compared to the real ear sound level. PhD thesis, Technical University of Denmark, Lyngby, Denmark, 85 p.

Howell, K. and A.M. Martin. 1975. « An investigation of the effects of hearing protectors on vocal communication in noise ». *Journal of Sound and Vibration*, Vol. 41, n° 2, p. 181—196.

Hudde, H. and A. Engel. 1998. « Measuring and modeling basic properties of the human middle ear and ear canal. Part II: Ear canal, middle ear cavities, eardrum and ossicles ». *Acustica - Acta Acustica*, Vol. 84, p. 894–913.

Hughson, G.W., R.E. Mulholland and H.A. Cowie. 2002. *Behavioural studies of people's attitudes to wearing hearing protection and how these might be changed*. Research report No. 028. Edinburgh, UK: Institute of Occupational Medicine, 125 p.

Huizing, E. H. 1960. « Bone conduction-the influence of the middle ear ». *Acta Oto-Laryngol.*, Vol. Suppl. 155, p. 1–99.

ISO. 1992. « *Acoustics -- Audiometric test methods -- Part 2: Sound field audiometry with pure-tone and narrow-band test signals* ». 8253-2. Geneva, Switzerland: International Organization for Standardization, 16 p.

Jahn, A.F. and J. Santos-Sacchi. 2001. *Physiology of the Ear,* 2nd ed. San Diego, CA, USA: Singular Thomson Learning, 689 p.

James, C. 2006. Finite Element Modeling and Exploration of Double Hearing Protection Systems. Master thesis, Virginia Polytechnic Institute and State University, Blacksburg, Virginia, 135 p.

Johansen, P.A. 1975. « Measurement of the human ear canal ». *Acustica*, Vol. 33, p. 349–351.

Khanna, S.M., J. Tonndorf and J.E. Queller. 1976. « Mechanical parameters of hearing by bone conduction ». *The Journal of the Acoustical Society of America*, Vol. 60, n° 1, p. 139–154.

Kirikae, I. 1959. « An experimental study on the fundamental mechanism of bone conduction ». *Acta Oto-Laryngol.*, Vol. Suppl. 145, p. 110.

Klodd, D.A. and B.J. Edgerton. 1977. « Occlusion effect: Bone Conduction speech audiometry using forehead and mastoid placement ». *International Journal of Audiology*, Vol. 16, n° 6, p. 522–529.

Lamarche, D., J. Aubin and S. Blouin. 2011. *Statistiques annuelles 2011*. Numéro de document: DC 200-1046-19. Ville de Québec, Canada: CSST, 155 p.

Lamarche, D., J. Aubin and S. Blouin. 2013. *Statistiques annuelles 2012*. Numéro de document: DC 200-1046-20. Ville de Québec, Canada: CSST, 155 p.

Lamarche, D., J. Aubin and S. Blouin. 2014. *Statistiques annuelles 2013*. Numéro de document: DC 200-1046-21. Ville de Québec, Canada: CSST, 158 p.

Lee, K. 2011. *Effects of earplug material, insertion depth, and measurement technique on hearing occlusion effect*. PhD thesis, Virginia Polytechnic Institute and State University, Blacksburg, Virginia, 127 p.

Lee, K. and J.G. Casali. 2011. « Investigation of the Auditory Occlusion Effect with Implications for Hearing Protection and Hearing Aid Design ». In *Proceedings of the Human Factors and Ergonomics Society Annual Meeting*. (Las Vegas, NV, USA, Sept. 19-23), p. 1783 –1787.

Lorensen, W.E. and H.E. Cline. 1987. « Marching Cubes: A High Resolution 3D Surface Construction Algorithm ». *Computer Graphics*, Vol. 21, n° 4, p. 163–169.

Lowy, K. 1942. « Cancellation of the electrical cochlear response with air- and bone-conduction ». *J. Acoust. Soc. Am.*, Vol. 14, p. 156–158.

Lucente, F.E., W. Lawson, and N.L. Novik. 1995. *The External Ear*. Philadelphia, PA, USA: W.B. Saunders Company. 311 p.

Mach, E. 1863. « Zur Theorie des Gehörorgans ». *Sber. Akad. Wiss. Wien, math-naturw. Kl., Abh. II*, Vol. 48, p. 283–300.

Melamed, S., S. Rabinowitz and M.S. Green. 1994. « Noise exposure, noise annoyance, use of hearing protection devices and distress among blue-collar workers ». *Scand J Work Environ Health*, Vol. 20, n° 4, p. 294–300.

Naunton, R. 1963. « The measurement of hearing by bone conduction ». In *Modern Developments in Audiology,* Jerger, J. (eds.), pp. 1–29. New York: Academic.

Nélisse, H., C. Le Cocq, J. Boutin, J. Voix and F. Laville. 2013. « Comparison of subjective and objective methods for the measurements of hearing protector devices attenuation and occlusion effect. ». In *Proceedings ICA 2013*. (Montreal, QC, Canada, June 2-7 2013), p. 1-7.

Oliveira, R.J. and G. Hoeker. 2003. « Ear Canal Anatomy and Activity ». *Semin Hear*, Vol. 24, n° 04, p. 265–276.

Organisation mondiale de la santé (OMS). 2001. « *Le bruit au travail et le bruit ambiant* ». Aide-mémoire N°258. Genève, Suisse: Organisation mondiale de la santé, 6 p.

Peterson, J. and P.C. Dechow. 2003. « Material Properties of the Human Cranial Vault and Zygoma ». *Anat. Rec.*,n° 274A, p. 785–797.

Pierce, A. D. 1991. *Acoustics. An introduction to its Physical Principles and Application,* New York: The Acoustical Society of America. 678 p.

Pohlmann, A.G. 1930. « Correlations Between the Acuity for Hearing Air and Bone Transmitted Sounds in Rinne Negative and Rinne Positive Cases ». *Ann. Otol., Rhin. & Laryng.*, n° 39, p. 927.

Québec, Province. À jour au 1 août 2014. « *Loi sur la santé et la sécurité du travail (L.R.Q., c. 2.1). Règlement sur la santé et la sécurité au travail (D. 885-2001), Section XV, articles 130 à 141)* ». En ligne. Québec (QC) : Éditeur officiel du Québec. http://www2.publicationsduquebec.gouv.qc.ca/dynamicSearch/telecharge.php?type=3&file=/S_2_1/S2_1R13.HTM. Consulté le 27 août 2014.

Reinfeldt, S., S. Stenfelt, T. Good and B. Hakansson. 2007. « Examination of bone-conducted transmission from sound field excitation measured by thresholds, ear-canal sound pressure, and skull vibrations ». *The Journal of the Acoustical Society of America*, Vol. 121, n° 3, p. 1576–1587.

Reinfeldt, S., S. Stenfelt and B. Håkansson. 2013. « Estimation of bone conduction skull transmission by hearing thresholds and ear-canal sound pressure ». *Hearing Research*, Vol. 299, n° 0, p. 19–28.

Rinne, H.F. 1855. « Beitraege zur Physiologie des menschlichen Ohres. ». *Praegers Vierteljahrsschriften*, n° 1, p. 113.

Sarvazyan, A.P., A.R. Skovoroda, S.Y. Emelianov, J.B. Fowlkes, J.G. Pipe, R.S. Adler, R.B. Buxton, et al. 1995. « Biophysical bases of elasticity imaging ». In A*coustical Imaging 1995,* Jones J. P. (Ed.), pp. 223–240. Vol. 21. New York and London: Plenum Press.

Schroeter, J. and C. Poesselt. 1986. « The use of acoustical test fixtures for the measurement of hearing protector attenuation. Part II : Modeling the external ear, simulating bone conduction, and comparing test fixture and real-ear data ». *The Journal of the Acoustical Society of America*, Vol. 80, n° 2, p. 505–527.

Sgard, F, H. Nélisse and F. Laville. 2008. *Développement d'outils et de méthodes pour mieux évaluer et améliorer la protection auditive individuelle des travailleurs*. Protocole de recherche 0099-7630. Montréal (QC): IRSST, 56 p.

Sgard, F., H. Nélisse, M.A. Gaudreau, J. Boutin, J. Voix and F. Laville. 2010. *Study of sound transmission through hearing protection device and application of a method to better assess their real efficiency in workplace. Part 2 : preliminary study of finite element models of hearing protection devices (in french: Étude de la transmission sonore à travers les protecteurs auditifs et application d'une méthode pour évaluer leur efficacité effective en milieu de travail. Partie 2 : étude préliminaire d'une modélisation des protecteurs auditifs par éléments finis)*. Technical report No. 099-494. Montréal (QC): IRSST, 24 p.

Sgard, F., M. Brummund, G. Viallet, S. Boyer, Y. Petit, F. Laville and J. Boutin. 2012. « Acoustic finite element modeling of hearing protection devices ». In *Proceedings Internoise 2012*. (New York, USA, Aug. 19-22 2012).

Shaw, E.A.G. 1976. « Diffuse field sensitivity of the external ear as a sound collector ». *J. Acoust. Soc. Am.*, Vol. 60, p. 102.

Shaw, E.A.G. 1977. « Eardrum representation in middle-ear acoustical networks ». *J. Acoust. Soc. Am.*, Vol. 62, n° 1, p. S 12.

Shaw, E.A.G and M.R. Stinson. 1981. « Network concepts and energy flow in the human middle ear. ». *J. Acoust. Soc. Am.*, Vol. 69, n° 1, p. 43.

Stenfelt, S., T. Wild, N. Hato and R. Goode. 2003. « Factors contributing to bone conduction: The outer ear ». *J. Acoust. Soc. Am.*, Vol. 113, n° 2, p. 902–913.

Stenfelt, S. and R.L. Goode. 2005. « Bone-conducted sound: physiological and clinical aspects ». *Otol. Neurotol*, Vol. 26, n° 6, p. 1245–1261.

Stenfelt, S., N. Hato and R.L. Goode. 2002. « Factors contributing to bone conduction: The middle ear ». *J. Acoust. Soc. Am.*, Vol. 111, n° 2, p. 947–959.

Stenfelt, S. and S. Reinfeldt. 2007. « A model of the occlusion effect with bone-conducted stimulation ». *Int. J. of Audiology*, Vol. 46, n° 10, p. 595 – 608.

Stenfelt, S., T. Wild, N. Hato and R.L. Goode. 2003. « Factors contributing to bone conduction: the outer ear ». *J. Acoust. Soc. Am.*, Vol. 113, n° 2, p. 902–913.

Stinson, M,R. and B.W. Lawton. 1989. « Specification of the geometry of the human ear canal for the prediction of sound-pressure level distribution ». *The Journal of the Acoustical Society of America*, Vol. 85, n° 6, p. 2492–2503.

Tak, S.W, R.R. Davis and G.M. Calvert. 2009. « Exposure to hazardous workplace noise and use of hearing protection devices among US workers—NHANES, 1999–2004 ». *American Journal of Industrial Medicine*, Vol. 52, n° 5, p. 358–371.

Tonndorf, J. 1966. « Bone conduction. Studies in experimental animals. ». *Acta Oto-Laryngol.*, Vol. Suppl. 213, p. 1–132.

Tonndorf, J. 1972. « Bone Conduction ». In *Foundations of Modern Auditory Theory,* Tobias, J.V. (Ed.), pp. 195–237. Vol. 2. New York: Academic Press.

Tufts, J.B., S. Chen and L. Marshall. 2013. « Attenuation as a function of the canal length of custom-molded earplugs: A pilot study ». *J. Acoust. Soc. Am*, Vol. 133, n° 6, p. 446.

Viallet, G., F. Sgard and F. Laville. 2013. « Influence of the external ear tissue domains on the sound attenuation of an earplug predicted by a finite element model ». *Proceedings of ICA 2013*. (Montreal, QC, Canada, June 2-7 2013), p. 1-8.

Watson, N.A. and R.S. Gales. 1943. « Bone-Conduction Threshold Measurements: Effects of Occlusion, Enclosures, and Masking Devices ». *J. Acoust. Soc. Am.*, Vol. 14, n° 4, p. 207–215.

Wever, G., and M. Lawrence. 1954. *Physiological Acoustics*. Princeton: Princeton U.P. 454 p.

Yu., J.F., G.L.Tsai, C.C. Fan, C.I. Chen, C.C. Cheng and C.C. Chen. 2012. « Non-invasive technique for in vivo human ear canal volume measurement ». *Journal of Mechanics in Medicine and Biology*, Vol. 12, n° 04, p. 1250064 1–9.